

SABATAIR

Deliverable 3b:

Test Report of the Selected Additional Mitigating Measures

Task	3	Identification and assessment of additional mitigating measures to packaging and multi-layered approaches
-------------	----------	---

Dissemination level¹	CO	Due delivery date	31/12/2018
Nature²	R	Actual delivery date	07/05/2020

Lead beneficiary	Algolion
Contributing beneficiaries	VITO, ImpactSolutions, Airbus

Document Version	Date	Author	Comments³
V0	18/11/2019	Alex Gorodnev (ALGOLiON) Steven Burns (Impact solutions) Praharsh Pai Raikar (VITO) André Freiling (AIRBUS)	Creation
V1.0	20/01/2020	Khiem Trad (VITO)	Review and submission
V1.1	23/04/2020	Enzo Canari (EASA)	Review
V1.2	06/05/2020	Niles Fleischer (ALGOLiON) Steven Burns (Impact solutions) André Freiling (Airbus) Khiem Trad (VITO)	Minor changes, Added executive summary, Appendix and final conclusions; Final

¹ Dissemination level: **PU** = Public, **PP** = Restricted to other programme participants (including the JU), **RE** = Restricted to a group specified by the consortium (including the JU), **CO** = Confidential, only for members of the consortium (including the JU)

² Nature of the deliverable: **R** = Report, **P** = Prototype, **D** = Demonstrator, **O** = Other

³ Creation, modification, final version for evaluation, revised version following evaluation, final



Table of Contents

Table of Contents	2
List of Figures	3
List of Tables	6
Executive summary	7
Introduction	9
Chapter I: Evaluation of battery safety with early warning diagnostic software	10
I.1 Introduction	10
I.2 Brief Description of the Technology	10
I.3 Development of Point Heating Method	11
I.4 Results of Thermal Runaway (TR) Testing with Point Heating	12
I.4.1 TR test results for cells with 30% SOC:	12
I.4.2 Thermal runaway test results for cells with 100% SOC	14
I.5 Conclusion	17
Chapter II: Thermal Modelling for Thermal Runaway Mitigation Strategies	18
II.1 Introduction	18
II.2 Brief description of the thermal model	18
II.3 Numerical Simulations for Thermal Runaway Mitigation Strategies	19
II.3.1 Base Case – Case 1	19
II.3.2 Mitigation Cases	21
II.4 Results Summary and Conclusion	30
Chapter III: Testing of Additional Mitigating Measures on Packaging Level	32
III.1 Brief description of the test procedure	32
III.2 Test Results	33
III.2.1 Reference test: no mitigation measure using cells at 30% SOC	33
III.2.2 Base case: no mitigation measure using cells at 100% SOC	34
III.2.3 Experimental assessment of Case 4 modelling results	35
III.2.4 Experimental assessment of Case 2 modelling results	37
III.2.5 Experimental assessment of Case 8 modelling results	38
III.3 Conclusion	39
Chapter IV: Full scale test on external fire impact mitigation	40
IV.1 Introduction	40
IV.2 Brief description of the test setup and procedure	40
IV.3 Test Results Summary	44
IV.4 Conclusions	48
Chapter V: Conclusions	49
Bibliography	50
Appendix	51

List of Figures

Figure 1. The laptop computer hosts the diagnostic software. The instrument on the right is used to access cell voltage and current in response to discharge or charge profiles applied to the cell (on top of the instrument).	11
<i>Figure 2: A point heater applied to the side of a cell. The numbers refer to four locations of thermocouples.....</i>	<i>11</i>
Figure 3: (Left) generation I cylindrical heating element, (Middle) generation II small area point contact tip, and (Right) various larger area point contacts with tip geometries selected for the geometry of the test cell casing.	12
<i>Figure 4: (a) Change in temperature measured by the four thermocouples with heating time. The cell swelled and then vented. (b) Voltage profile of cell during test. (c) Change of the EA cathode parameter during the course of the heating. The red dotted line indicates the alert value for the EA parameter.</i>	<i>13</i>
Figure 5: The dc resistance, (R_{ir} blue) as measured by the iR drop and the cell temperature (gray), corresponding to the experiment in Figure 5.	14
Figure 6: (Upper) change in temperature measured by the four thermocouples with heating time. The cell entered into thermal runaway at about 180° C. (Lower) Change of the HC parameter (green) compared to conventional dc resistance iR drop (red) during the course of the heating.	15
Figure 7: Change of the EMS parameter (green) compared to conventional dc resistance iR drop (black) during the course of the heating to thermal runaway for a A type 18650 cell.....	15
Figure 8: Temperature profiles as measured by the four thermocouples for B type cell with bottom heating. The numbers in the graph legend refer to the position of the thermocouples as noted in Figure 7.....	16
Figure 9: Temperature graphs of a B type cell heated to thermal runaway; the four lines are from the four different thermocouples located on the cell as per Figure 2. The top line is thermocouple number 1 which is located next to the heating point.....	16
Figure 10: Heat generation definition used for TR modelling.....	18
Figure 11: Base case for study of TR propagation mitigation strategies with computational mesh (right).....	19
Figure 12: Base case cells maximum temperature temporal evolution of cells in the initiation row and farthest column.....	20
Figure 13: Temperature contour at mid-height level plane for base case at different times	21
Figure 14: Temperature contour at mid-height level plane for case 0 at different times.....	22
Figure 15: Temperature evolution for initiation cell and adjacent cells for Case 0.....	22
Figure 16: Temperature contour at mid-height level plane for case 2 at different times.....	23

Figure 17: Temperature evolution for initiation cell and adjacent cells for Case 1 (top) and Case 2 (bottom).....	24
Figure 18: Temperature evolution for initiation cell and adjacent cells for Case 3.....	25
Figure 19: Temperature evolution for initiation cell and adjacent cells for Case 4 (top) and Case 5 (bottom).....	26
Figure 20: Temperature evolution for initiation cell and adjacent cells for Case 6.....	27
Figure 21: Temperature evolution for initiation cell and adjacent cells for Case 7.....	28
Figure 22: Temperature evolution for initiation cell and adjacent cells for Case 8.....	29
Figure 23: Temperature evolution for initiation cell and adjacent cells for Case 9 (top) and Case 10 (bottom).....	30
Figure 24: Thermal runaway initiation test setup. (PC stands for Periphery Cell; IC for Initiation Cell; and t for thermocouple).....	33
Figure 25: GB6232 certification status.....	33
Figure 26: Reference test results using cells at 30%SOC	34
Figure 27: Reference test results using cells at 100%SOC	35
Figure 28: Test setup for test 36	36
Figure 29: Experimental results of Case 04 modelling scenario	36
Figure 30: Picture of the package after experimental test of Case 04 modelling scenario	36
Figure 31: Experimental results of Case 02 modelling scenario	37
Figure 32: Picture of the package after experimental test of Case 2 modelling scenario	37
Figure 33: Experimental results of Case 08 modelling scenario	38
Figure 34: Photograph of the fire test chamber	40
Figure 35: Arrangement of Cardboard Boxes as fire load for the Bulk load fire test of the Minimum Performance Standard for Aircraft Cargo Compartment Halon Replacement Fire Suppression Systems (2012 Update)	41
Figure 36: Cardboard Box filled with shredded paper acting as fire source for the external fire test (left) – Cardboard Box arrangement in the test compartment (right)	41
Figure 37: Type B cell packaging.	42
Figure 38: Type C cell packaging.	42
Figure 39: Arrangement of cardboard boxes for the full scale fire test	43
Figure 40: Position of the thermocouples of the cell packs located directly on the pallet. The blue markers indicate thermocouple location outside of the outer cardboard boxes. The pink/green	

positions indicate thermocouple locations directly on the respective cells (green= B type and pink=C type) The graphics also indicates the State of Charge 43

Figure 41: Position of the thermocouples of the cell packs located on the metallic support. The blue positions indicate thermocouple location outside of the outer cardboard boxes. The pink/green positions indicate thermocouple locations directly on the respective cells (green= B type and pink=C type). The graphics also indicates the SoC. In a mixed configuration with 50 cells at 50% SoC and 50 cells with 100% SoC, the cells with 100% SoC were located at the outer rim as indicated in the upper left image..... 44

Figure 42: Temperatures during the external fire test without fire suppression 45

Figure 43: Impact on Cells after the test without fire suppression 45

Figure 44: Temperatures during the external fire test with fire suppression 46

Figure 45: Impact on Cells after the test with fire suppression 46

Figure 46: Temperatures during the external fire test with fire suppression and Fire Containment cover..... 47

Figure 47: Fire Containment Cover within cardboard boxes before the test 47

Figure 48: Fire Containment Cover after the test 47

Figure 49: Impact on Cells after the Test with Fire Suppression and Fire Containment Cover 48

List of Tables

Table 1: Comparison of properties of the two 18650 cells used in the tests. In the rest of the document they will be referenced as A type and B type.....	15
Table 2: Thermal properties of simulation materials.....	20
Table 3: Test plan of additional mitigation measures.....	32

Executive summary

A technology of early warning safety diagnostic algorithms was demonstrated. It was shown that it can detect changes in the cell due to thermal degradation from external heating significantly before the threshold of thermal runaway. The algorithms analyze changes in the cell current and voltage and then calculates several key output parameters that are indicators of internal defects that may lead to internal shorting and then thermal runaway. This new method responds to changes in cells associated with defects significantly earlier than conventional techniques of dc resistance and ac impedance. The test results support the possible use of the ALGOLiON software as a mitigating measure within a multi-layer approach for enhancing the safety of batteries during air transport. It is recommended to continue to refine this technique under an expanded set of conditions. It is also recommended to design and build a measurement instrument incorporating this software to check its effectiveness on a larger population of cells and possible use as a maintenance check for cells prior to air transport.

Thermal modelling was performed for developing some suggested thermal runaway mitigation strategies. Ten cases and a baseline reference were simulated. The thermal numerical model provided a good understanding of heat propagation from a thermal runaway (TR) initiation cell to neighbouring cells in a box packaging. From the different cases analysed, and for the specific cell models, the cell group topology, and their state of charge, the following observations were made:

1. Thicker cardboard separators between cells in a box is suggested to prevent TR propagation. This is related to increasing the minimum safe distance between cells.
2. A box filled with cells placed in a cold environment with high heat transfer coefficient can reduce TR propagation relative to warmer environments under the full set of conditions in this study.
3. Thicker thermal conductive fibreboard is more effective in mitigating TR relative to less conductive cardboard in the conditions of this work.
4. The presence of vermiculite instead of air is a good mitigating option in these scenarios when used with cardboard separators in the conditions of this work.
5. A container filled with sand can effectively mitigate TR propagation in these test conditions when the cells are kept with sufficient separation distance between them.
6. Thermally conductive boxes made from graphite or alumina helps in thermal dissipation and prevents TR propagation for the conditions used in this study.

The above recommendations are suggested to be evaluated with other cell types, SOC, and cell grouping configurations to gain a more comprehensive view of the effectiveness of possible mitigating measures in packaging.

While the model provides good basis for qualitative assessments, it should be noted that the thermal model has several limitations. The simulations can be used to predict well the heat propagation by conduction and radiation. However a thermal runaway event has other critical effects, such as the release of toxic gases, flames, etc. which are not addressed in the current model. The model currently utilizes only thermal properties of the materials to predict heat propagation. Thus, the benefit of vermiculite, for example, compared to just air is not highlighted by this model. Another consideration is that for dividers and boxes made from cardboard the results from this particular study indicate that it would be better to have a flame-resistant coating. While the model predicts temperatures as high as 600°C, it does not simulate ignition of the packaging.

For the optimization of design solutions that could mitigate the effects of a thermal runaway to acceptable levels, it would be preferred that the model is supported with more experimental data. However, the results from the model highlight trends and principles that could be used as a reference to develop mitigation strategies for prevention of thermal runaway propagation.

Actual testing of some proposed mitigating measures was performed. The testing was carried out using a setup based on the reduced cell configuration test method specified in the draft SAE AS6413 (version November 2018). The test chamber and all equipment were built based on the description in the draft standard. A total of 8 cells were used during this testing. 30 dummy cells made of aluminum were arranged around these. The results for the conditions used in this study showed that it is possible to undertake thermal modelling to closely align with actual results. The testing also highlighted that small differences in the environment (e.g., temperature) can have an appreciable influence on the test results.

Full scale tests of an external fire to cells were performed in an 1:1 aircraft cargo compartment mock-up with an operable aircraft Halon 1301 fire suppression system calibrated to replicate the concentration levels that are typical for a wide body lower deck class C cargo compartment. It was found in these tests that a state-of-the-art Class C cargo compartment built-in fire suppression system inhibited propagation of thermal runaways for the tested configurations. This outcome can be considered specific to the types, quantities, distribution and SOC of cells involved in the performed tests. It was also found in this study that for the tested scenario, a Fire Containment Cover provides an appreciable level of protection against the threats of an external fire event.

Introduction

The goal of Task 3 was to propose mitigating measures that can be used as part of a multi-layered approach for mitigating safety hazards associated with the transport of lithium cells/batteries by air cargo.

As the first step towards achieving this objective, the work that identified mitigating measures, including packaging standards, and multi-layered approaches was presented in the report Deliverable 3a. A test plan was formulated in D3a for assessing several of these measures that were recognized by the project in coordination with the Scientific Committee and EASA as high priority and feasible to test within the scope of the Sabatair project.

This report (Deliverable 3b) covers the results of the testing and modelling done in the project to evaluate the selected mitigating measures.

Disclaimer: Although the survey of possible mitigating measures was comprehensive it was not exhaustive. Thus other mitigation measures may exist which were not examined in Sabatair .

The topic of safety hazards and thermal runaway of lithium cells/batteries (batteries are composed of two or more cells) in air cargo transport has already been covered in this project's deliverable reports D2a and D3a, and so will not again be covered in this report.

Four major sets of evaluations were performed at different locations by various partners of the selected mitigation measures. The major results for each are presented in four different sections of the this report.

Section 1 presents results of the application of ALGOLiON's proprietary predictive early warning prognostic software on single cells via a technique developed in the project for external point heating of cells to drive them into thermal runaway. Point heating closely simulates the location and area of heat generation due to internal short circuit.

Section 2 presents a summary of thermal modelling done by VITO of the propagation of thermal runaway from cell to cell in a package with and without mitigating measures. Experimental data from thermal runaway tests done at Impact Solutions were used to formulate the model.

Section 3 summarizes the results of experimental tests performed by Impact Solutions to validate the modelling results. The tests were done according the procedure described in the November 2018 draft version of SAE AS6413.

Section 4 summarizes the outcome of tests conducted in a test chamber representative of a large aeroplane Class C cargo compartment to evaluate the scenario in which large quantities of cells are involved in a cargo fire event. The tests were done under the supervision of Airbus.

Chapter I: Evaluation of battery safety with early warning diagnostic software

I.1 Introduction

This prevention measure was identified in D3a for testing within the project with high priority. It was evaluated in Task 2 and Task 3. The software outputs a state of risk notification that can be used to implement measures that may prevent thermal runaway.

The cause of thermal runaway that might be prevented and/or detected with this measure are internal short circuits that might be initiated by cell defects induced by manufacturing or post-manufacturing. This technique can be used after the cell production and prior to packaging and shipment. The cell or battery manufacturer may supply the shipper with a certificate on the state of safety of the cells for transport.

Determining when a cell or a battery is close to becoming hazardous is not easy. Some of the failure detection methods like monitoring of cell temperature and visual observations for swelling provides information that might be too late to prevent thermal runaway. Diagnostic algorithms may be used to examine electrochemical developments that are precursors to thermal runaway. The software can be integrated into a purpose-built measuring instrument for testing batteries.

I.2 Brief Description of the Technology

A description of the algorithm, with first test results, was provided in the D3a Report.

In short, the program measures regular cell dc current and voltage, processes and analyzes the signals with algorithms. It then calculates quantitative value for several unique parameters that have been shown in extensive laboratory testing to correlate with electrochemical changes in the cell that can lead to thermal runaway.

The parameters include: a) a surrogate dc resistance parameter (HC) which is more sensitive than dc resistance and ac impedance to precursors of cell faults, b) a measurement of the solid electrolyte interface (SEI), material and structure of the electrode surface (EMS) which tracks for example dendrite growth, c) a measurement of the active electrode area for the anode and the cathode (EA) which also follows dendrite growth and other changes in the electrode, and d) two curve fitting parameters.

A purpose built hardware platform, Figure 1, was built by ALGOLiON for the project to use the software for tests in Task 2 and Task 3.



Figure 1. The laptop computer hosts the diagnostic software. The instrument on the right is used to access cell voltage and current in response to discharge or charge profiles applied to the cell (on top of the instrument).

I.3 Development of Point Heating Method

Internal shorts are characterized by intense local heating. To simulate such local heating a point heating method was developed and validated. In this technique, an external heat source was used at a point contact on the casing of the cell.

The concept for using a point contact heating method to drive cells into thermal runaway was generated by joint collaboration between Impact Solutions, VITO and ALGOLiON. It was based on observations from tests run according to the in preparation SAE AS6413 standard performed in Task 2. This section describes the rationale for the point heating method and its further development at ALGOLiON.

Factors that needed to be taken into account in the development of the technique include: geometry of the heating element and its relation to making effective contact with the cell surface, the contact area of the heating element in relation to the cell size, the position of heating point on the cell, the effect of cell state of charge, rate of heating, and other factors.

Figure 2 shows a schematic view of the point heating setup. A heating tip is applied to the side of a cell and thermocouples follow the temperature at several points on the cell enclosure.

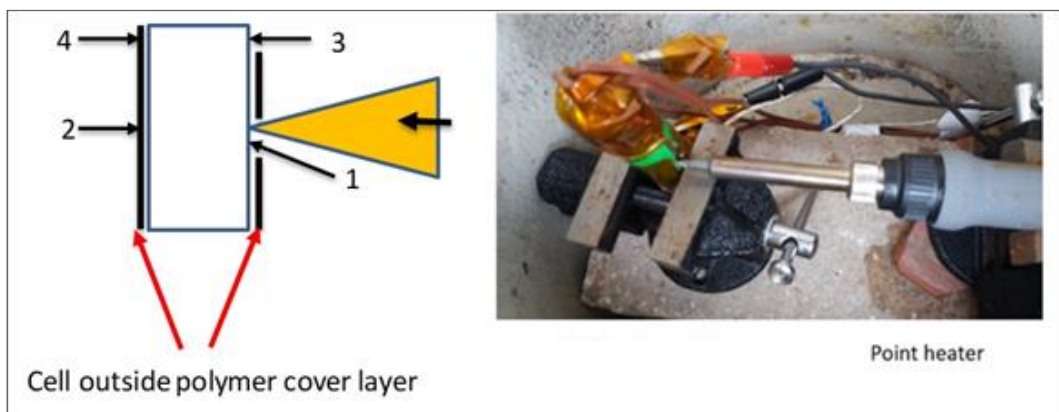


Figure 2: A point heater applied to the side of a cell. The numbers refer to four locations of thermocouples.

Figure 3 shows the progressive enhancement in the geometry of the heating tips developed in this work. The cylindrical heating element makes a line contact with the cell (its end is not applied to the cell). The initial point contact used a tip with a very small surface area tip. This limited the amount of heat that could be transferred to the cell. The improved point contact tips had a larger area for contacting the cell and were either concave with a radius appropriate for the curvature of cylindrical cells, *e.g.*, the 18650 model cells used in these tests, or flat for pressing up against the side of prismatic or pouch cells (also used in some thermal runaway testing).



Figure 3: (Left) generation I cylindrical heating element, (Middle) generation II small area point contact tip, and (Right) various larger area point contacts with tip geometries selected for the geometry of the test cell casing.

Cells were reproducibly driven into thermal runaway using the setup shown in Figure 2 (and use of insulating glass wool wrapped around the cell to achieve quasi-adiabatic conditions). Conclusions from the tests include:

- heating conditions should be adjusted for cell size, capacity and SOC in order to achieve reproducible results;
- the area of tip contact should be scaled within limits with the amount of heat desired to be transferred into the cell;
- the geometry of the heating tip affects the heat transfer properties and cell temperature rise;
- Overall, from the variety of tests conducted with different tip-cell type combinations, it was deduced that there is no ‘one size – fits all’ protocol for reproducible, repeatable thermal runaway results.

1.4 Results of Thermal Runaway (TR) Testing with Point Heating

Some test results examples are provided below for different conditions. The tests were done to validate the algorithm with the point heating method.

1.4.1 TR test results for cells with 30% SOC:

During first stage of the work the experiments were carried out with commercially available pouch cells at 30% SOC as per the point contact heating method described above. Cell capacity is 830 mAh and nominal voltage is 3.7 volts. Dimensions are: 20 x 62 x 7 mm and the cell weight is 16 grams. The cathode is based on a NMC 523 stoichiometry material and the anode is based on graphite.

The upper portion of Figure 4 shows the temperature profile of the cell during heating as measured at the four thermocouples as per the point heating method (see Figure 2). The middle portion tracks the open circuit voltage during the heating process. Upon venting as expected the voltage falls to zero. The interesting part of the experiment is in the lower portion of Figure 4. It shows the response of the EA parameter as measured during the experiment. The change in EA early in the heating process can be used to predict the eventual swelling and venting. The EMS Parameter shows similar behavior (data not shown in the present report).

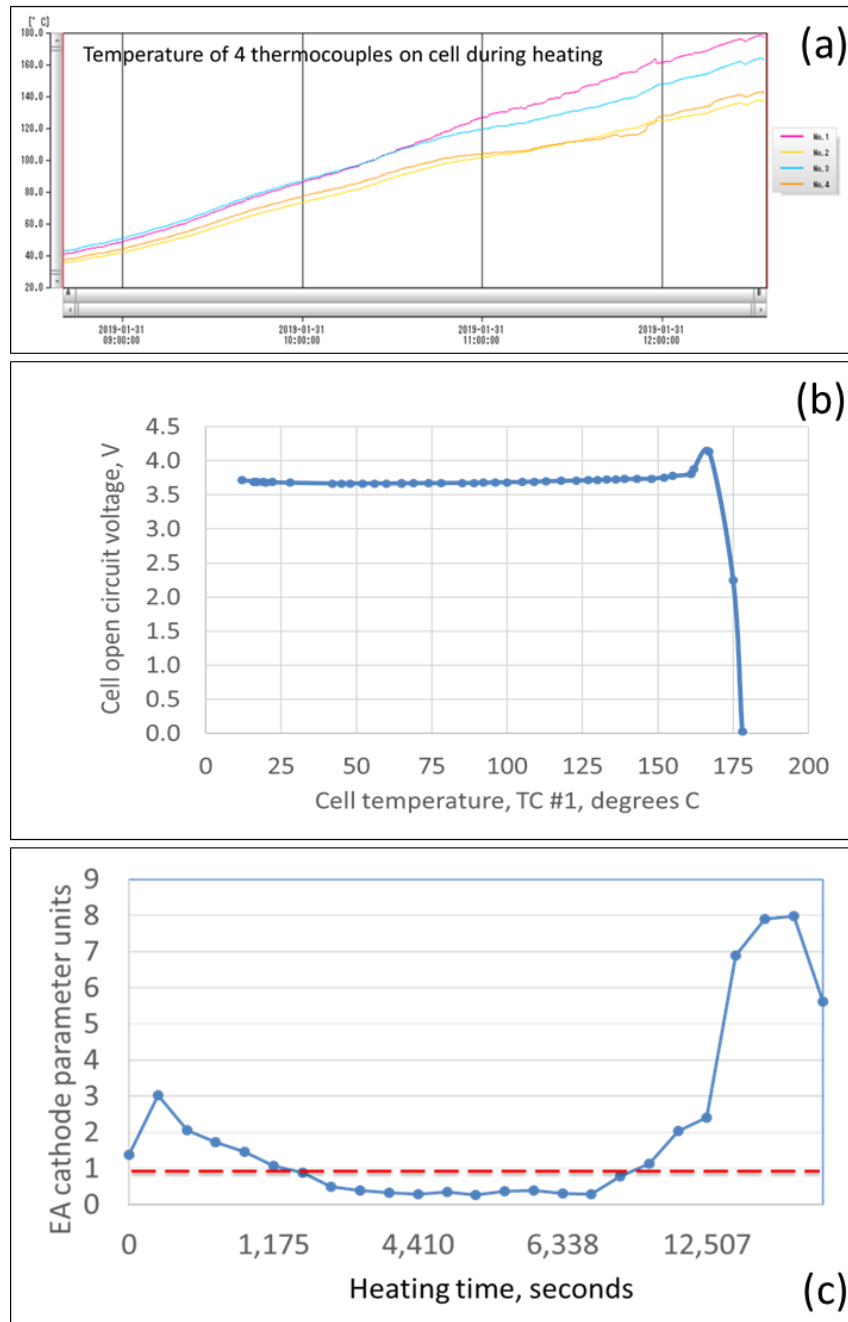


Figure 4: (a) Change in temperature measured by the four thermocouples with heating time. The cell swelled and then vented. (b) Voltage profile of cell during test. (c) Change of the EA cathode parameter during the course of the heating. The red dotted line indicates the alert value for the EA parameter.

In comparison to the predictive EMS and EA parameters the conventional dc resistance shows no significant change during the experiment (blue line on Figure 5).

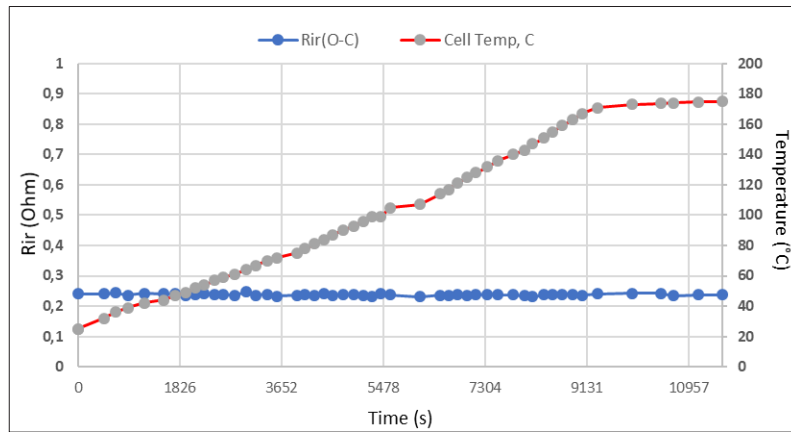


Figure 5: The dc resistance, (*Rir* blue) as measured by the *iR* drop and the cell temperature (gray), corresponding to the experiment in Figure 5.

I.4.2 Thermal runaway test results for cells with 100% SOC

Pouch Cells:

Using the same type of pouch cells as in the previous experiments, additional cells (at total of 10 tests were carried out) in this phase of the work were charged to 100% SOC. Point heating was performed as described above. Cells reached the threshold to thermal runaway at approximately 180°C as measured at the heating point (Figure 6). The maximum measured thermal runaway temperature recorded was 680°C at the heating point. The heating rate was 6 degrees/minute.

As shown in Figure 6, the response of the HC parameter occurs appreciably prior (12.5 minutes) to the thermal runaway. This makes it an effective predictor of the hazard. The algorithm EMS and EA parameters show similar behavior (data not shown in the present report). In contrast, the dc *iR* does not change in any significant way.

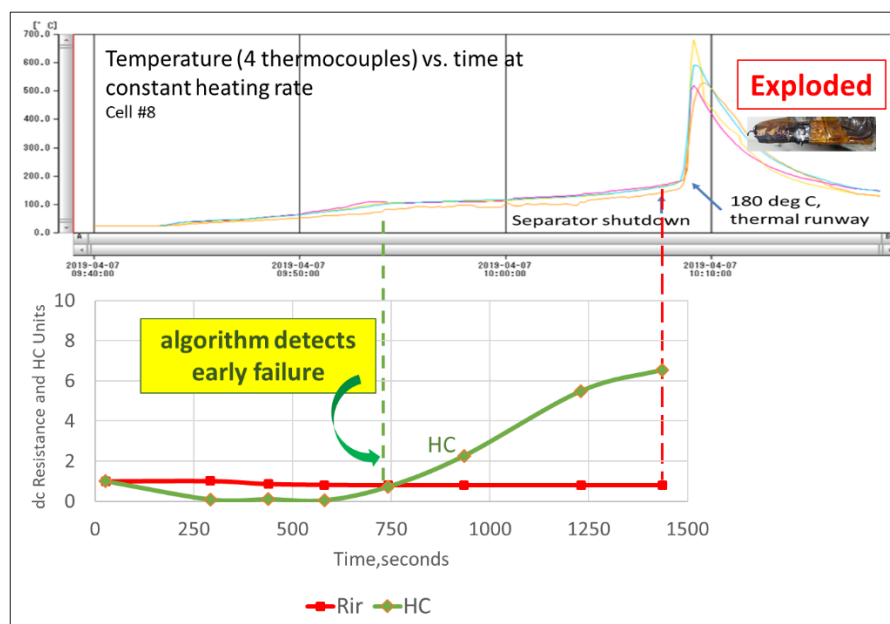


Figure 6: (Upper) change in temperature measured by the four thermocouples with heating time. The cell entered into thermal runaway at about 180° C. (Lower) Change of the HC parameter (green) compared to conventional dc resistance iR drop (red) during the course of the heating.

18650 Cells:

Two types of 18650 cylindrical cells were tested. The cell properties are shown in **Table 1**.

Table 1: Comparison of properties of the two 18650 cells used in the tests. In the rest of the document they will be referenced as A type and B type.

Cell Model, 18650	Capacity (Ah)	Voltage (V)	Weight (grams)	Anode	Cathode
Manufacturer A	3.2	3.7	45	Graphite	NMC, Ni rich
Manufacturer B	3.5	3.6	49	Graphite/Si	NMC, Ni rich

A type cell, bottom heating – 30% SOC:

In one test of a A type cell at 30% SOC a cylindrical heating element was located at the base of the cell. Thermal runaway occurred at about 180° C using a heating rate of 5 degrees/minute.

Figure 7 shows the development of the EMS parameter during the heating compared to dc resistance. The EMS parameter curve (in green in Figure 7) shows a distinct change starting 40 minutes prior to thermal runaway. In comparison the conventional measurement of dc resistance does not change prior to the onset of thermal runaway. The maximum cell temperature after TR was over 900°C.

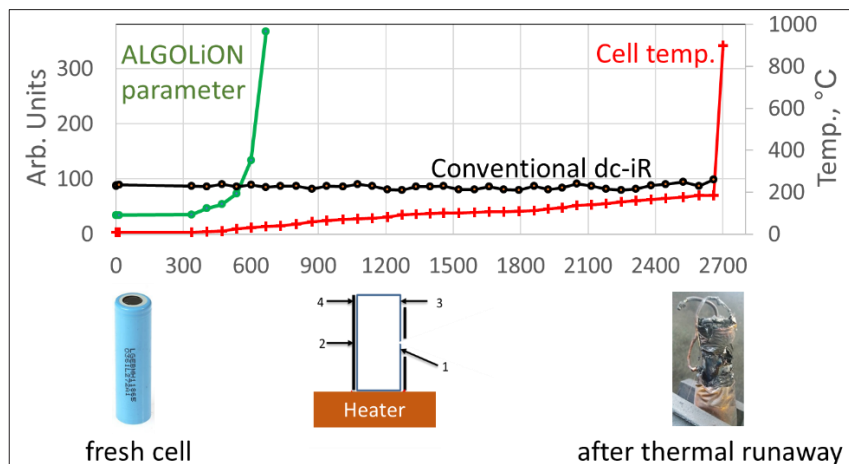


Figure 7: Change of the EMS parameter (green) compared to conventional dc resistance iR drop (black) during the course of the heating to thermal runaway for a A type 18650 cell.

B type cell, bottom heating – 100% SOC:

In another test of the MH1 type cell, the test was run at 100% SOC with bottom heating as portrayed in the lower center portion of Figure 8. The average heating rate was 6° C/minute. The thermal runaway threshold temperature was 177° C, and a maximum temperature of 602° C was reached (Figure 9). In the tests portrayed in Figure 8 and Figure 9 the positions of the thermocouples were as shown in Figure 2.

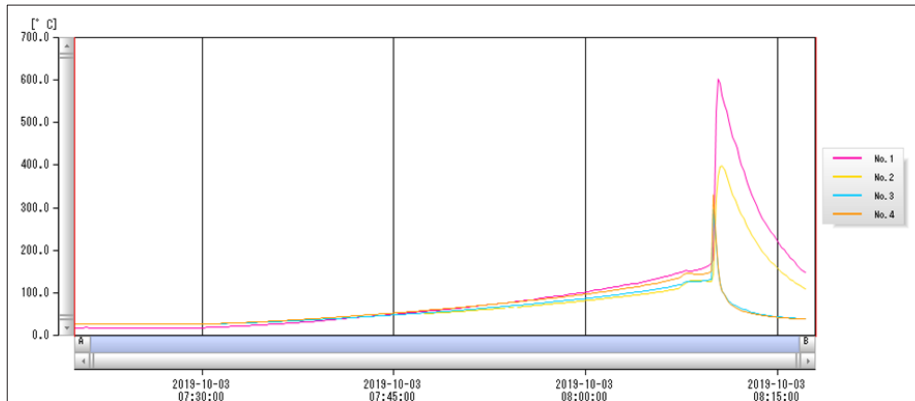


Figure 8: Temperature profiles as measured by the four thermocouples for B type cell with bottom heating. The numbers in the graph legend refer to the position of the thermocouples as noted in Figure 7.

B type cell, 100% SOC, point contact heating at cell's mid-height:

Other tests were run on a different cell brand, the high capacity B type cell. An example of the temperature during heating of a cell tested at 100% SOC and the TR event is presented in Figure 9. Recordings of the temperature from the four different thermocouples are given by the four lines in the graph. The TR threshold (as measured at the point of heating by thermocouple #1 (red in the graph below) temperature was 192° C at the point of heating. Temperatures at more distant locations and on the opposite side of the cell were lower (see Figure 2 for their positions). The maximum temperature recorded during thermal runaway was almost 800°C.

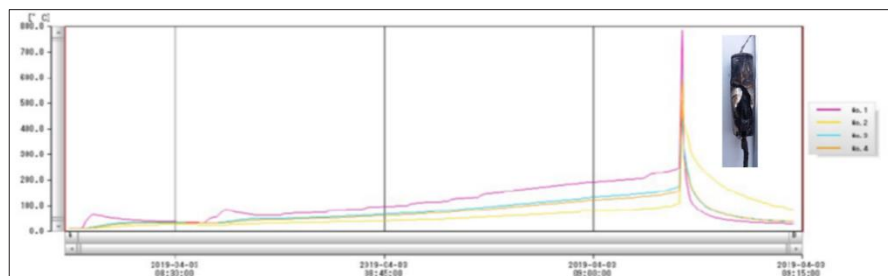


Figure 9: Temperature graphs of a B type cell heated to thermal runaway; the four lines are from the four different thermocouples located on the cell as per Figure 2. The top line is thermocouple number 1 which is located next to the heating point.

1.5 Conclusion

A new method for simulation of the internal shorts was proposed and developed that reproducibly drove cells into thermal runaway by heating the cell surface at a point contact with an external heater. This new technique was applied to cells of various brands and characteristics, at different State of Charge.

It was found that various factors seem to influence the thermal runaway event including the shape and position of the heater, heating rate, and properties of the cell such as the SOC.

Separator shut-down does not prevent thermal runaway if heating continues above the shut-down temperature.

It was demonstrated that the ALGOLION early warning safety diagnostic algorithms detect changes in the cell due to thermal degradation from external heating significantly before the threshold of thermal runaway, and significantly better than conventional techniques of dc resistance and ac impedance.

The test results support the possible use of the ALGOLION algorithm as a prevention measure for monitoring changes in cell properties which could degrade due to external heating leading to thermal runaway. Implementation could be as embedded programs in test stations at cell OEMs, battery pack assemblers and tests would run before packing the cells for shipment by the OEM to detect damaged cells. This seems to be an attractive method for combining within a multi-layer approach for safety of batteries during air transport.

Chapter II: Thermal Modelling for Thermal Runaway Mitigation Strategies

II.1 Introduction

Experimental work to study thermal runaway can be relatively risky. Moreover, exploring different mitigation measures with experimental methods is expensive and time-consuming. To help with these challenges, a thermal model has been developed and validated to be used as a tool to select mitigating measures for further experimental investigation.

In this chapter, a brief description of the model used in this study is provided. This model is used for conducting numerical simulations of different cases to evaluate mitigation measures. Finally, the results and key conclusions are presented.

Document Heat transfer modelling of a Li-Ion cell pack undergoing thermal runaway, dated 10/12/2020 is reported in Appendix A of the present deliverable and provides a more detailed description of the model and of the related simulation output.

II.2 Brief description of the thermal model

The thermal model objective is to simulate heat propagation (by conduction and radiation) for an array of Li-Ion cells within a transportation package. The thermal runaway is modelled with a 'black-box' approach where rather than describing the detailed electrochemical mechanisms leading to the heat generation in the cell, the heat generation is modelled directly. The heat generation at two stages of thermal runaway is linked with the onset temperatures which can be an input in the model.

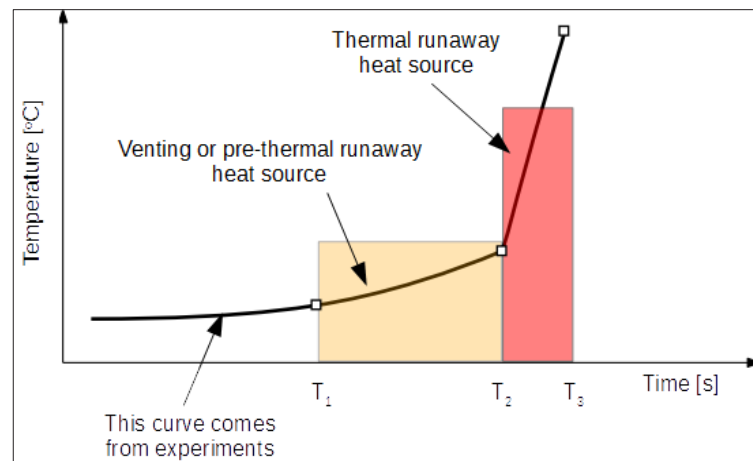


Figure 10: Heat generation definition used for TR modelling

In this simple model, only energy equation is solved in the computational domain. Computational domain can be set depending on the case of interest with appropriate material properties and boundary conditions.

Before the application of the model for exploring TR mitigation strategies, the model is formulated based on experimental data from thermal runaway induced tests performed during

this project. Within the limitations of experimental measurement data and numerical results, the thermal model can be considered as validated and can be used to provide qualitative assessment of various mitigation strategies for prevention of thermal runaway.

II.3 Numerical Simulations for Thermal Runaway Mitigation Strategies

In this study, the thermal model is applied to study different mitigation strategies for a reference case of transport of 25 cells of type 18650 B type cell at 100% SOC packaged in a 5x5 configuration. A cell at the corner of the cell array is simulated to instantaneously go into thermal runaway and the heat propagation to neighbouring cells is investigated. The cases of investigation are with and without mitigation strategies. The location of corner cell as initiation cell is chosen as it represents a worst case scenario in terms of risk of abuse as well as in terms of thermal propagation behaviour. The worst case as corner location was determined from literature as well performed simulations. The initiation in the numerical simulation can be considered similar to thermal transience effects from nail-penetration where 1 cell's temperature suddenly increases.

The study is performed for a base case scenario with solid cardboard dividers between the cells to prevent thermal runaway propagation. The base case is presented in section II.3.1. Further mitigation cases are simulated with changes in appropriate parameters and properties from the base case as proposed improvements and the mitigation cases are presented in section II.3.2.

II.3.1 Base Case – Case 1

The base case chosen for this study is one in which 25 cells are transported in a corrugated cardboard of 5 mm thickness in a 5 x 5 cell configuration separated with 2 mm thick solid cardboard dividers as shown in Figure 11. The outer box is fully closed making the box with cells air-packed. The initial temperature of all cells are 20°C and the box is placed in an environment at 20°C with heat transfer coefficient of 5 [W/m²K].

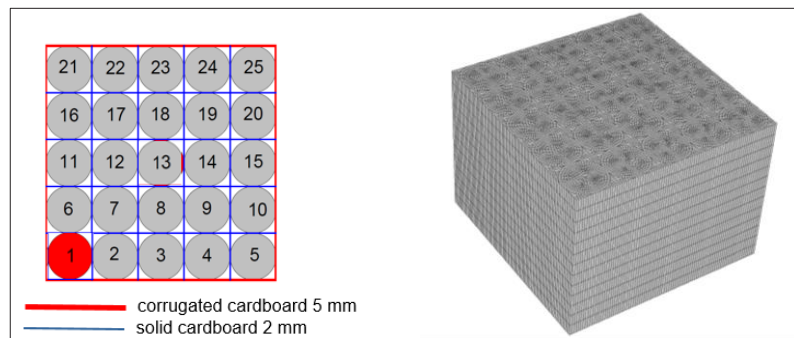


Figure 11: Base case for study of TR propagation mitigation strategies with computational mesh (right)

In this study, the temperature of the initiation cell suddenly increases from above cell onset temperature, starting from 180°C and reaches temperature of around 600°C in about 14 seconds (see Cell 1 in Figure 12). This heat is propagated to the neighboring cells and the focus is to study how far and fast is thermal runaway propagated to the neighboring cells. The thermal runaway properties for heat generation profile have onset temperature for pre-thermal runaway heat generation is 118°C and onset temperature for thermal runaway is 176°C. These input parameters are based on experimental tests. The heat generation power for pre-thermal runaway and

thermal runaway are 9.5[W] and 1320[W] respectively. These values correspond to Li-ion 18650 cell at 100% SOC as observed from the experiments. In the numerical model, the heat generation is initiated when any computational control volume within the cell reaches these onset temperatures.

The thermal properties of the cell as well as other materials input are presented in Table 2:

Table 2: Thermal properties of simulation materials

Thermal Properties	18650 B type Cell	Air	Corrugated Cardboard	Solid Cardboard
Cp [J/KgK]	918.8	1006	1700	1260
K [W/mK]	radial – 2.3 axial – 24.3	0.0242	0.065	0.07
Rho [Kg/m3]	2761.7	Ideal gas	200	802

The results for this base case are as follows:

The temporal evolution of maximum temperature in each of the cells can be seen in the following Figure 12. In this base case, all 25 cells go into thermal runaway before 45 minutes from the start of initiation of the first cell thermal runaway.

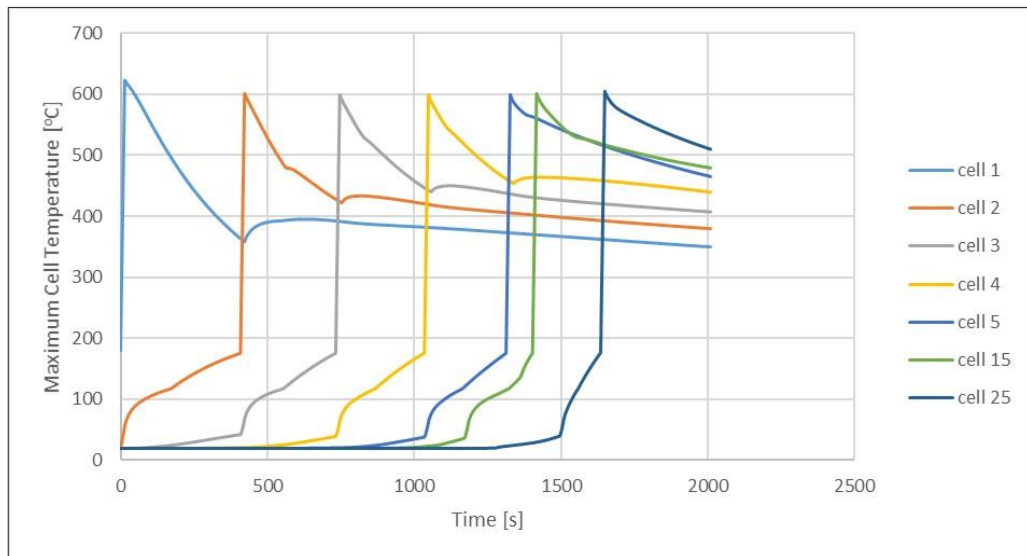


Figure 12: Base case cells maximum temperature temporal evolution of cells in the initiation row and farthest column

The heat is propagated from the initiation cell at position 1 to its adjacent cells first, i.e. cells 2 & 6 in Figure 11. Once they reach their onset temperatures they have heat generation and reach TR temperature. The temperature contour at mid-height of the cells can be seen in Figure 13.

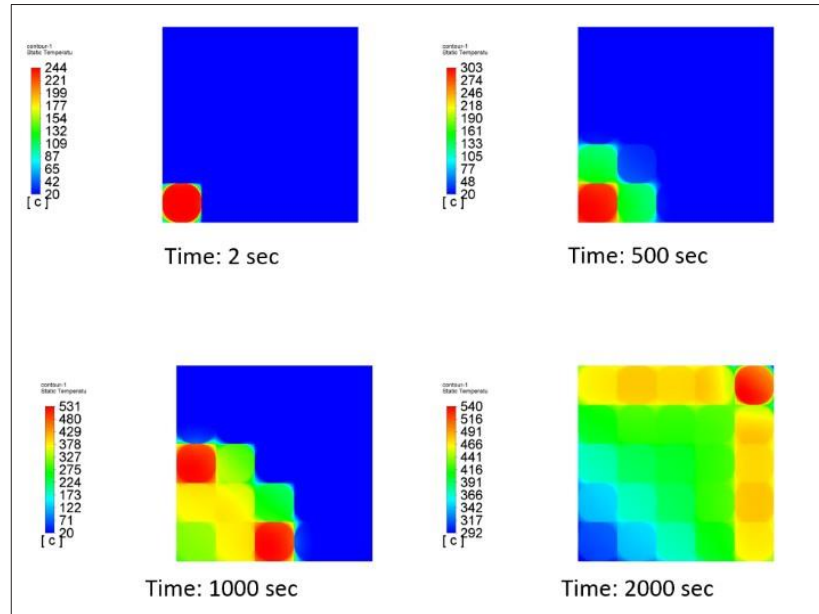


Figure 13: Temperature contour at mid-height level plane for base case at different times

From this base case, it can be understood that the current settings of dividers do not suffice to prevent propagation of thermal runaway. Another important observation from this is that once the adjacent cells to the initiation cells go into complete thermal runaway, it is highly likely that all the cells would go into thermal runaway. This is because the environment for each subsequent cell gets hotter and it increases the chances of thermal runaway for the neighboring cells. Thus, in the further cases cells adjacent to initiation cell are focused to check thermal runaway.

From the current setting of cell properties, environmental conditions and initial conditions, different mitigation strategies are proposed in subsequent section to prevent thermal runaway propagation.

II.3.2 Mitigation Cases

In the base case in previous sub-section, it is seen that thin solid cardboard separators of 2 mm thickness do not prevent propagation of thermal runaway for the above case conditions. Thus, it was of interest to find different methods for prevention of thermal runaway propagation for this case of box-cell configuration and initial conditions. In this sub-section several cases are examined to study the heat transfer propagation with different measures. In each case, everything is same as base case except for the parameter change of interest described for each case. The simulation temperature results are analysed with special focus on temperature of TR initiation cell and 2 cells adjacent to the TR initiation cell. The description of the cases and results are provided as follows:

Case 0

This case is a step back from the base case. In this case, there are no dividers separating the cells in the box. Thus, cells are placed in direct contact with one another while rest all of the conditions are exactly same as the base case. The temperature contour at mid-height of the cells for this case 0 can be seen in Figure 14.

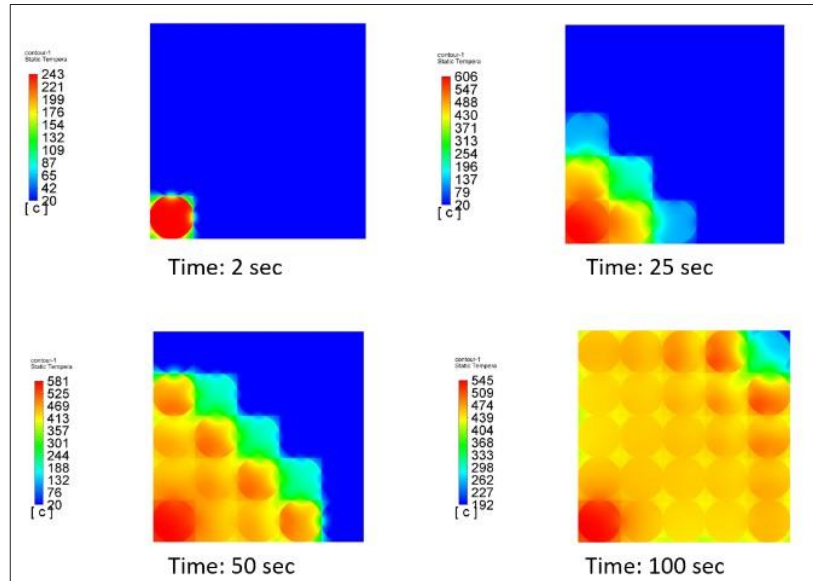


Figure 14: Temperature contour at mid-height level plane for case 0 at different times

As can be seen from Figure 14, TR propagates through whole box for Case 0 just as for Case 1. However Case 0 shows that without any dividers the propagation is much faster. All cells in the box undergo thermal runaway by around 100 seconds. This is 20 times faster than the base case which has thin cardboard dividers. Thus, it can be said that having thin dividers help reduce the rate at which TR propagation takes place. The temperature evolution profile for initiation cell and its adjacent cells TC2 and TC6 can be seen in the following figure:

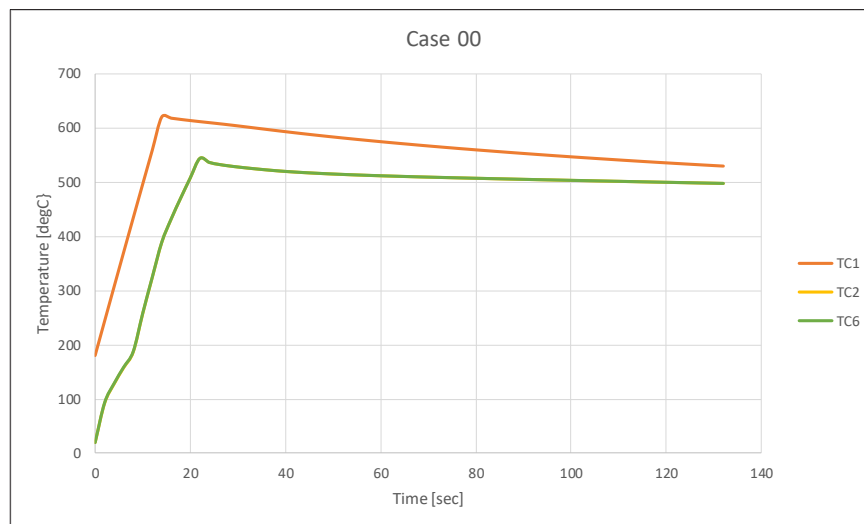


Figure 15: Temperature evolution for initiation cell and adjacent cells for Case 0

Once the initiation cell and adjacent cells undergo thermal runaway, the rest of the cells experience a hotter surrounding and undergo thermal runaway as well. As a next step to propose mitigation measures, thickness of cardboard separators are increased and simulations are performed as Case 2.

Case 2

In this case the thickness of the dividers is increased from 2mm to 4mm. The thermal properties of the cardboard are same as in base case. All other conditions are also kept exactly same as in the base case. The temperature contour at mid-height of the cells for this case 0 can be seen in Figure 16.

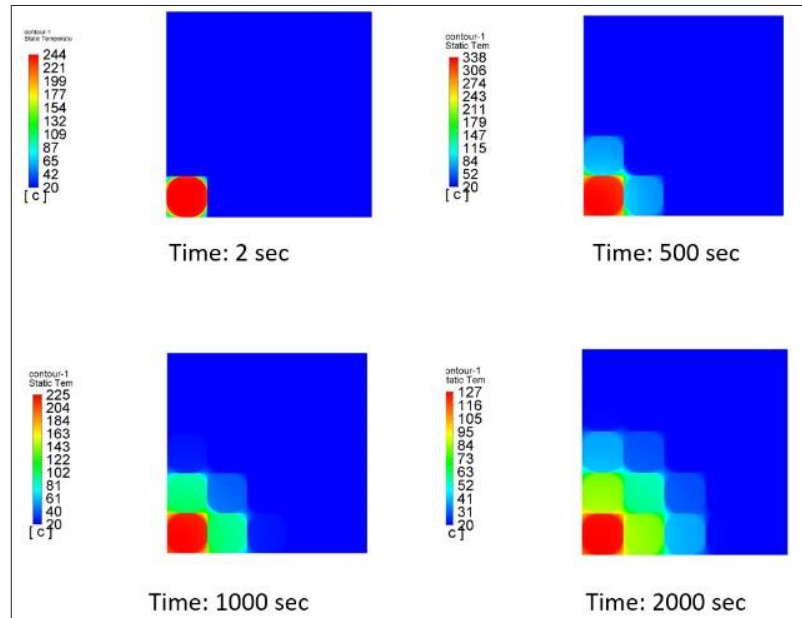


Figure 16: Temperature contour at mid-height level plane for case 2 at different times

As can be seen from the temperature contours of Case 2 simulation, cells adjacent to the initiation cell do not undergo thermal runaway. Thus, the other cells also do not undergo thermal runaway. This is with the increase in the thickness of separators which increases the effective thermal resistance between two adjacent cells. Also, the presence of thicker cell dividers adds more thermal mass to the system which reduces the rate of heat transfer from one cell to another. Thus, cell separators with 4mm thickness can prevent TR propagation while cell separators with 2mm thickness fail to do so.

The temperature evolution profile for initiation cell and its adjacent cells for the base case (case 1) and case 2 can be compared as follows:

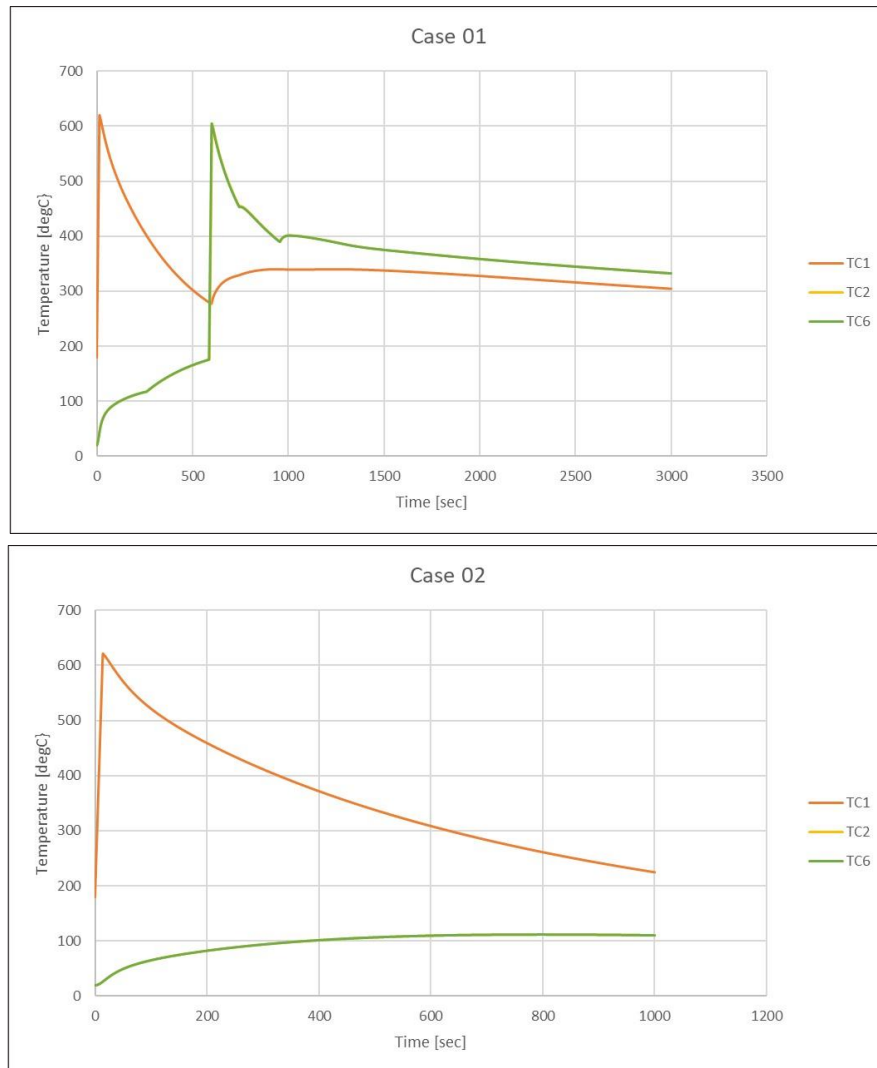


Figure 17: Temperature evolution for initiation cell and adjacent cells for Case 1 (top) and Case 2 (bottom)

As can be seen in the Figure 17, temperature of cells at position 2 and 6 never reach onset temperature and do not undergo thermal runaway. Thus, none of the other cells go into thermal runaway as the temperature of the initiation cell slowly reduces with time and heat dissipation. With this understanding, other possible measures for prevention of TR propagation can be seen in the subsequent cases.

Case 3

This case is same as the base case with the difference of external conditions outside of the cardboard box. For this case the effect of larger heat transfer coefficient and a colder environment is investigated. In this case 3 the heat transfer coefficient is increased from 5 W/m²K in base case to 50 W/m²K. Along with this the outer environment temperature is reduced from 20°C to 0°C. The temperature evolution profile for initiation cell and its adjacent cells can be seen in the following figure:

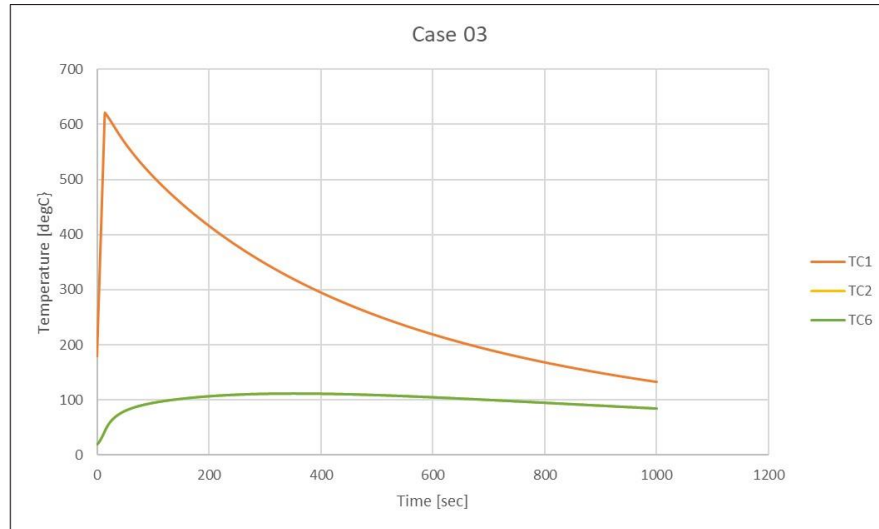


Figure 18: Temperature evolution for initiation cell and adjacent cells for Case 3

As can be seen from Figure 18, the temperature of the initiation cell reduces much faster due to larger heat dissipation rate to the environment. This is due to lower external temperature and larger heat transfer. Larger heat transfer is achieved for example by having forced convection by a fan blower. The temperature of the adjacent cells do not reach onset temperature values so they do not undergo thermal runaway, nor do the rest of the cells. Thus, having mechanisms to cool down the box transporting cells can be one of the mitigation measures to prevent TR propagation.

Case 4 and Case 5

In Case 4 and Case 5, the effect of presence of fiberboard instead of thin cardboard separators is investigated. In both these cases, the base case is modified from having 2 mm thick cardboard separators to 2 mm thick fiberboard dividers. Fiberboard is selected as it is a commonly used material in transportation boxes. The thermal properties of fiberboard input in the simulations are as follows : $C_p = 1700$ [J/KgK], $Rho = 750$ [Kg/m³], $K = 0.3$ [W/mK]. The rest of the properties and conditions for case 4 are same as in base case. For case 5, effect of presence of vermiculite instead of air in case 4 is investigated. The thermal properties of vermiculite input are as follows: $C_p = 920$ [J/KgK], $Rho = 100$ [Kg/m³], $K = 0.06$ [W/mK].

The temperature evolution profile for initiation cell and its adjacent cells for case 4 and case 5 can be compared as follows:

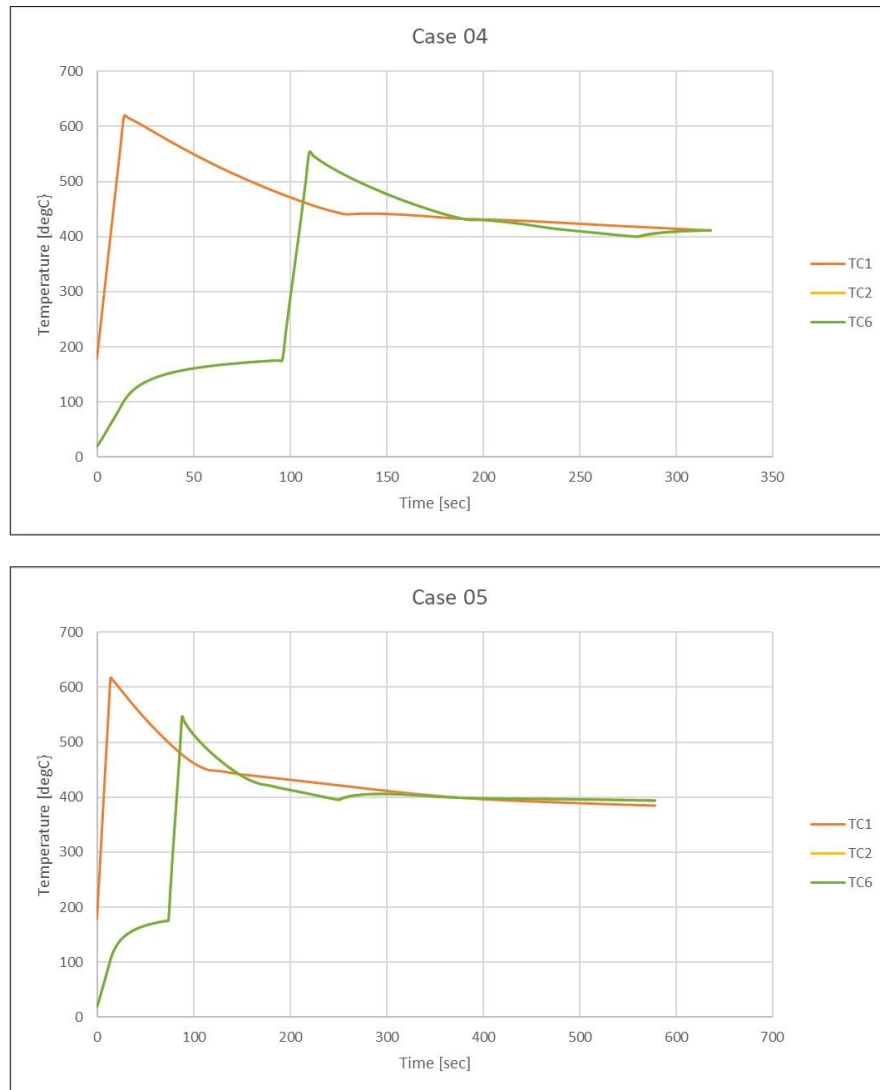


Figure 19: Temperature evolution for initiation cell and adjacent cells for Case 4 (top) and Case 5 (bottom)

For both the cases, Case 4 and Case 5 adjacent cells and further all the remaining cells undergo thermal runaway. Thus, having fiberboard of only 2mm thick is insufficient to prevent TR propagation in this case. The difference between presence of air and vermiculite is minimal for heat propagation. However it should be kept in mind that this is only in terms of heat conduction and propagation and the model does not capture the benefits which vermiculite has in terms of absorption of electrolyte and gases.

Case 6

In this case, the study of presence of fiberboard is extended from the previous cases and 4 mm thick fiberboard separators are used. All the other inputs are exactly the same as in Case 4. Since moving from case 1 (2mm) to case 2 (4mm) worked with solid cardboard separators to prevent TR propagation, it was of interest to see if it also works with fiberboard separators.

The temperature evolution profile for initiation cell and its adjacent cells can be seen in the following figure:

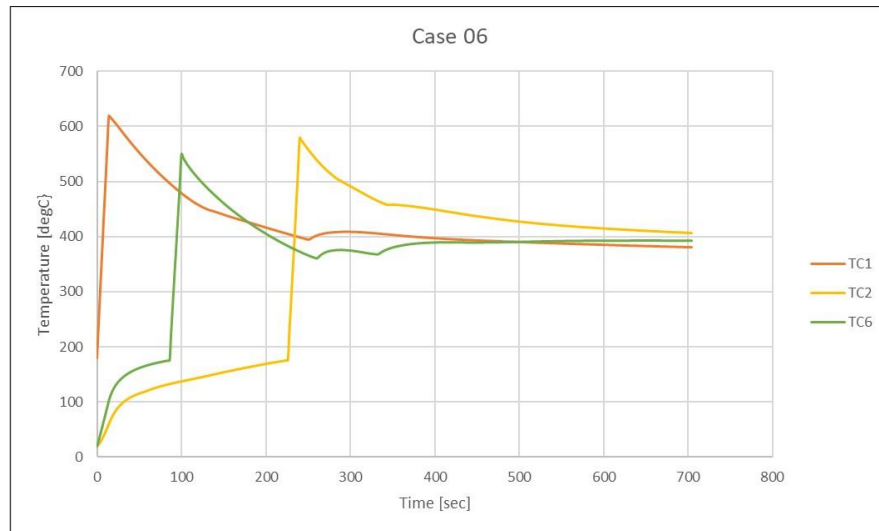


Figure 20: Temperature evolution for initiation cell and adjacent cells for Case 6

It can be seen from Figure 20 that for the case of using thicker fiberboard with the input thermal properties does not prevent propagation of thermal runaway. Both the adjacent cells went into thermal runaway and subsequently all the cells went into thermal runaway. Moreover, it was interesting that in this case compared to previous cases the temperature profiles TC6 and TC2 were not identical indicating heat propagation to be asymmetric. As this kind of output was not to be expected, thus, the use of fiberboard with the input thermal properties as mitigation measure, requires further investigation.

Case 7

In this case the effect of presence of vermiculite in combination of thick solid cardboard dividers is investigated. Thus, Case 7 is exactly same as case 2 - in which no TR propagation occurred, except of addition of vermiculite instead of air. Though the thicker cardboard prevents TR propagation in the simulations, gas and electrolyte release from cells in TR is not modelled in the simulations. Thus, it was of interest to observe what is the effect of gas and electrolyte observing material like vermiculite in heat propagation simulations. Results are plotted as for the other cases and it is seen that solid cardboard dividers of 4mm thickness along with vermiculite can prevent TR propagation.

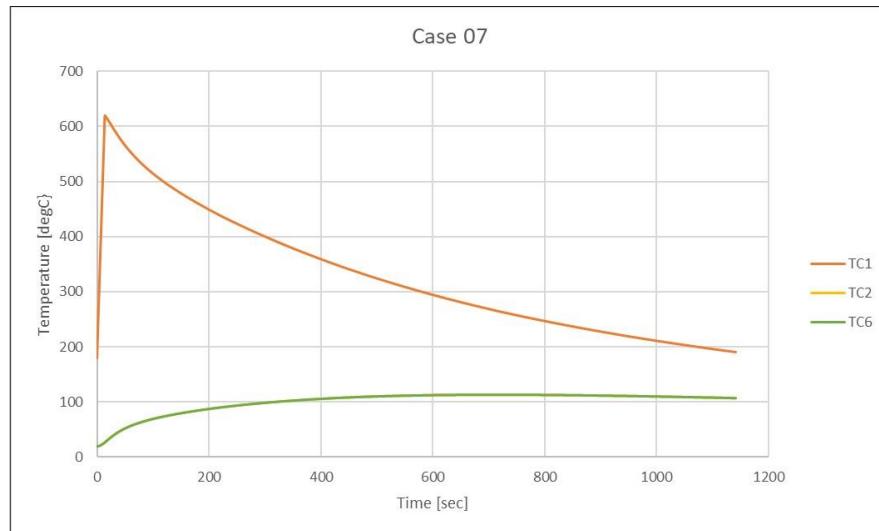


Figure 21: Temperature evolution for initiation cell and adjacent cells for Case 7

Case 8

This case is different from the previous cases as there are no cardboard solid dividers. Instead the whole box is filled with sand between the cells to prevent thermal runaway propagation. Presence of sand is investigated as other literature studies present sand as one of the possible options to prevent TR propagation. The gap between the two cells is kept as 2 mm and is considered to be filled with sand. The remaining properties, as well as the initial and boundary conditions are same as in Case 1. The temperature evolution profile for initiation cell and its adjacent cells can be seen in the following figure:

As can be seen from Figure 22, the adjacent cells do not undergo thermal runaway and so is the case for the rest of the cells in the box. This is because the packaging configuration and sand thermal properties lead to sufficient heat insulation for neighboring cells in the initial phase of the event and then ensure dissipation of heat such that onset temperatures are not reached for the adjacent cells. However, it should be noted that the cells do reach onset temperature of pre-thermal runaway self-heating. This indicates that the model of the configuration studied in Case 8 does not offer sufficient factor-of-safety to be sure of thermal runaway propagation prevention. A possible means of improvement can be to increase the gap between the adjacent from 2 mm to 4 mm or higher to ensure that there is no thermal runaway propagation.

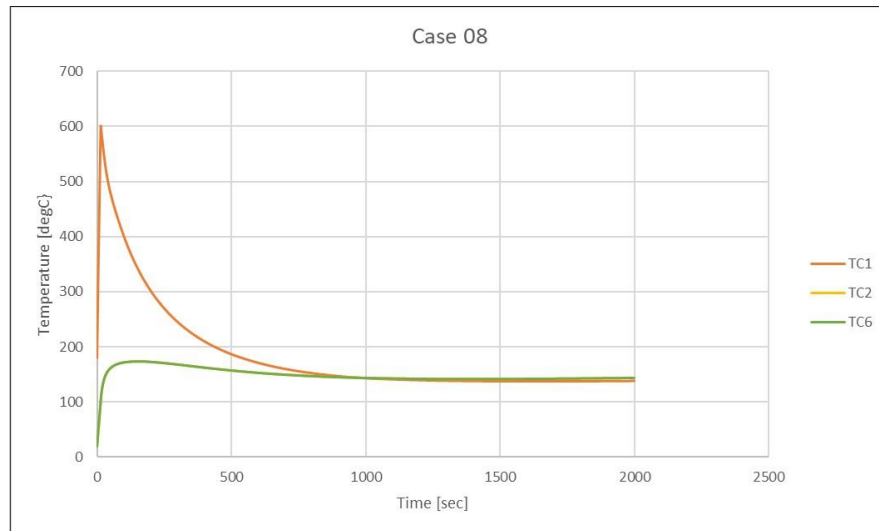


Figure 22: Temperature evolution for initiation cell and adjacent cells for Case 8

Case 9 and Case 10

All the previously reviewed cases mainly rely on the fact that the adjacent cells are sufficiently insulated from the initiation cell and the heat release out of the box is sufficient that the remaining cells do not undergo thermal runaway. While for Case 9 and Case 10, the main mitigation strategy is to have material with high thermal conductivity between the cells such that the heat is dissipated away from the initiation cell much faster and the adjacent cells do not reach onset temperatures. For these cases special boxes with materials covering the whole box and inter-cell region are used. Thus, they act as heat sinks when one cell goes into thermal runaway. The material used in case 9 is alumina (Al_2O_3) with following properties: $C_p = 3970$ [J/KgK], $\text{Rho} = 765$ [Kg/m^3], $K = 36$ [W/mK]. For case 10 graphite is used instead of alumina with the properties as follows: $C_p = 850$ [J/KgK], $\text{Rho} = 1600$ [Kg/m^3], $K = 160$ [W/mK]. It can be observed that the thermal conductivity for these materials is more than 100 times higher than for the previous cases. The gap between the adjacent cells is fixed to be having 4 mm made of the respective dissipative material while the outer box is made with same material having 5 mm thickness. From the temperature evolution profile for initiation cell and its adjacent cells for Case 9 and Case 10, it can be seen that the temperature of the initiation cell is reduced very fast and within 100 seconds the risk of TR propagation is eliminated. The temperature evolution for the 2 cases vary due to differences in thermal properties but both act as good heat sinks and provide extremely efficient measure for preventing risks of thermal runaway propagation. This observation, though valid for this setup of small number of cells in a box, when the number of cells would be much more and in a different configuration like boxes piled up on one another; further numerical and experimental investigations would be necessary to provide optimal solutions.

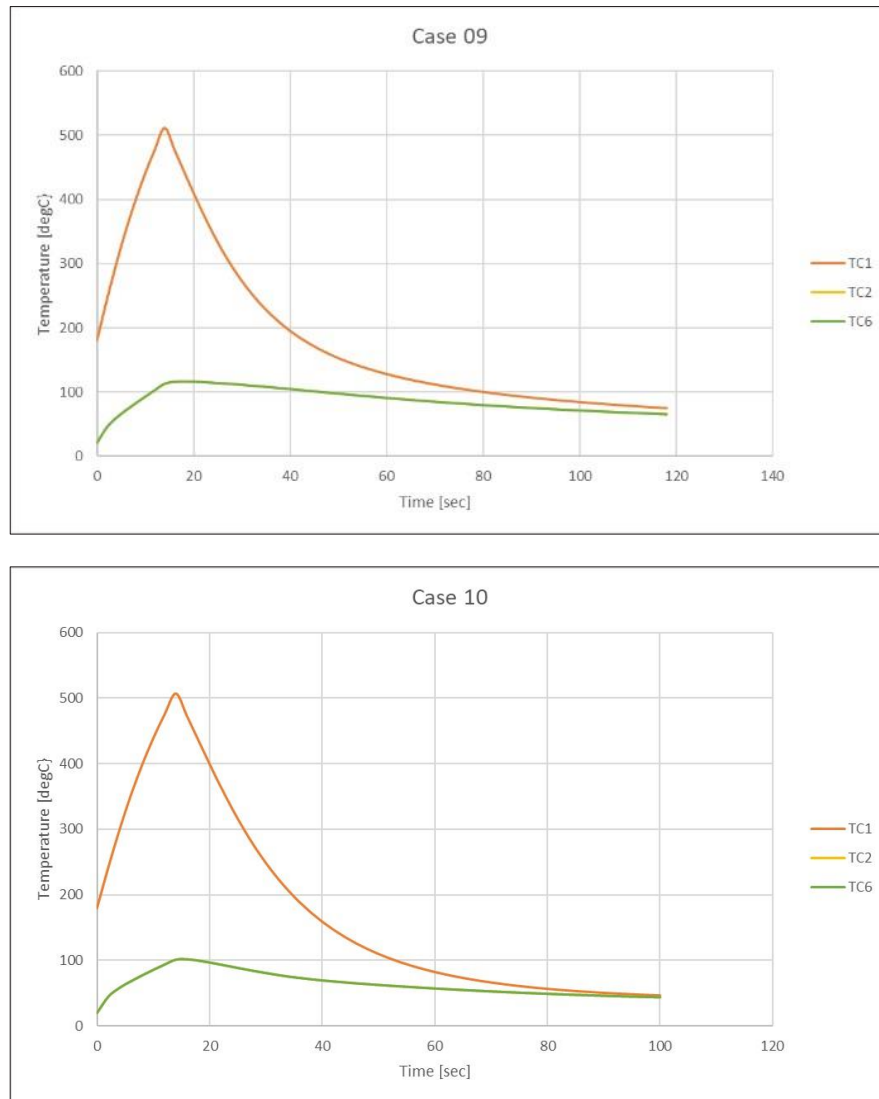


Figure 23: Temperature evolution for initiation cell and adjacent cells for Case 9 (top) and Case 10 (bottom)

II.4 Results Summary and Conclusion

The thermal numerical model provides good understanding of heat propagation from a TR initiation cell to remaining cells in a box. It is also used to study the effect of different mitigation strategies for prevention of thermal runaway propagation.

From different cases analysed, the following results can be summarised:

1. Thicker cardboard separators are required to prevent TR propagation.
2. Box placed in a colder environment with high heat transfer coefficient can prevent TR propagation.
3. Thermal conductive fibreboard needs more thickness for TR prevention in comparison to less conductive cardboard.

4. Presence of vermiculite instead of air is a good option when used with cardboard separators. In addition it can absorb any liquid that would spill from the cell after venting.
5. Container filled with sand can prevent TR propagation when the cells are kept with sufficient separation distance between them.
6. Thermally conductive holder boxes made from graphite or alumina helps in thermal dissipation and prevents TR propagation.

The summary of results of all cases presented in section II.3 is provided as follows:

Case Name	Mitigation Strategy	Description	Result
Case 00	None	No separators	TR for all cells
Case 01	Thin cardboard separators BASE CASE	Base Case of 5x5 with TR cell at a corner	TR for all cells
Case 02	Thicker cardboard separators	Base Case with 4mm separator thickness	no TR propagation
Case 03	Colder environment with higher h	Base Case with more convection heat transfer: h=50, T=0	no TR propagation
Case 04	Thin fiberboard separators	Base Case with 2mm fiberboard separators	TR for all cells
Case 05	Thin fiberboard + vermiculite	Base Case with 2mm fiberboard separators & vermiculite	TR for all cells
Case 06	Thicker fiberboard	Base Case with 2mm fiberboard separators	TR for all cells
Case 07	Thicker cardboard + vermiculite	Base Case with 4mm separator thickness & vermiculite	no TR propagation
Case 08	Sand filled cardboard box	Base Case sand filled with cells at 2mm separation	adjacent cells vented but no TR propagation
Case 09	Alumina full container	Base Case layout in Alumina container with 4mm cell separation	no TR propagation
Case 10	Graphite full container	Base Case layout in Graphite container with 4mm cell separation	no TR propagation

Thus, from these possibilities in the above cases, appropriate thickness of dividers, material for filling and holding of the cells can be selected. Furthermore, it should be noted that the success or failure from the above simulation cases is for one type of thermal runaway i.e. one cell suddenly goes into TR while the other cells are at room temperature. This can be considered similar to the case of a sudden nail penetration for the corner cell. If the initial condition and initiation conditions are changed then some measures can become more effective or less effective depending on the case at hand.

While the model provides good basis for qualitative assessments, it should be noted that the thermal model has several limitations. The simulations can be used to predict well the heat propagation by conduction and radiation. However a thermal runaway event has other critical effects, such as the release of toxic gases, flames, etc. which are not addressed in the current model. The model currently utilizes only thermal properties of the materials to predict heat propagation. Thus, the benefit of vermiculite, for example, compared to just air is not highlighted by this model. Another consideration which is important is that for dividers and boxes made from cardboard it would be better to have flame-resistant coating as the temperatures reach up to 600°C while flame point of most carboards is around 450°C. While the model predicts temperatures as high as 600°C, it does not simulate ignition of the packaging.

For the optimization of design solutions that could mitigate the effects of a TR to acceptable levels, it would be preferred that the model is supported with more experimental data. However, the results from the model highlight trends and principles that could be used as a reference to develop mitigation strategies for prevention of thermal runaway propagation.

Chapter III: Testing of Additional Mitigating Measures on Packaging Level

The present chapter describes the testing activities that were carried out in the context of Task 2, using certain mitigations identified in Task 3. The testing was designed to identify whether the physical results of testing would match those of the thermal modelling (Chapter II).

The test plan was as follows in Table 3. Physical tests were carried out as described below (labelled as “TestXX”). These can be differentiated from the simulated runs which are labelled as “CaseXX”.

Details of the test reports are included in separate and individual reports.

Table 3: Test plan of additional mitigation measures

Modelling Case N°	Test N°	Cells SOC (%)	Mitigation
Reference test	34	30	None
Base case (no mitigation)	35	100	None
Case 04	36	100	2mm fibreboard divider
Case 02	37	100	4mm fibreboard divider
Case 08	38	100	2mm fibreboard divider + Sand between the cells

III.1 Brief description of the test procedure

The testing was carried out using a setup based on the reduced cell configuration test method specified in the draft SAE AS6413 (version November 2018). The test chamber and all equipment were built based on the description in the draft standard.

A total of 8 cells were used during this testing. 30 dummy cells made of aluminum were arranged around these to act as placebos. They were arranged as shown in Figure 24: Thermal runaway initiation test setup. (PC stands for Periphery Cell; IC for Initiation Cell; and t for thermocouple) shown below. The cell skin temperature was recorded and thermocouples were placed at mid-height of the cell and distributed as shown in Figure 24.

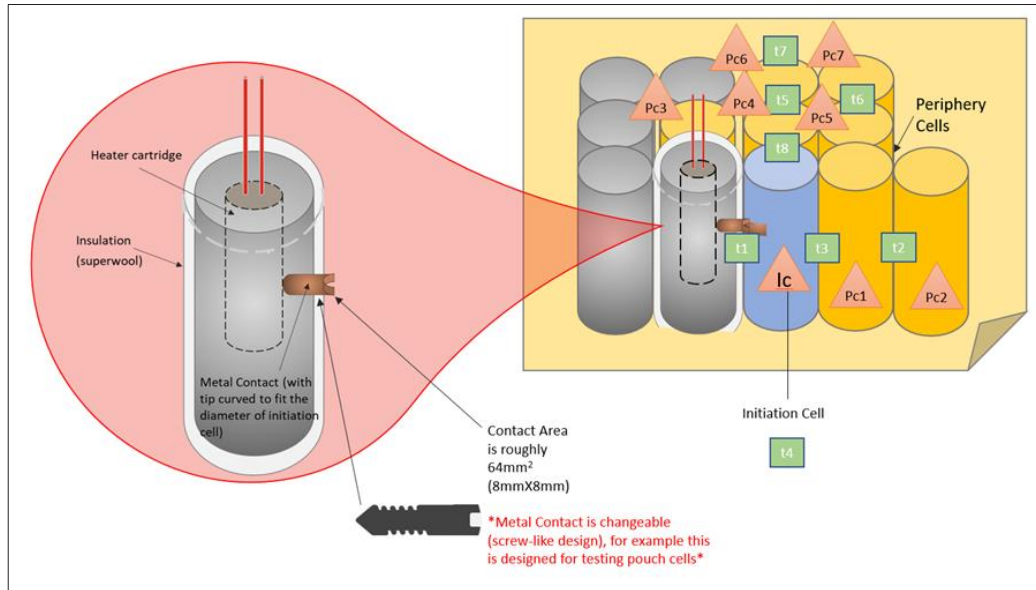


Figure 24: Thermal runaway initiation test setup. (PC stands for Periphery Cell; IC for Initiation Cell; and t for thermocouple)

Temperatures were measured by thermocouples attached to a data logger. Temperatures can be considered accurate for the positions shown in figure 24 only up to the point of thermal runaway, visible in graphs from temperature spikes. After thermal runaway there can be no certainty on the temperatures recorded due to damage to thermocouples, or dislodgement of thermocouples and/or cells contained within the test pack.

The testing was carried out using a heating ramp rate target of 5°C/min. In all tests ambient temperature varied between 0°C and 9°C. In all tests the cells were placed inside a UN approved fibreboard boxes bearing the mark 4G/X13/GB6232. Information on this type of packaging can be found on the VCA DGO (the UK competent authority for UN marking) database and is reported in Figure 34.

6232	4G	Current	2023	4G/X13/S/**/GB/6232	Lithium batteries in plastics bags	AIR SEA CONTAINERS LTD
------	----	---------	------	---------------------	------------------------------------	------------------------

Figure 25: GB6232 certification status

III.2 Test Results

A summary of the results obtained in the testing campaign is reported in the present chapter. Detailed test results can be found in individual test reports.

III.2.1 Reference test: no mitigation measure using cells at 30% SOC

This test was designed to have establish a baseline considering a packaging configuration in which no mitigation measure is introduced and where the cells are at 30% SOC. As expected from other similar tests performed in Task 2, only the initiation cell went into thermal runaway. The packaging was locally damaged resulting in a failed test as per the draft SAE AS6413 standard, as shown in figure 26 below.

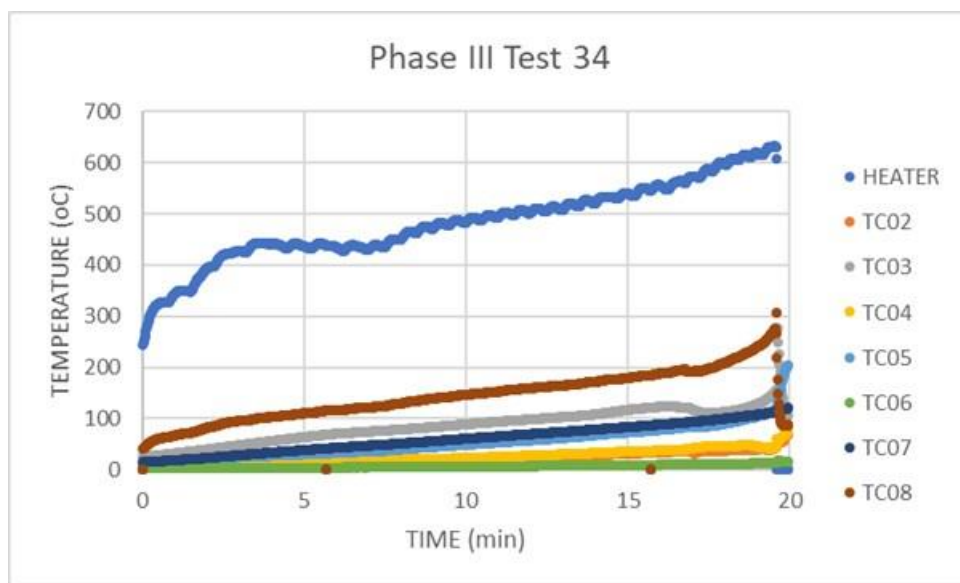


Figure 26: Reference test results using cells at 30%SOC

III.2.2 Base case: no mitigation measure using cells at 100% SOC

Test 35 was a repeat of test 34, but using 8 cells at 100%SOC to provide the worst case scenario. From the thermal modelling (Case00) it was expected that all 8 cells would enter thermal runaway.

The ambient temperature was not as modelled in Case00, with test 35 carried out at an ambient temperature of 2°C. Based on the output given by the thermal modelling, this should reduce the impact of the thermal runaway event, and therefore it was expected that not all 8 cells would enter thermal runaway.

As shown in Figure 27, two cells, the initiation and the cell Pc1, entered thermal runaway, with another cell (Pc5) venting.

This made the testing more comparable to Case03 which showed no thermal runaway propagation.

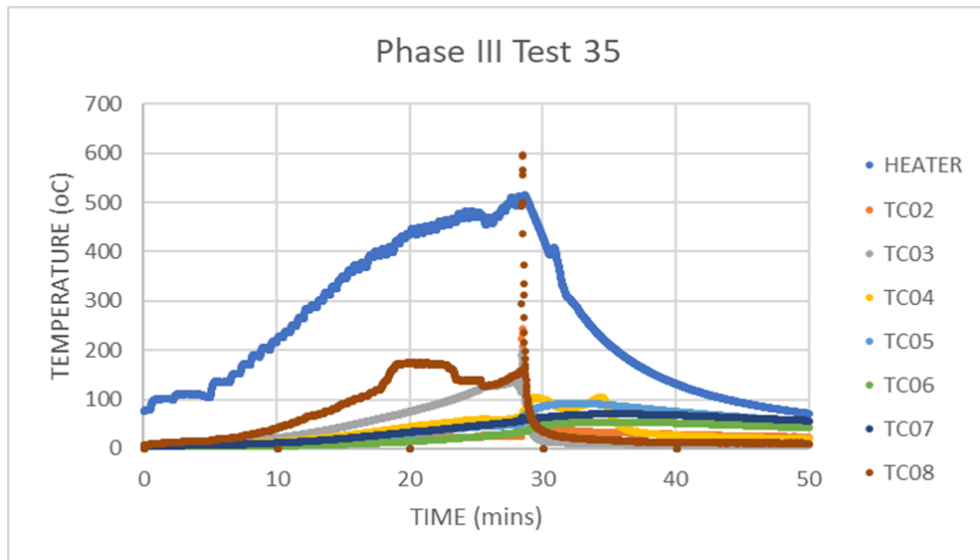


Figure 27: Reference test results using cells at 100%SOC

III.2.3 Experimental assessment of Case 4 modelling results

Test 36 was carried out using cells at 100% SOC, separated by 2 mm fibreboard dividers in a ‘reduced cell configuration’ setup (see Figure 28). This test configuration is similar to Case 04 modelling, where results shows that all cells entered thermal runaway. However the results plotted in Figure 29 shows that ‘only’ two cells went into thermal runaway (the initiation cell and one of the neighbouring ones).

It’s worth to notice that like test 35, this test was carried out at a low ambient temperature (3°C) and therefore differences with the modelling results might be expected. Due to the change in ambient temperature, difficulty was experienced in controlling the ramp rate of the heater, leading to a non-linear increase in temperature. From previous testing this would be expected to cause a more extreme thermal runaway event. The heat transferred from the heater to the initiation cell was a parameter which was difficult to control throughout the testing, however the temperature increase rate was still in the middle of the range prescribed by SAE AS6413.

Considering the above, the 2 mm dividers might have made a small difference to the severity of the result. The packaging was destroyed as shown in Figure 30.

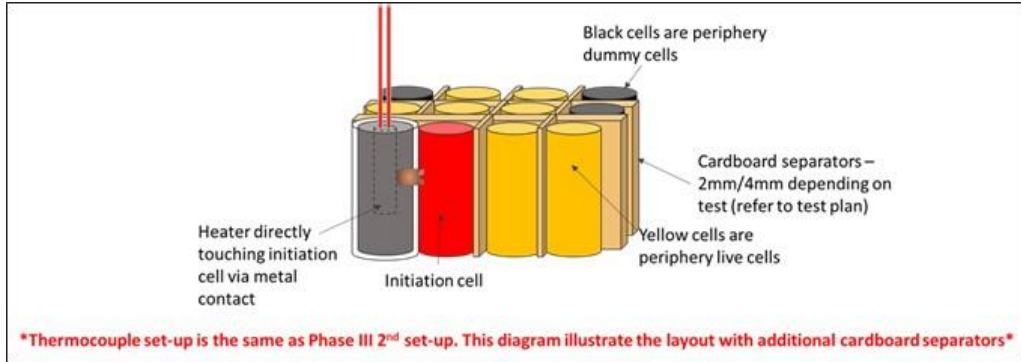


Figure 28: Test setup for test 36

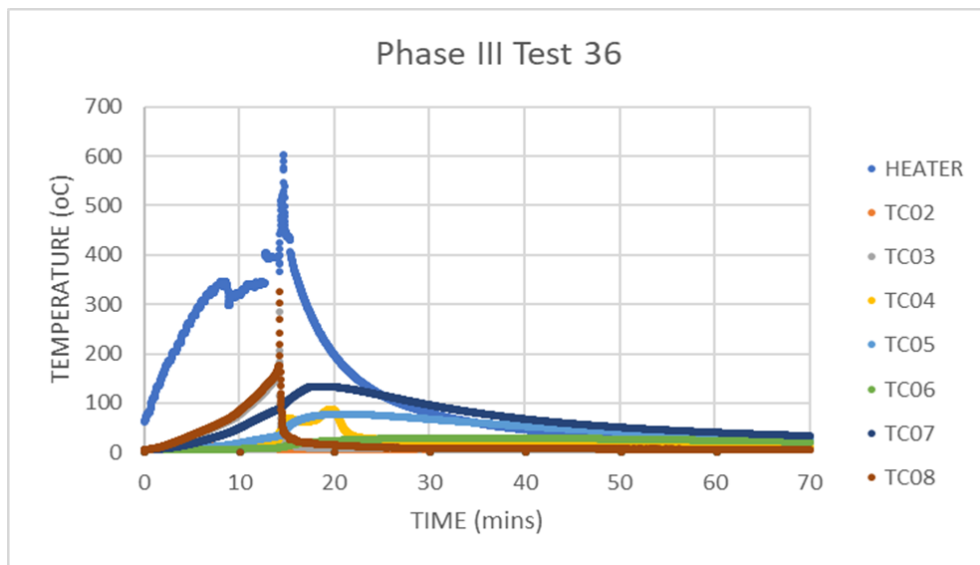


Figure 29: Experimental results of Case 04 modelling scenario



Figure 30: Picture of the package after experimental test of Case 04 modelling scenario

III.2.4 Experimental assessment of Case 2 modelling results

In Test 37, 4 mm thick fibreboard dividers were used instead of 2 mm thick dividers. It was expected, based on modelling, that propagation and severity of thermal runaway would be reduced in this case. Ambient temperature was 3°C when the test started.

However, this turned out to be the most severe result of the D3b testing, as shown in Figure 31 and Figure 32.

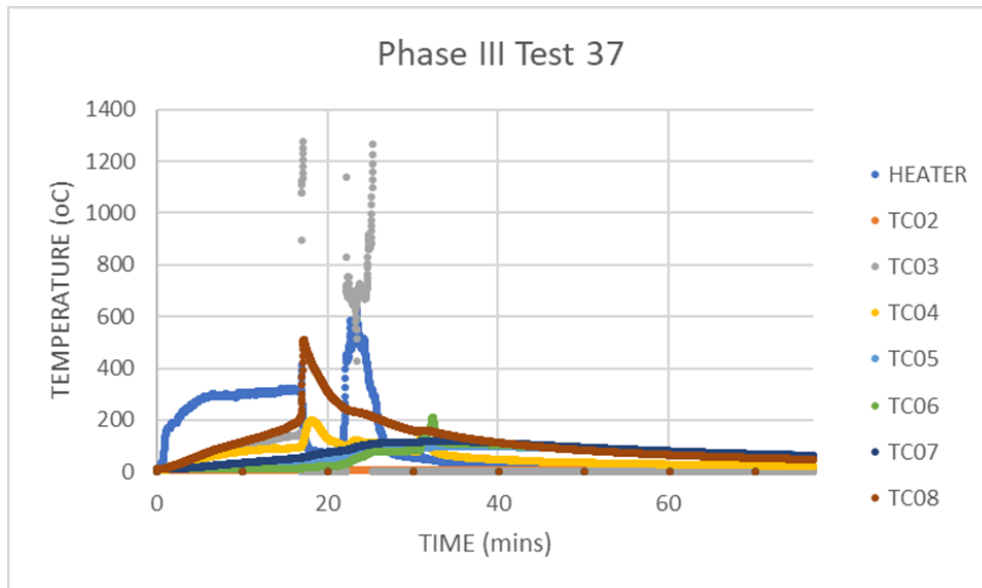


Figure 31: Experimental results of Case 02 modelling scenario



Figure 32: Picture of the package after experimental test of Case 2 modelling scenario

Following the initial thermal runaway of the initiation cell, it appeared that propagation had been prevented. However, following the initial thermal runaway the box was observed to catch fire. Approximately 7 minutes after the fire was observed to start the rest of the cells started to enter thermal runaway with the end result being a completely destroyed package. From the graph data it is observed that following the initial thermal runaway of the initiation cell, only Pc4 (shown by TC5) went into thermal runaway, however this was not the case. The data recorded is deemed inaccurate due to the dislodgment of thermocouples during the initial thermal runaway.

It is likely the 4 mm dividers did the job envisaged by the thermal modelling (Case02), however the additional packaging material, in close contact with the initiation cell, might have acted as a fuel source and allowed the package to fully catch alight (which had not been seen on other tests), leading to the complete destruction.

III.2.5 Experimental assessment of Case 8 modelling results

The final test was to look at Test 36, but with sand included to fill in the remaining spaces between the cells.

The thermal modelling showed no thermal runaway propagation should take place. The actual results are shown in Figure 7.

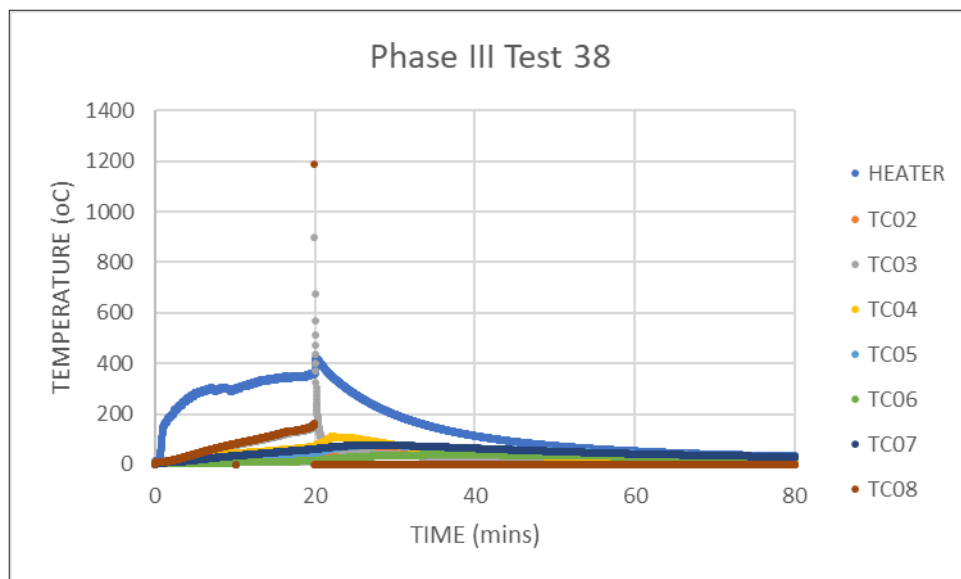


Figure 33: Experimental results of Case 08 modelling scenario

As can be seen in the figures, only the initiation cell entered thermal runaway. No venting, or voltage loss was observed in the other cells. The result was that only a small rip was observed at the top seam of the package, with otherwise no damage, as shown in Figure 34.



Figure 34: Picture of the package after experimental test of Case 08 modelling scenario

While the test was a fail against the SAE AS6413 draft protocols, it was a marginal fail which could be fixed by using better tapes. The test results confirmed the outcome predicted by the thermal modelling.

III.3 Conclusion

The results of this chapter showed that it is possible to undertake thermal modelling to closely align with physical results obtained during AS-6413 testing. The testing also highlighted that small differences in the environment (e.g., temperature) can have an appreciable influence on the test results.

Chapter IV: Full scale test on external fire impact mitigation

IV.1 Introduction

While Task 2 mainly addresses the scenario in which a thermal runaway event occurs inside the package in which cells /batteries are (**internal** fire), Task 4 evaluates scenarios in which lithium cells/ batteries are involved in a cargo fire event (**external** fire).

The purpose of the full scale fire tests conducted within the scope of the Sabatair project was to assess the effectiveness of state-of-the-art fire cargo compartment built-in fire suppression systems in controlling the severity of a cargo fire potentially involving high quantities of cells at high state of charge, with and without the protection offered by additional mitigation measure such as Fire Containment Covers (FCCs).

A detailed description of the test procedure and results can be found in deliverables D4a and D4b.

IV.2 Brief description of the test setup and procedure

The test chamber has a volume of 56.6 m³ (see Figure 34) and is in accordance with the Minimum Performance Standard for Aircraft Cargo Compartment Halon Replacement Fire Suppression Systems [2].



Figure 34: Photograph of the fire test chamber

This Minimum Performance Standard published by the Federal Aviation Administration (FAA) contains a test procedure that simulates a bulk-load fire scenario by using cardboard boxes filled with shredded paper (see Figure 35). The MPS test setup was followed as close as possible but was adapted to take into account the objectives of Task 4, in particular the presence of boxes containing lithium cells/batteries the need to install a FCC in conjunction with a pallet.

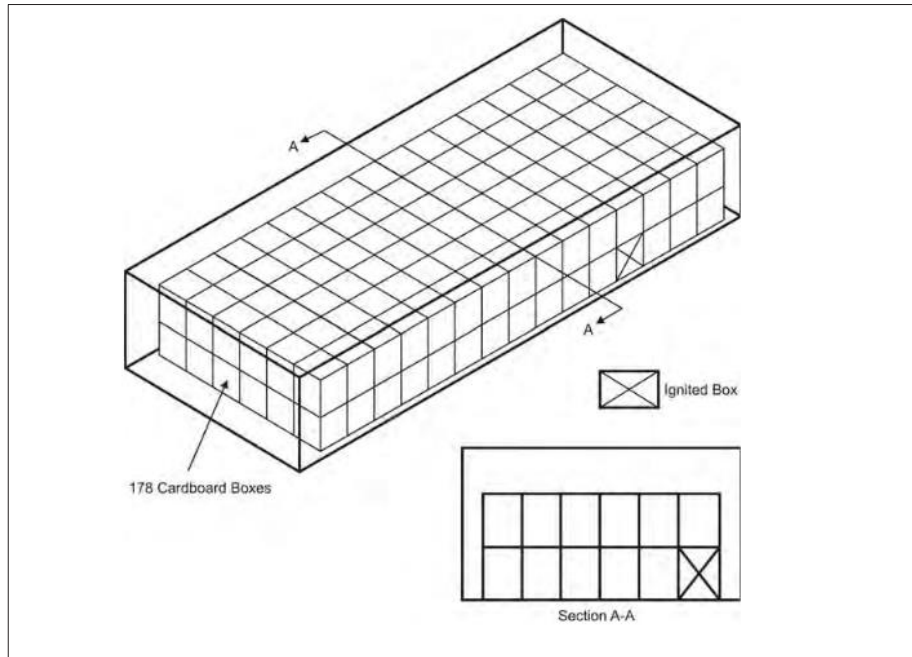


Figure 35: Arrangement of Cardboard Boxes as fire load for the Bulk load fire test of the Minimum Performance Standard for Aircraft Cargo Compartment Halon Replacement Fire Suppression Systems (2012 Update)

Cardboard boxes filled with shredded paper are used as fire load (see Figure 35). One box is ignited in by means of a resistance wire heater.



Figure 36: Cardboard Box filled with shredded paper acting as fire source for the external fire test (left) – Cardboard Box arrangement in the test compartment (right)

The cells tested were standard 18650 Lithium ion cells. More details related to the cell selection are available in deliverable D2a. Two different cell brands (Figure 37 and Figure 38) have been selected to represent a random mix. The cells underwent successfully the UN38.3 tests. The technical specification of the cells are as follows:

Brand	B type	C type
Nominal Capacity	3500mAh	3500mAh
Chemistry	LiNiCoAlO ₂	LiNiCoMnO ₂
Dimensions	18650	18650
SOC	50%	50%

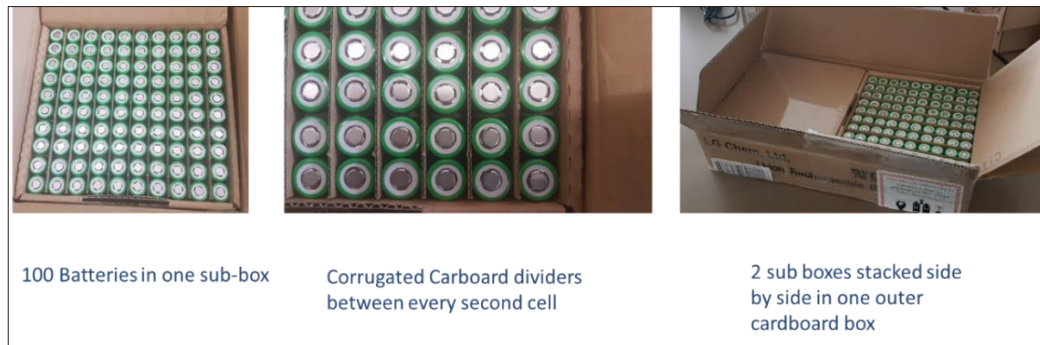


Figure 37: Type B cell packaging.



Figure 38: Type C cell packaging.

The arrangement of the cardboard boxes was not exactly the same as specified in the MPS [2]. Deviating from the MPS arrangement, some cardboard boxes were placed on a pallet to allow installation of the Fire Containment Cover. In total, 800 cells were involved per test with 600 cells at 50%SOC and 200 cells at 100%SOC.

They were arranged in a way that they would receive as much energy from the ignition source as possible. The cells were arranged in 2 layers, corresponding to the layers of cardboard boxes filled with shredded paper. The top layer of the cells was supported by a metal structure to prevent the cells from dropping when the cardboard boxes become unstable during the burning process (see Figure 39).

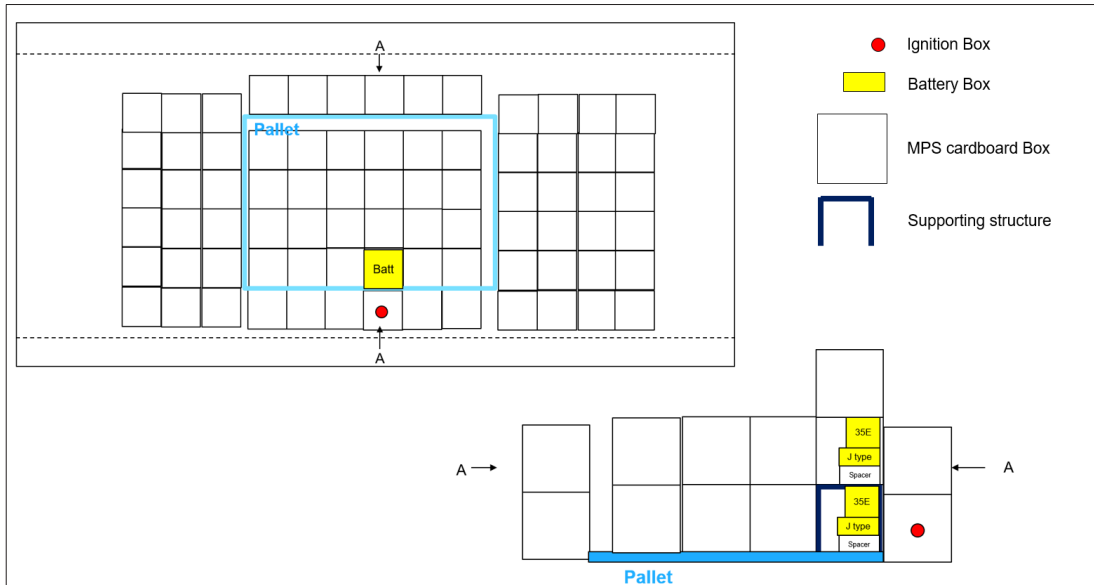


Figure 39: Arrangement of cardboard boxes for the full scale fire test

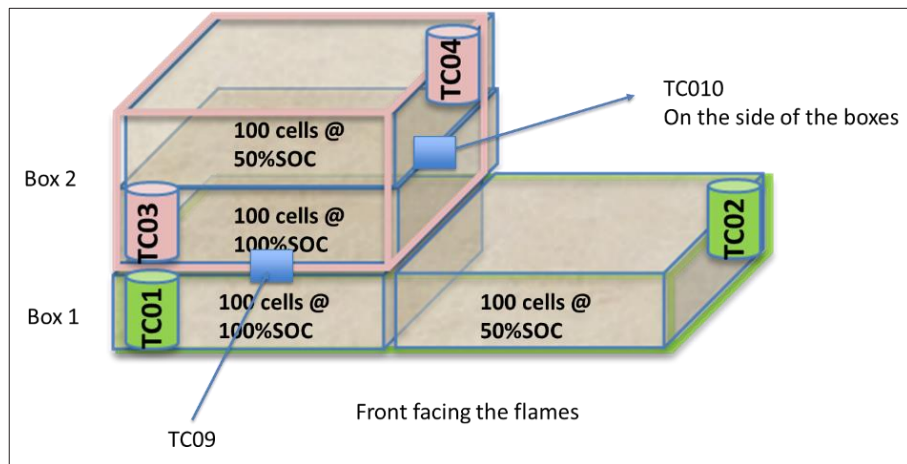


Figure 40: Position of the thermocouples of the cell packs located directly on the pallet. The blue markers indicate thermocouple location outside of the outer cardboard boxes. The pink/green positions indicate thermocouple locations directly on the respective cells (green= B type and pink=C type) The graphics also indicates the State of Charge

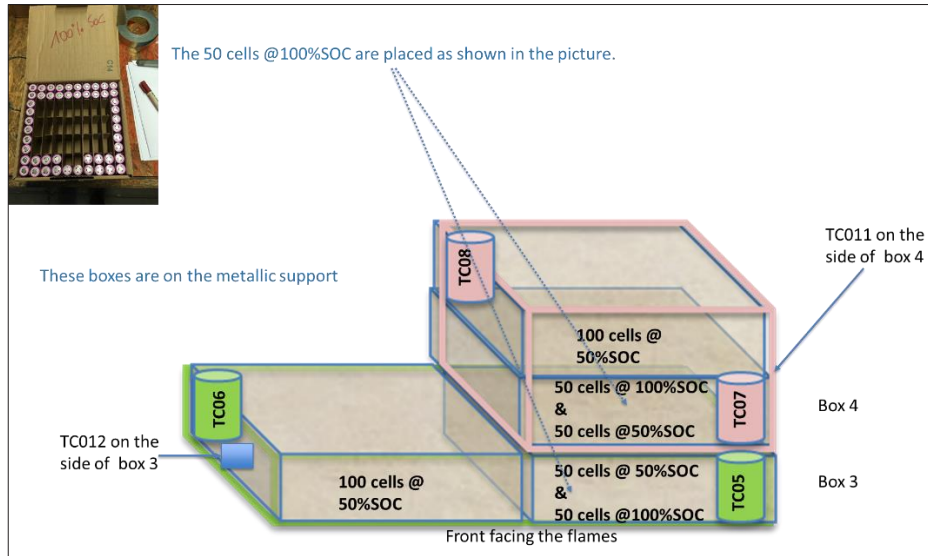


Figure 41: Position of the thermocouples of the cell packs located on the metallic support. The blue positions indicate thermocouple location outside of the outer cardboard boxes. The pink/green positions indicate thermocouple locations directly on the respective cells (green= B type and pink=C type). The graphics also indicates the SoC. In a mixed configuration with 50 cells at 50% SoC and 50 cells with 100% SoC, the cells with 100% SoC were located at the outer rim as indicated in the upper left image.

IV.3 Test Results Summary

The test results are summarized in the following set of charts.

1. No Halon 1301 discharge:

Several temperature measurement points directly on the cells show readings in the order of magnitude of 700°C. Although the exact amount of involved cells was not counted, it was estimated that around 100 cells went into thermal runaway. The cells located towards the ignition box were involved first.

The test was stopped after approximately one hour. Cells were continuously involved during this time period. Thermal runaways obviously propagated throughout the packaging boxes without a tendency that this process would be interrupted.

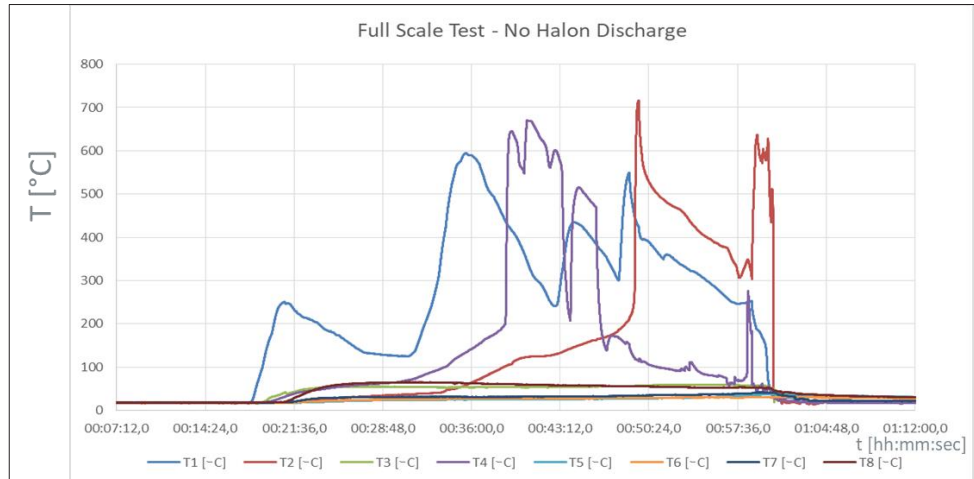


Figure 42: Temperatures during the external fire test without fire suppression



Figure 43: Impact on Cells after the test without fire suppression

2. Halon Fire Suppression

The aircraft Halon Fire Suppression system was activated as soon as the temperature reading at the level of any of the cells exceeded 145 °C. This trigger criterion deviates from the trigger criterion in the MPS test [2]. The MPS requires a temperature of 93,3°C (200°F) at the ceiling level of the compartment. At the time this criterion was reached, the temperature at cell level was far from being critical. The thermal runaway was finally initiated and propagated between several cells.

The Halon suppressed further propagation of thermal runaways. In the temperature profile recorded during the test (Figure 28), it can be observed that one reading reaches values that indicate thermal runaway. This reading is limited to a single high peak. As the test progressed, no further temperature rise was observed at any measurement point. All thermal runaway processes occurred before the Halon discharge.

Although the exact amount of involved cells was not counted, it was estimated that around 30 cells went into thermal runaway.

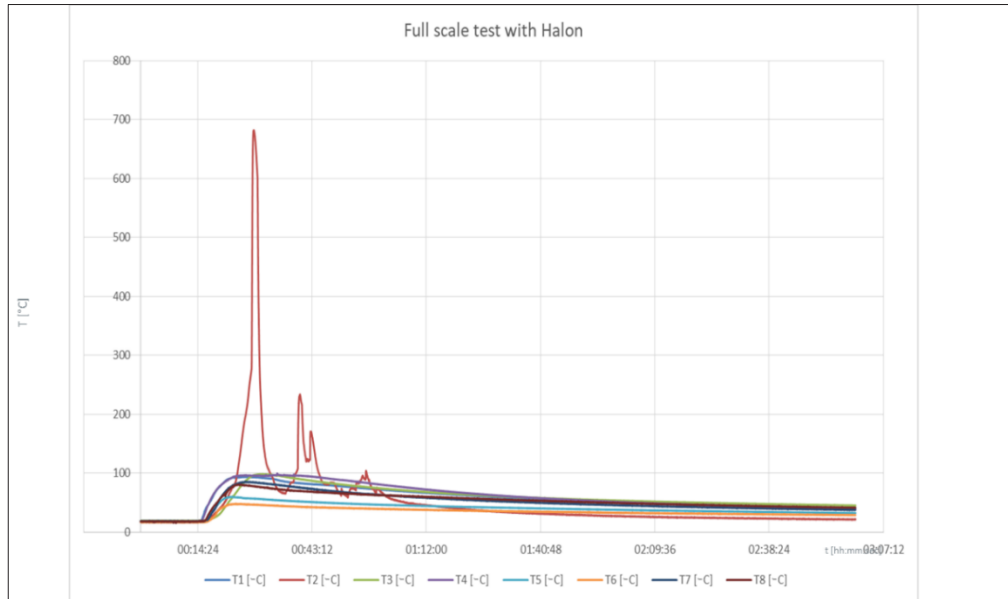


Figure 44: Temperatures during the external fire test with fire suppression



Figure 45: Impact on Cells after the test with fire suppression

3. Halon Fire Suppression and Fire Containment Cover

Adding the fire containment cover to the test setup showed further improvement, resulting in the fact that the fire impact was reduced significantly.

The trigger criterion for the Halon discharge was set to replicate the evolution of the previous test in terms of timing. The time from reaching a threshold temperature of 93.3°C for the Halon discharge was identical to the test previously conducted without a fire containment cover in order to ensure consistent conditions in the chamber between the two tests.

The maximum temperature observed during this test was 145°C in a location close to the ignition box. Analyzing the impacted cells after the test showed that only one corner of one box was affected.

The fire containment cover itself showed burn marks but was not burnt through. However, the temperature behind the cover was high enough to cause burn marks on cardboard boxes covered by the fabric of the cover.

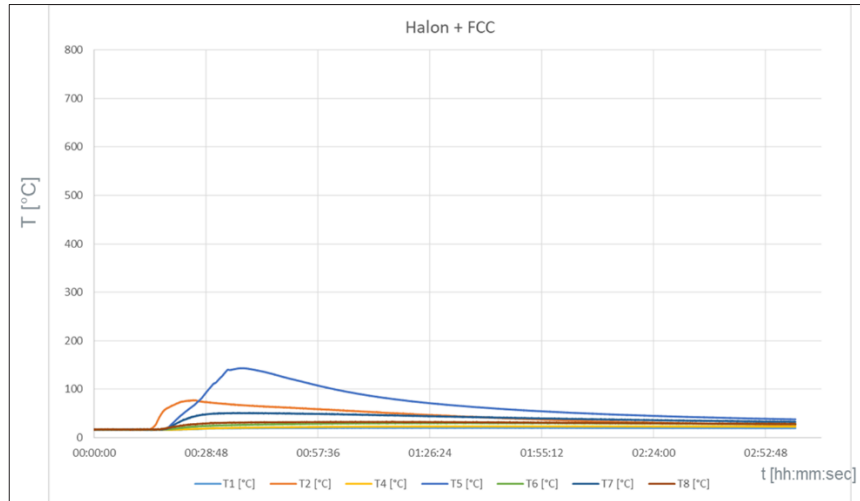


Figure 46: Temperatures during the external fire test with fire suppression and Fire Containment cover



Figure 47: Fire Containment Cover within cardboard boxes before the test



Figure 48: Fire Containment Cover after the test



Figure 49: Impact on Cells after the Test with Fire Suppression and Fire Containment Cover

For a more detailed description of the test results, refer to deliverable D4b.

IV.4 Conclusions

Two main conclusions are derived from the test results:

- A state-of-the-art Class C cargo compartment built-in fire suppression system inhibited propagation of thermal runaways for the tested configurations. This outcome can be considered specific to the types, quantities, distribution and SOC of cells involved in the performed tests.
- For the tested scenario, a Fire Containment Cover provides an appreciable level of protection against the threats of an external fire event.

Statistical relevance: Each test was performed only once. The MPS test specification [2] requires every test to be conducted 5 times in order to gather statistical relevance. Within the scope of the Sabatair project, resources were limited, so no statistical evidence is provided. However, the tests show a clear tendency to provide enough confidence to support the conclusions.

Chapter V: Conclusions

One of the main Sabatair objectives was the assessment of the effectiveness of the test methods as described in the draft SAE AS6413.

An initial experimental test plan was designed to evaluate the tests as described in the SAE AS6413 draft standard. Quickly a lack of test repeatability was encountered. The focus was then directed to the thermal runaway initiation process. Actually first tests showed that the thermal runaway is strongly depending on the type of heater used and the heating control. As the draft standard gives little information on the properties of the equipment that should be used, the Sabatair test results showed that the thermal runaway severity is strongly dependent on how the thermal runaway was initiated. In fact the heating rate range as specified in the standard version used during this project may lead the test to a fail or to a pass. As a slow heating rate may not lead to a severe thermal runaway with subsequent damages on the package.

The lack of repeatability of the test results may be justified by the fact that the SAE AS6413 standard includes a high level of flexibility cover the many potential combinations of cells and packaging to be tested as well as future evolution of the design of lithium batteries. However more detailed recommendations should be given on some key parameters like the heater size and the heating rate.

The second main objective of the Sabatair project is to study and assess the effectiveness of potential mitigating measures against fire risk related to the transport of lithium batteries on cargo aircrafts. The idea is that how to prevent a thermal runaway to propagation inside a package but also between packages. Several commercially available solutions were identified and some of them were tested and/or simulated during this project. Results have shown that simple measures like adding cardboard dividers between the cells can be effective in slowing down or even stopping the thermal runaway propagation inside the package. Solutions like using graphite or alumina casing packaging or adding sands between the cells helps in thermal runaway dissipation and prevents thermal runaway propagation but it's up to the cell distributor to take its decision as such solutions may increase the costs of shipping lithium cells/batteries by air. A compromise should be found between safety, practicality and cost effectiveness.

Finally, the full scale external fire tests performed during the Sabatair project showed that a state-of-the-art built-in fire suppression system of a Class C cargo compartment, combined with the use of Fire Containment Covers, could prevent the involvement of lithium cells/batteries in an external cargo fire event. However, due to the limited number of tests, statistical evidence could not be satisfactorily produced for the tested combinations of cell types, quantities and states of charge. To confirm the effectiveness of these protection measures, further investigation and repetitions of the tests would be required.

Bibliography

- [1] SAFO - Safety Alert for Operators 10017, U.S. Federal Aviation Administration, Flight Standards Service Washington, DC, October 2010
- [2] Minimum Performance Standard for Aircraft Cargo Compartment Halon Replacement Fire Suppression Systems (2012 Update), U.S. Federal Aviation Administration, DOT/FAA/TC-TN12/11, May 2012

Appendix

An extensive thermal modelling work has been carried out during this project. More details on the thermal model and the different simulations cases are presented in this report.

As this document is not an official deliverable, it is presented here as an appendix.

Heat transfer modeling of a Li-Ion cell pack undergoing thermal runaway

Pai Raikar Prahars (VITO)
Vladimir Jovanovic (InsPyro) (temporary consultant 2018)
Khiem Trad (VITO)

Study accomplished under the authority of
2020/Unit/R/2220

December 2019

Contents

1	Introduction.....	3
2	Cell pack geometry (CAD) model.....	3
3	Computational mesh	4
4	Model setup	5
5	Summary of numerical simulations results	6
5.1	Thermal runaway modeling of a cylindrical cells pack (simulation g05m01s02).....	7
5.2	Thermal runaway modeling of a cylindrical cells pack (simulation g05m01s03).....	9
5.3	Thermal runaway modeling of a cylindrical cells pack (simulation g05m01s04).....	11
5.4	Thermal runaway modeling of a cylindrical cells pack (simulation g05m01s05).....	14
5.5	Thermal runaway modeling of a cylindrical cells pack (simulations g05m01s07 -> g05m01s12)	17
5.6	Simulations with 5x5 cell arrangement.....	23
6	Heat propagation modelling in a pouch type cell and pouch cell array.....	30
6.1	Heat distribution modelling in a pouch cell with tabs and pouch cell array with tabs	31
7	Heat propagation modelling in cylindrical cell packs.....	34
8	Validation of thermal model	36
8.1	Comparison with temperature measurements for one 1 cell.....	36
8.1.1	Experimental Setup	37
8.1.2	Computational Setup & Boundary Conditions	37
8.1.3	Results	38
8.2	Comparison with temperature measurements for a group of cells	40
8.2.1	Experimental Setup	40
8.2.2	Computational Setup & Boundary Conditions	40
8.2.3	Results	41
8.3	Conclusions.....	42
9	Thermal model application for mitigation strategies.....	42
9.1	Base Case – Case 1	42
9.2	Mitigation Cases.....	45
9.3	Results Summary.....	50

1 Introduction

Heat propagation simulation over an array of Li-Ion cells within a transportation package has been performed to get better insight into transient heat flow across the package. The assumption is that one of the cells in a package accidentally goes into thermal runaway either by being mechanically penetrated with a sharp pointy object, which causes internal short circuiting, or by being thermally abused with an external heat source. In either case, this mechanical or heat forcing triggers a chain of electro-chemical exothermic reactions and a rapid heat release occurs accompanied with high temperatures of the cell. This in turn may or may not, depending on the state-of-charge (SOC) of the batteries (which directly influences the amount of heat it will release if in thermal runaway), trigger other cells in the immediate vicinity. The most detrimental situation is when the whole cell package burns out, due to a so called thermal runaway cascade effect. The cascade effect refers to the event when all the cells in a package go off in thermal runaway one after the other with a certain (not necessarily regular) time period in between. Although the SOC is likely to be the most influential parameter in the heat release intensity during the thermal runaway, it is also important to take into account the way cells are stacked in a package, staggered apart or not, and in case they are apart, which material in between the cells may be a good insulator to prevent TR cascading effect. All these questions may be tackled by a numerical simulation along with some necessary inputs from thermal or mechanical cell abuse experiments.

2 Cell pack geometry (CAD) model

A CAD model is designed based on a few requirements. It has to contain enough cells to properly observe thermal runaway propagation in a package, and to be flexible in terms of adding or removing dividing walls in between the cells and fluid/insulator regions in the package. Ansys Fluent v19.2 is used to model heat generation and propagation across the cell package. It is assumed that thermal conduction is the only mechanism by which heat propagates through the package. Since the air space in between the cells is rather small (in case of tightly packed cylindrical cells), and the box containing cells is closed, it is assumed that heat propagates through the air region only by conduction as well. In other words, air is taken to behave like a solid with its own thermophysical properties. Figure 1 shows a schematic of a geometrical model for a 5x5 cell package. The box around the cells (red line on the picture), and dividers (blue line on the picture), are not included in the CAD model with their real thickness. They are designed as zero-thickness plane surfaces in the CAD model, however, in the Fluent solver they are virtually given a finite thickness. This offers a great flexibility since it is not necessary to make a new model and a computational mesh every time thickness of the dividers or the box around the cells is slightly modified.

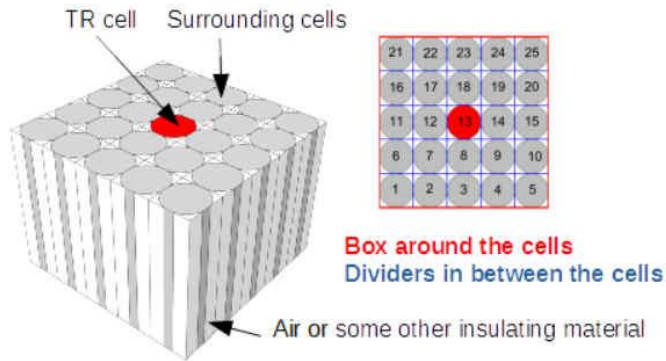


Figure 1: Geometrical model for a 5x5 cell package

3 Computational mesh

Ansys Fluent is a finite volume based general thermo-fluids solver and as a first step a finite volume good quality computational mesh must be generated. For this purpose Ansys Workbench package is used as a pre-processor since it can generate high quality meshes which are dominated by extrusions. If a surface mesh is defined on one side of the domain it can be easily extruded to the other side with a specified pitch. Moreover, the Ansys Workbench Mesher is capable of automatic naming of the interior mesh surfaces which exist in between the cells as well as in between fluid region. This provides a great flexibility while using these interior faces later on in the Fluent solver to place dividers of a certain virtual thickness and certain properties to examine insulation effects of the dividers. It is also worth clarifying, as already mentioned above, that the box around the cells as well as dividers are not actually meshed, they do not contain computational cell volumes. They are very thin regions and for that reason a special feature of Fluent is used where one can impose virtual thickness through which heat conduction can be modeled only in a surface normal direction. Taking into account a very small thickness of these regions, this should be a fair approximation. Certainly, symmetry may be used in modelling geometries like this (box with regularly spaced cells) to build models which are even more simple and with a small number of computational cells, however this has been avoided. A model with symmetric boundaries would be useful if thermal runaway is initiated at the center of the box. However, if thermal runaway is initiated at the edge of the box or at the corner of the box, symmetry would be lost and a new model is needed. An example of a computational mesh is given on Figure 2 for a 5x5 cell package.

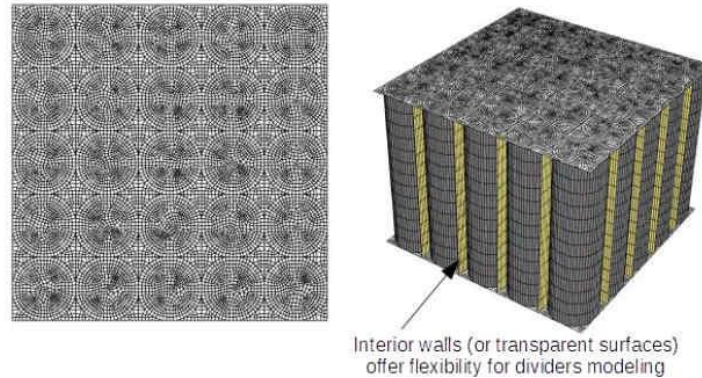


Figure 2: Computational mesh for a 5x5 cell package

4 Model setup

A black-box approach is utilized for the modeling of heat propagation across the cell package and in that case Fluent solves only one equation which defines heat propagation within the solid region.

$$\frac{\partial}{\partial t}(\rho h) = \nabla \cdot (k \nabla T) + S_h$$

Where:

- ρ = density
- h = sensible enthalpy
- k = conductivity
- T = temperature
- S_h = volumetric heat source

Black-box model actually means that, rather than describing the mechanisms leading to the heat generation in the battery, the heat generation is modelled directly. A volumetric heat source of a certain strength is imposed inside the cell volume which should result in temperatures which are observed in the experiments. Therefore, solving all the equations which describe thermo-chemical and electro-chemical processes within a cell is avoided. Each cell is considered to be a made up of a homogeneous material with its own thermo-mechanical properties which should in case of a thermal runaway release a certain amount of heat. The strength of the heat source is estimated from the experimental temperature recordings. The computational model is transient which provides the time evolution of temperatures across the cells and the possibility to introduce cascading effect.

The model uses User Defined Functions (UDF) to describe the specific behavior. These functions are pieces of C-code run by the solver and allow to make additional calculations and to change boundary conditions during the simulation. A first UDF contains the heat source definition, describing the black box thermal behavior of the batteries. Other routines are run after each time-step of the simulation to track down maximum and average temperature of each cell, which are necessary to trigger the heat release.

A schematic in Figure 3 outlines how the temperature evolution during the experimental thermal runaway tests is used to define two heat sources as a function of time. These heat sources are constant

during a certain period of time, and approximate the power necessary to reproduce a certain temperature increase, as observed in experiments. A first smaller heat source is imposed during the time delay between reaching the venting temperature T_1 and the onset of fast thermal runaway T_2 . During a short time interval, a larger heat source is imposed, corresponding to the heat released during the fast thermal runaway stage (reaching T_3).

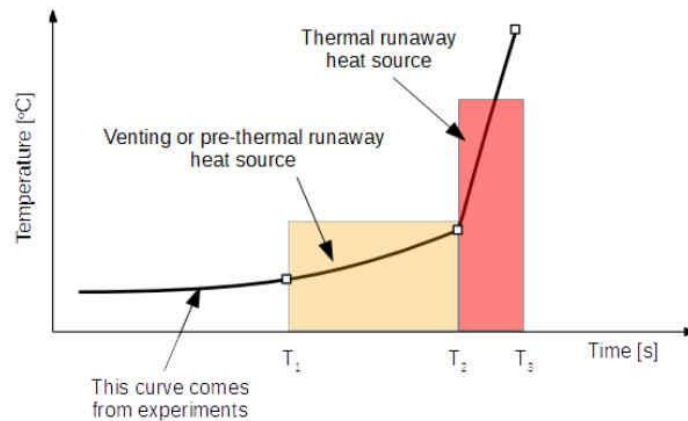


Figure 3: Heat source definition for the black-box modeling approach

Since only the energy equation is solved during the simulation, boundary conditions require the temperature to be defined at the faces of the box. Convective boundary conditions are chosen as the most suitable, meaning that the convective heat coefficient along with the free-stream temperature on the outside of the box must be defined. The simulation starts from an initial condition which may either be an environmental uniform temperature over the whole domain and possibly a temperature T_2 which is imposed within the cell which goes into thermal runaway.

5 Summary of numerical simulations results

A range of numerical simulations of thermal energy propagation across a cell pack have been performed for various conditions. Cells are not connected into an electrical circuit, they are only being stacked in a matrix pattern and either being separated by a thin sheet of some isolator material or touching each other. The conditions which are varied include:

- Intensity of the heat source which is applied to a cell which initially undergoes thermal runaway
- Location of an initial thermal runaway cell within a pack
- Environmental conditions around a cell pack
- Properties of the medium which is in between the cells: air or vermiculite
- Cell type: cylindrical or pouch
- State of charge of the cells

The term "cell" is used in this report both for a battery which is not being connected into a circuit and is called a cell, and also for a unit cell of the computational finite volume mesh. It is believed that the

potential reader will be able to infer what is meant from the context of the sentence within which the term cells is used. In the part 5 results are presented on the cylindrical cells while the part 6 discusses pouch cells. Since the only equation that is solved in the model is the energy equation, and the mode of thermal energy propagation is conduction only, the results will be presented in the form of temperature spatial distribution over the cells in a pack and the time evolution of temperature for a chosen set of monitoring points within domain.

5.1 Thermal runaway modeling of a cylindrical cells pack (simulation g05m01s02)

Initially we look into a 5x3 matrix of cells packed in a cardboard box of a given thickness of 5 mm. The goal is to use experimentally obtained temperature (TR101 in the VITO document) time evolution of a cell within pack which is thermally forced into thermal runaway (TR in the further text), estimate thermal energy release during that period, and impose the obtained value as an energy source term in our numerical simulation. Figure 4 outlines the simulation setup. In the model, air in between the cells is included only as a conductive medium. It is assumed that in a cell package as small as this one there will be no enough space in between the cells and time for the convective currents to develop during the TR stage to impose significant influence on temperature distribution on the cells.

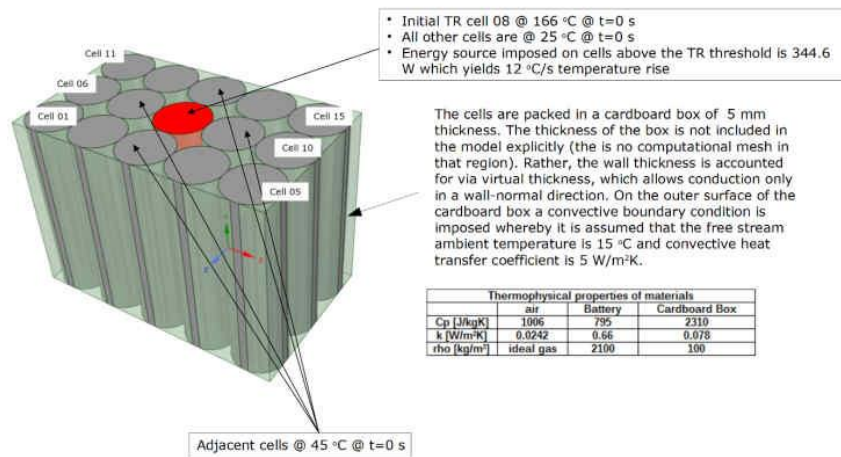


Figure 4: Schematic to accompany simulation g05m01s02 (internal simulation tagging convention).

One more important detail to mention is that the end of the venting stage of a cell is taken into account through the initial temperature. That is the reason why the cell number 8 is initially at 166 °C and the cells around it are at 45 °C. Therefore the cell number 8 goes into TR immediately while the other cells in a package are warming up and pending to reach the TR threshold temperature of 166 °C somewhere on their surface (normally at the contact line with the cell which is already in the TR stage). Therefore, the cascade mechanism is configured to work based on the maximum temperature in the cell. Figures 5 and 6 show the temperature evolution with time on the inner surface of the box. Figure 7 provides the maximum temperature time evolution within a cell.

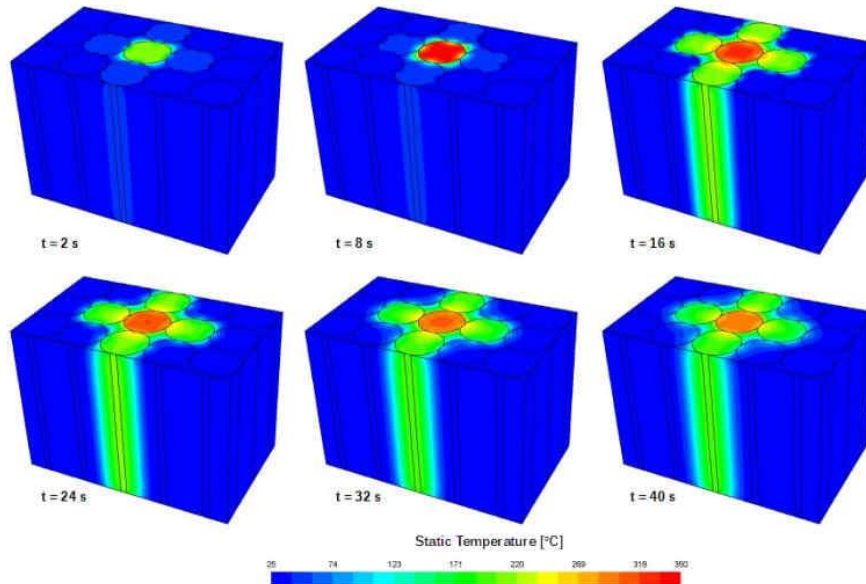


Figure 5: Temperature distribution on the inner surface of the box (g05m01s02)

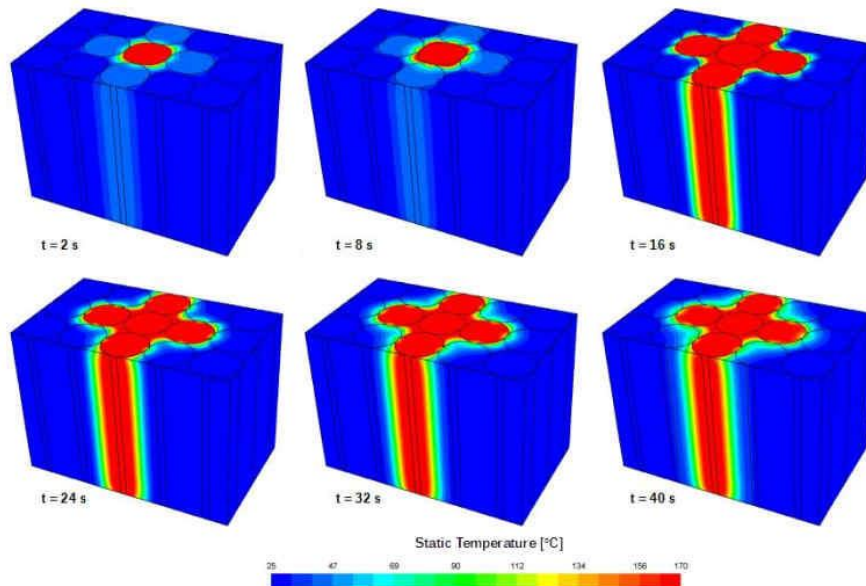


Figure 6: Temperature distribution on the inner surface of the box (g05m01s02). Upper limit of the scale is truncated to 170 °C

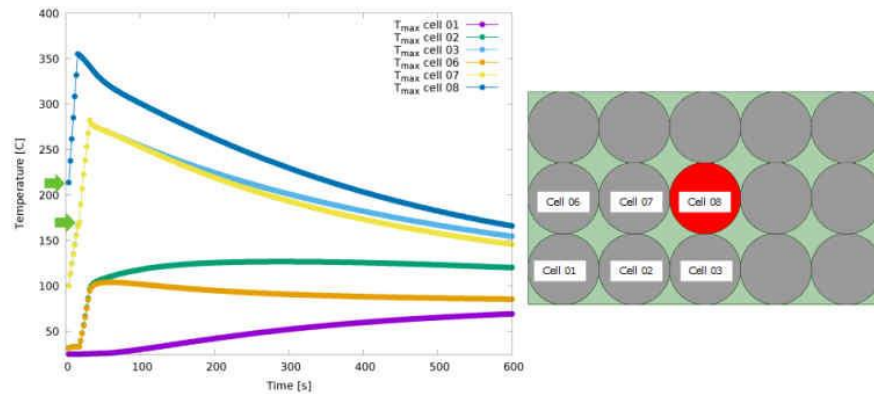


Figure 7: Maximum temperature within a cell vs time

From the simulation (g05m01s02) some observations and conclusions might be derived:

- An attempt to model TR propagation effect across all the cells in the package is performed based on the condition that the adjacent cell reaches T_{TR} (at least at one point) and then it goes into TR and temperature rise
- This is probably not the entirely true (one point in contact will always reach the trigger temperature, but probably not enough to trigger the cell into TR)
- TR propagation effect does not occur in the experiment, however in the simulation it does occur only in the cells around the initial TR cell
- In the experiments the initial TR cell has been brought into TR stage by continuous relatively slow thermal energy transfer into the cell therefore the temperature must have been evenly distributed across the cell volume prior TR occurs
- In the simulation model there is not enough time for the adjacent cells to get their temperature evenly distributed during the TR and the maximum temperature after the TR is lower than in the initial cell

5.2 Thermal runaway modeling of a cylindrical cells pack (simulation g05m01s03)

In this simulation the same boundary conditions are kept as in the g05m01s02. However, the location of the cell which is initially triggered into TR is moved from the center to the corner of the box. A pre-thermal-runaway warm-up stage is introduced in this model. This means that as soon as a cell reaches temperature of 60 °C at any point, a weak heat source is applied to that cell which results in a long-time slow increase in temperature. This “pre-thermal-runaway” stage lasts only for a short-time and is interrupted when the temperature of 160 °C appears somewhere at a cell boundary and it marks the beginning of thermal runaway (as before triggered by the maximum temperature in a cell criterion). Thermal-runaway is modeled by an intense short-time energy source which causes battery to reach high temperature and further induce thermal runaway in the adjacent ones. The schematic of the model is setup is shown on Figure 8. As it is currently modeled, thermal runaway will occur in all the

cells and its' propagation may only be prevented by introducing some gap in between the batteries and/or filling up the space in between the batteries with some sort of isolating material.

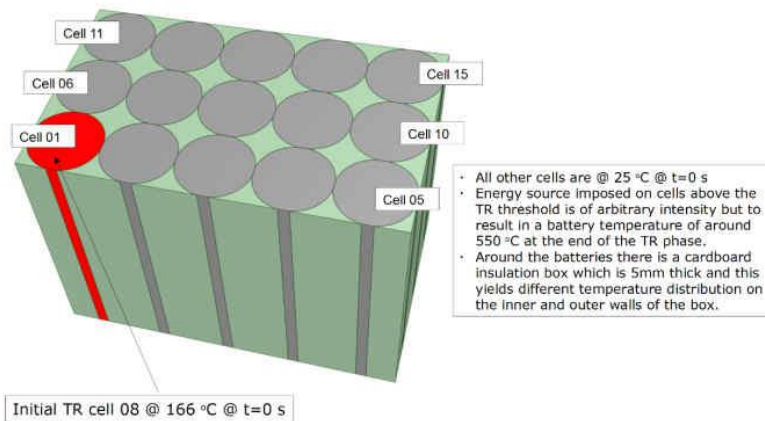


Figure 8: Schematic to accompany simulation setup for the model g05m01s03

One the Figures 9 and 10 temperature distribution on the inner and outer side of the box is shown respectively. Figure 11 shows the plot of maximum temperature recordings in time for each cell in the box.

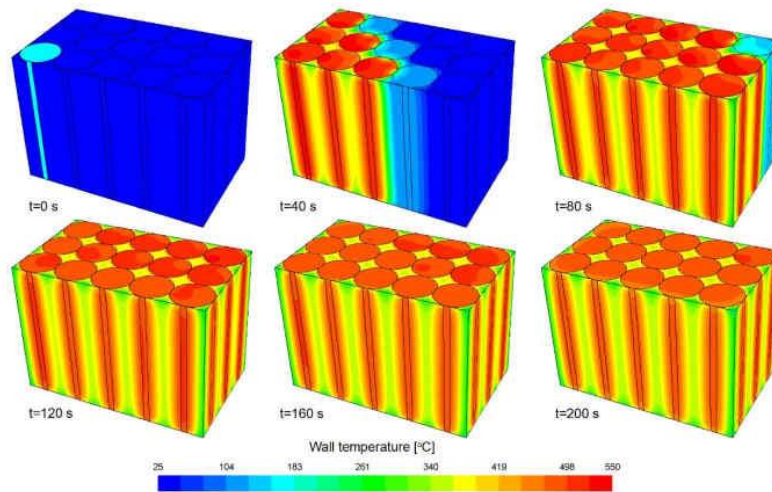


Figure 9: Temperature distribution on the inner surface of the box (g05m01s03)

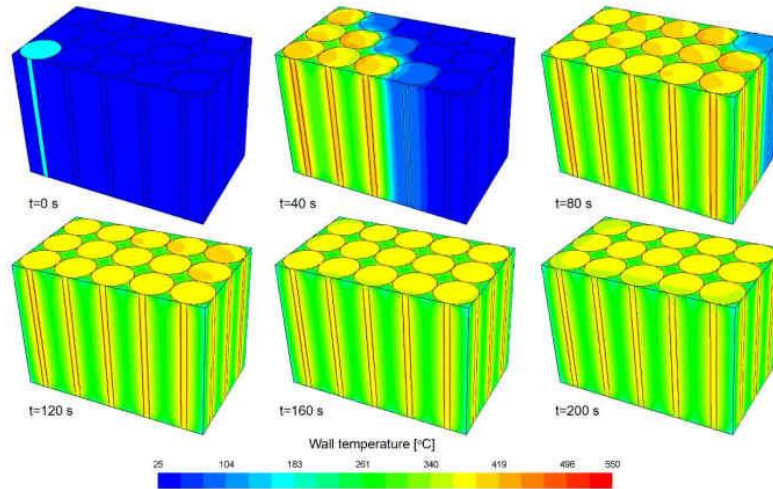


Figure 10: Temperature distribution on the outer surface of the box (g05m01s03)

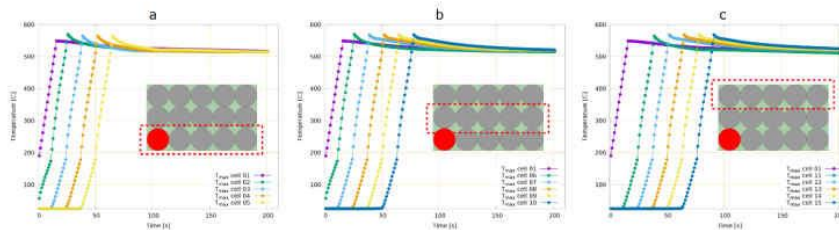


Figure 11: Maximum temperature vs time for a) cells 02-05, b) cells 06-10, c) cells 11-15. Maximum temperature evolution for the cell 01 is plotted on each graph for reference (g05m01s03)

5.3 Thermal runaway modeling of a cylindrical cells pack (simulation g05m01s04)

Simulation g05m01s04 is the continuation of g05m01s03. The description of the setup is as follows:

- The initiation of cell venting and thermal runaway phase are implemented based on the **volume averaged temperature** within a cell
- Air is in between the packaged cells and cell-to-cell radiation heat transfer is included
- Intensity of the venting phase heat source per unit time is 8.6 W
- This heat source is applied during the venting phase from $T_{start_venting} \rightarrow T_{end_venting}$
- The moment when temperature $T_{end_venting}$ occurs is influenced by both adjacent batteries as well as boundary condition imposed by the surrounding
- Intensity of the TR phase heat source per unit time is 860 W
- Unlike venting phase, TR phase lasts for a limited time period of 16 s

Simulation results are shown on Figures 12-16.

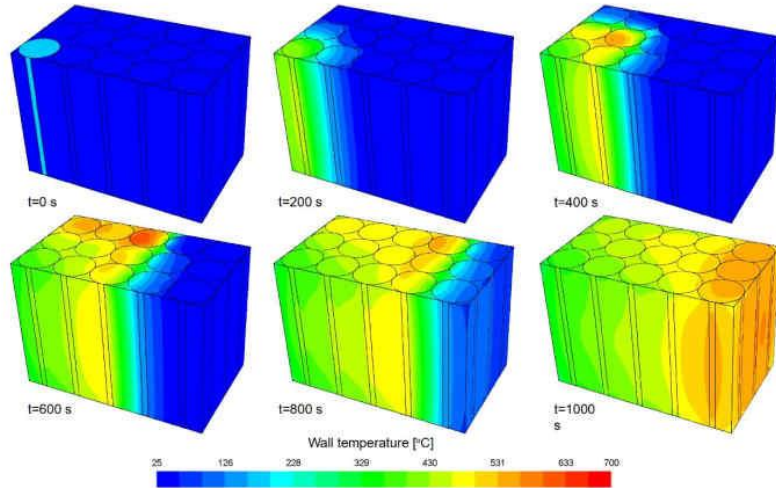


Figure 12: Temperature distribution on the inner surface of the box (g05m01s05)

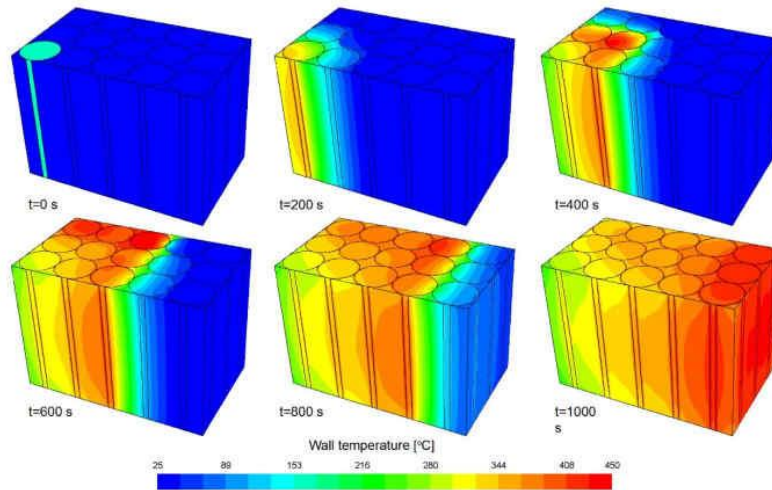


Figure 13: Temperature on the outer surface of the box (g05m01s04)

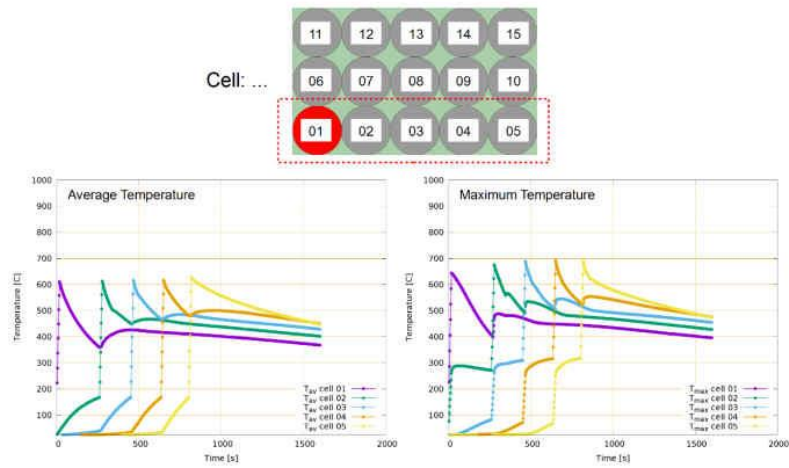


Figure 14: Maximum and volume-averaged cell temperature evolution in time for cells 01-05 (g05m01s04)

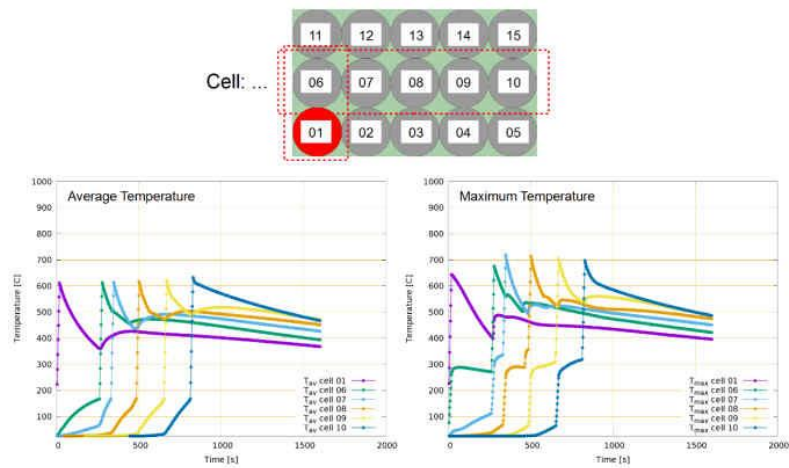


Figure 15: Maximum and volume-averaged cell temperature evolution in time for cells 06-10 (g05m01s04). Cell 01 plotted for reference

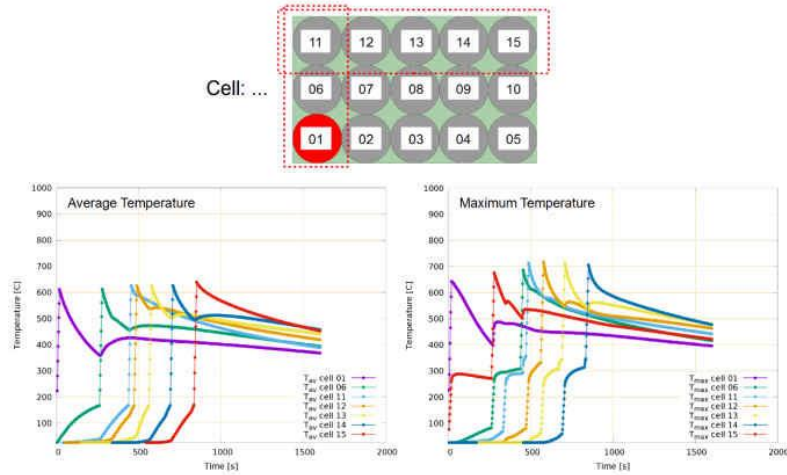


Figure 16: Maximum and volume-averaged cell temperature evolution in time for cells 11-15 (g05m01s04). Cell 01 and 06 plotted for reference

5.4 Thermal runaway modeling of a cylindrical cells pack (simulation g05m01s05)

In this simulation the influence of thermally insulating material vermiculite is investigated and its' ability to suppress cascading effect of thermal runaway. Vermiculite is placed in the space between cells instead of air. Boundary and initial conditions are the same as in the simulation g05m01s04. Thermophysical properties of the materials used in the model are outlined in the table below.

Thermophysical properties of materials				
	air	Battery	Cardboard Box	Vermiculite
Cp [J/kgK]	1006	795	2310	950
k [W/m ² K]	0.0242	0.66	0.078	0.064
rho [kg/m ³]	ideal gas	2100	100	90

Figure 17: Thermophysical properties of the materials used in simulation g05m01s05

Simulation results are shown on Figures 18 – 22.

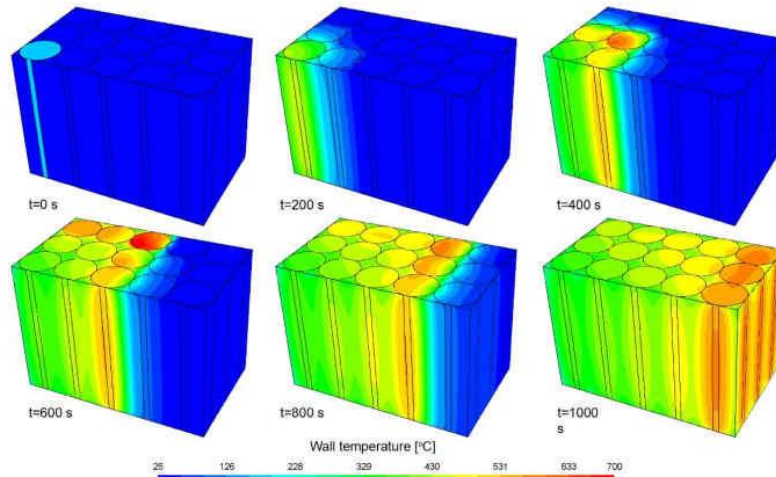


Figure 18: Temperature on the inner surface of the box (g05m01s05)

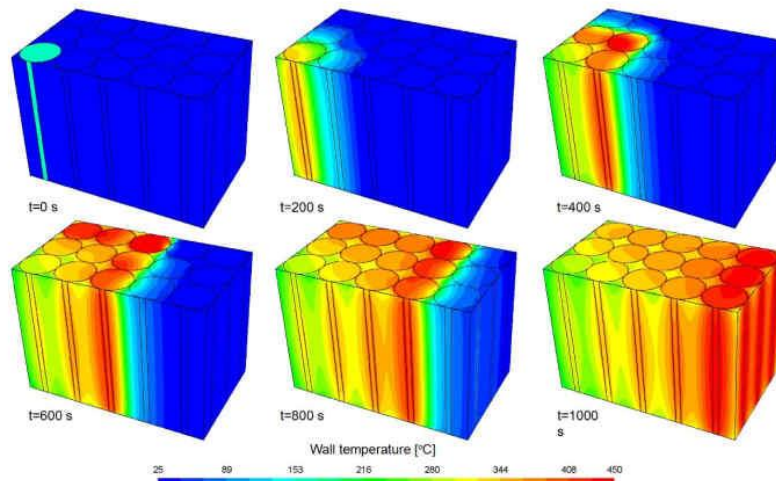


Figure 19: Temperature on the outer surface of the box (g05m01s05)

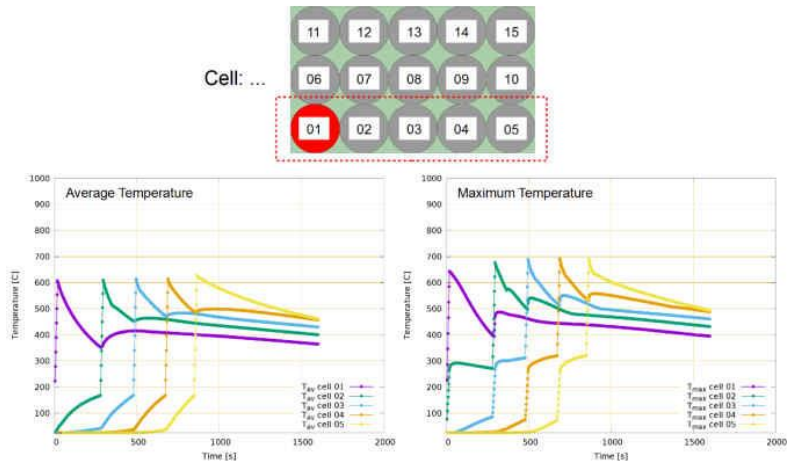


Figure 20: Maximum and volume-averaged temperature evolution in time, cells 01-05 (g05m01s05)

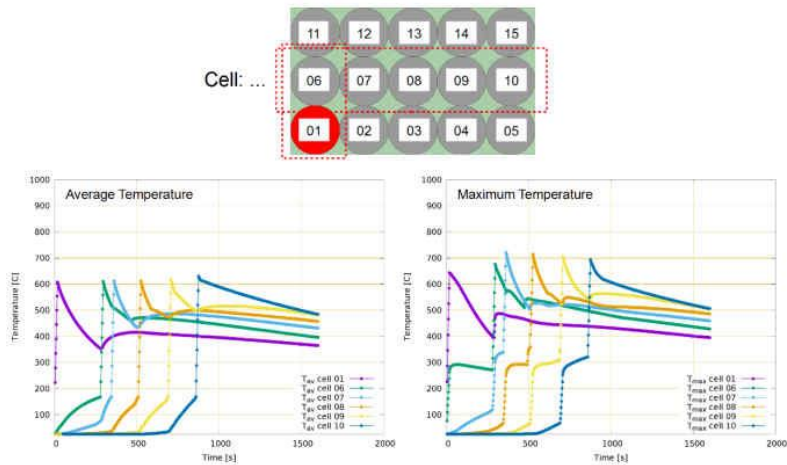


Figure 21: Maximum and volume-averaged temperature evolution in time, cells 06-10 (g05m01s05)

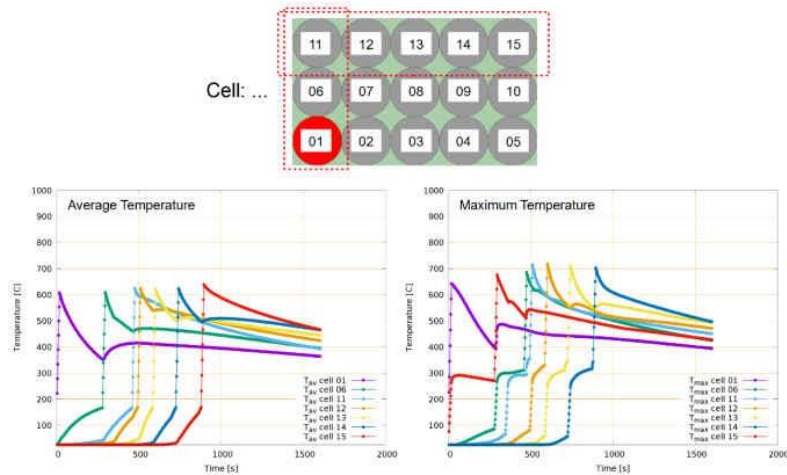


Figure 22: Maximum and volume-averaged temperature evolution in time, cells 11-15 (g05m01s05)

Replacing air with vermiculite as a thermal insulator has a limited impact on TR propagation (with thermodynamic properties of vermiculite as taken in the model). It is worthy pointing out again that in this model the TR trigger is based on the volume-averaged temperature in the cell.

5.5 Thermal runaway modeling of a cylindrical cells pack (simulations g05m01s07 -> g05m01s12)

In this part a range of simulations have been performed by varying cell location within a package and state of charge of cylindrical NCA cells. Only high and low values of SOC are taken into account which are 100 % for high SOC and 25 % for low SOC. Heat conduction is the only mechanism of thermal energy transfer. As before, cells are packed in a 5 mm carton box. Convective boundary condition is applied to the outer surface of the box with an environmental temperature of 15 °C and convective heat transfer coefficient of 5 W/m²K. All the input data which are summarized on the table below are taken from the reference “Thermal runaway of commercial 18650 Li-ion batteries with LFP and NCA cathodes – impact of state of charge and overcharge” (Khiem to put proper reference).

Simulation Code	Battery Type/Scenario	Capacity	density [kg/m ³]	Specific Heat Capacity [J/kgK]	NCA battery pack @ various arrangements						
					T ₀ @ venting onset [°C]	T ₀ @ venting onset = T ₀ @ start TR [°C]	T @ end TR [°C]	t @ venting onset [s]	t @ venting onset = t @ TR start [s]	t @ TR max [s]	t end of TR process [s]
g05m01s07	NCA @ 100% SOC/ Center, 1 layer	3.35Ah	2580	830	130	162	885	3384	4000	4417	4700
g05m01s08	NCA @ 25% SOC/ Corner, 1 layer	3.35Ah	2580	830	148	184	717	3634	5121	5484	5750
g05m01s09	NCA @ 100% SOC/ Edge, 1 layer	3.35Ah	2580	830	130	162	885	3384	4000	4417	4700
g05m01s10	NCA @ 25% SOC/ Edge, 1 layer	3.35Ah	2580	830	148	184	717	3634	5121	5484	5750
g05m01s11	NCA @ 100% SOC/ Center, 1 layer	3.35Ah	2580	830	130	162	885	3384	4000	4417	4700
g05m01s12	NCA @ 25% SOC/ Center, 1 layer	3.35Ah	2580	830	148	184	717	3634	5121	5484	5750

Further specific details about the simulations are as follows:

- A single cell which goes into thermal runaway is initiated with T₀@start TR temperature and an energy source with TR strength is assigned to that cell

- For high SOC the thermal power source strength in the TR stage is 3764140 W/m^3 , and for low SOC the strength is 3059963 W/m^3
- When the volumetric mean temperature of a neighbor cell reaches temperature $T_{\text{venting onset}}$ it goes into a venting stage and a venting power source is assigned to that cell which further increases temperature of that cell
- For high SOC the venting power source strength is 79955 W/m^3 , and for low SOC the strength is 64946 W/m^3
- All the cells in a pack are initiated with $25 \text{ }^\circ\text{C}$ at $t=0\text{s}$ apart from the one which is at $166 \text{ }^\circ\text{C}$ and at $t=0\text{s}$ immediately goes into TR without venting.
- Thermal conductivity of the battery (active) zone is taken to be $1.1 \text{ W/m}^2\text{K}$

Results will be presented in a form of graphs showing maximum and volume averaged temperature distribution for each cell in a pack and the maximum temperature on the outer surface of the box as a function of time.

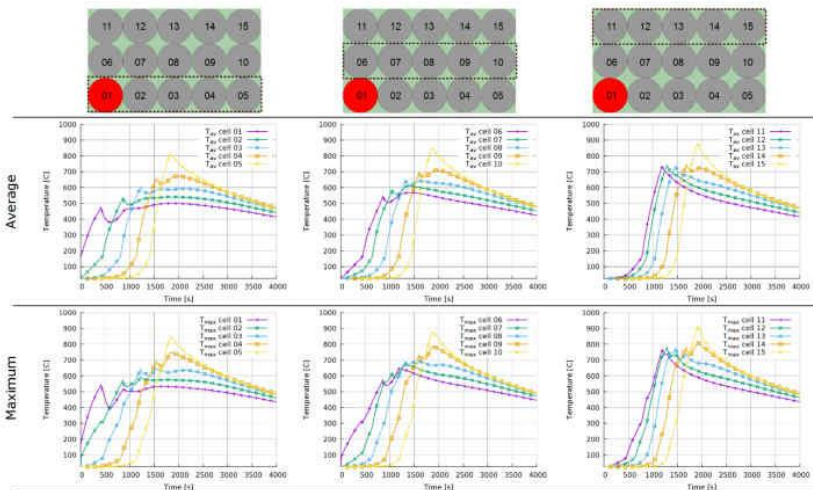


Figure 23: Average and maximum cell temperature as a function of time (g05m01s07)

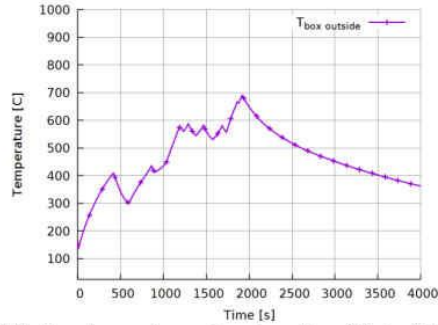


Figure 24: Maximum temperature on the outer surface of the box (g05m01s07)

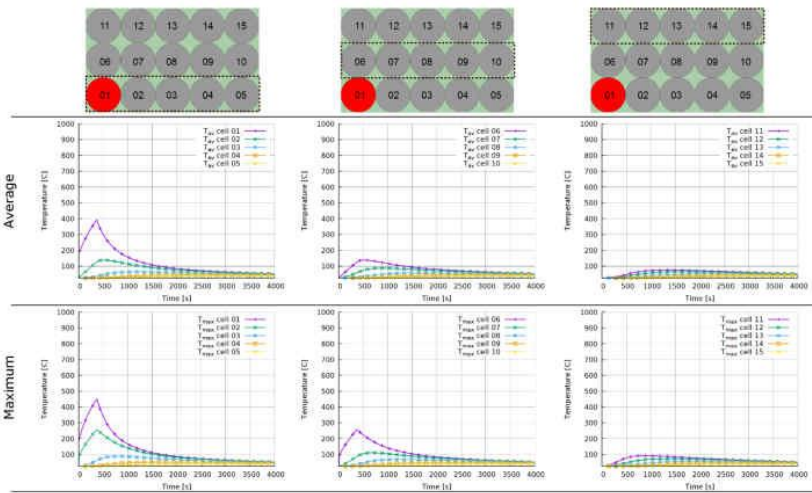


Figure 25: Average and maximum cell temperature as a function of time (g05m01s08)

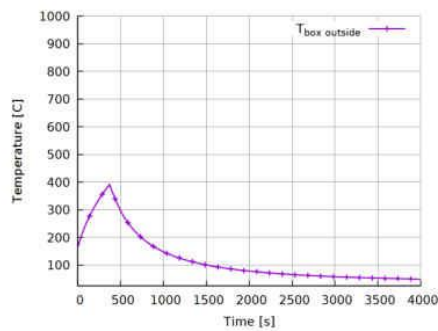


Figure 26: Maximum temperature on the outer surface of the box (g05m01s08)

08/05/2020

19/58

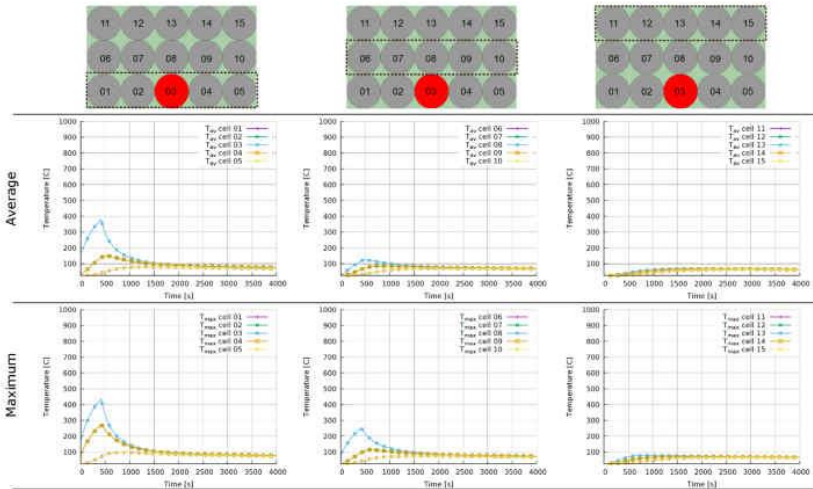


Figure 27: Average and maximum cell temperature as a function of time (g05m01s09)

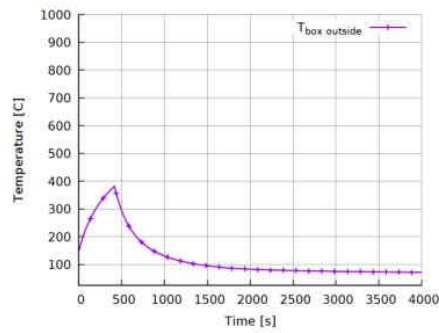


Figure 28: Maximum temperature on the outer surface of the box (g05m01s09)

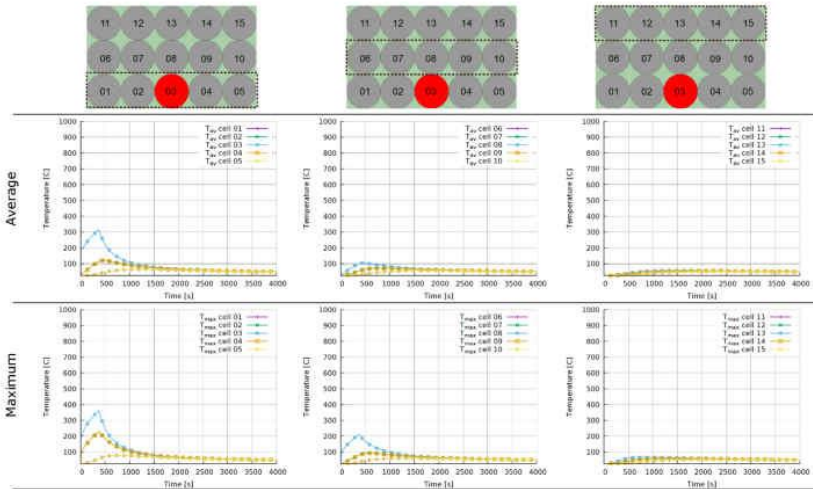


Figure 29: Average and maximum cell temperature as a function of time (g05m01s10)

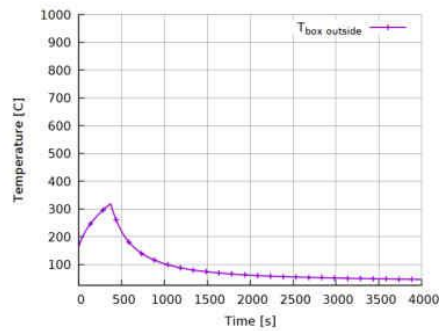


Figure 30: Maximum temperature on the outer surface of the box (g05m01s10)

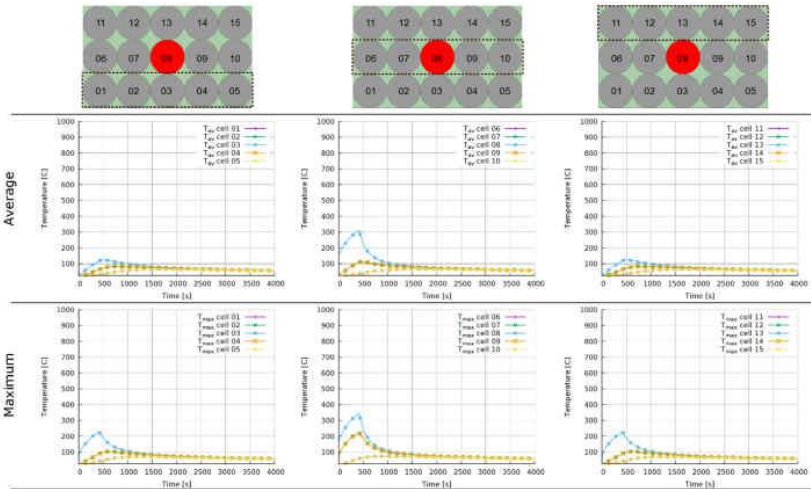


Figure 31: Average and maximum cell temperature as a function of time (g05m01s11)

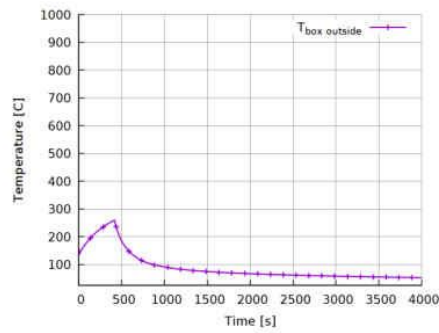


Figure 32: Maximum temperature on the outer surface of the box (g05m01s11)

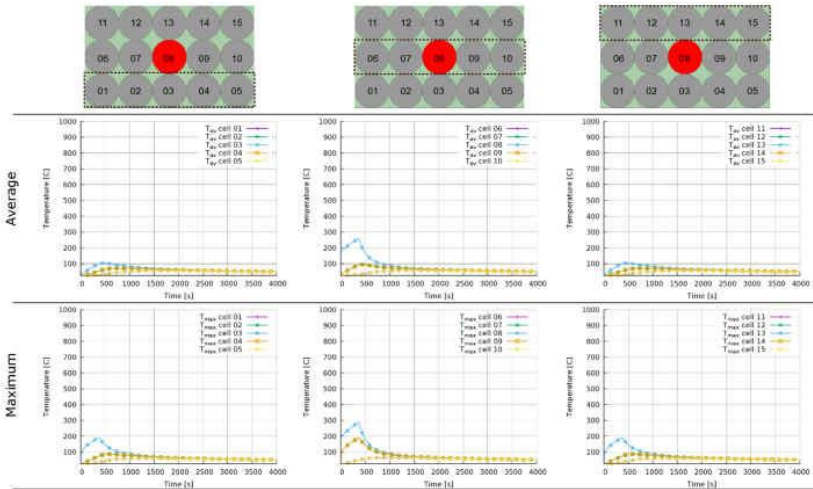


Figure 33: Average and maximum cell temperature as a function of time (g05m01s12)

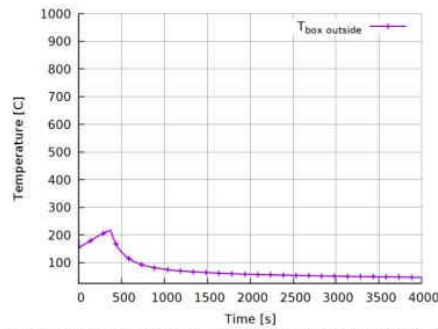


Figure 34: Maximum temperature on the outer surface of the box (g05m01s11)

5.6 Simulations with 5x5 cell arrangement

For this group of simulations on NCA cylindrical cells we use as a source of data experimental results obtained by UL. They used 5x5 cell package with some cardboard dividers and it was reported that all the cells in the package went into TR without clearly exhibiting venting stage. The whole package finally went into fire. No smoke was observed before TR started. It was clear from the experimental temperature logs that the TR occurs abruptly accompanied with a huge temperature gradient within a cell. Therefore, for the following set of simulations it was decided to use the maximum temperature in a cell as a trigger for TR. The cell matrix and package properties are shown on Figure 36. The summary of the data used in simulations g06m01s01->s03 is given in tabular form on the Figure 35.

Figure 35: Outline of the simulations g06m01s01->s03

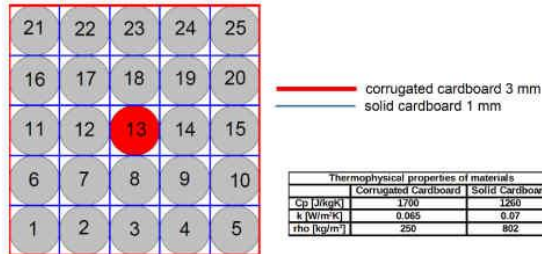


Figure 36: Cell arrangement and cardboard thermophysical properties

In the UL experiments the cell in the middle of the box which is heated up at a specific rate is labeled as 09. In our model that cell is labeled as 13. Maximum cell temperature as a function of time for the model g06m01s01 is presented on Figure 37. Wall temperature on the inner wall side of the box is shown on Figure 38.

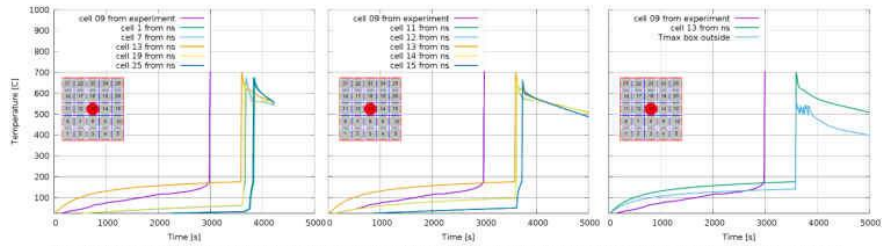


Figure 37: Maximum temperature as a function of time for the model g06m01s01 (ns = numerical simulation)

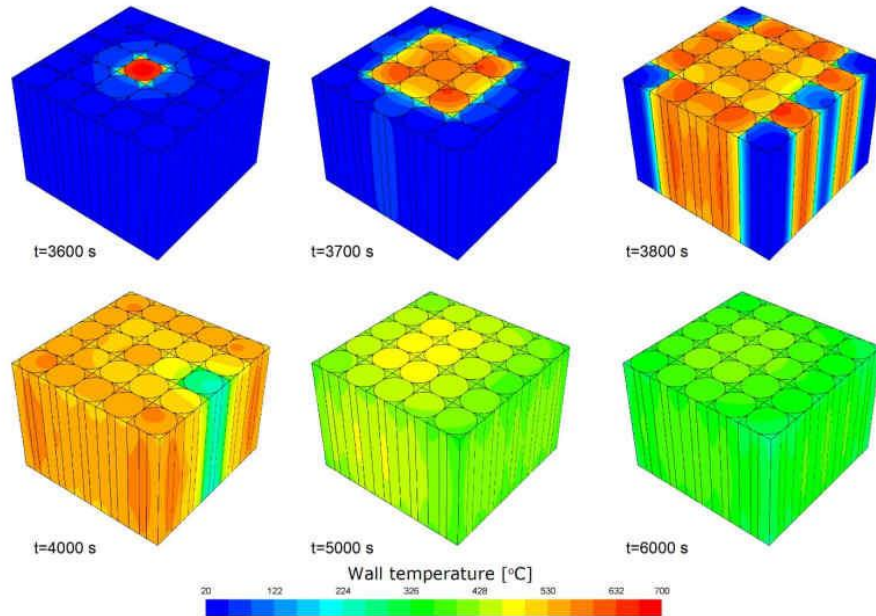


Figure 38: Temperature as a function of time on the inner wall surface of the box (g06m01s01)

Two more simulations are performed for the same geometrical 5x5 cell setup. In the model g06m01s02 the ambient temperature outside the box is 2 °C while for the model g06m01s03 the ambient temperature is 30 °C. Details are outlined in the table above. Cardboard walls are removed so the cells are in direct physical contact with each other. The box represents an enclosure around the cells, meaning the cells are sealed within the box. Schematic to accompany model setup for the simulations g06m01s02-s03 is given on the Figure 39.

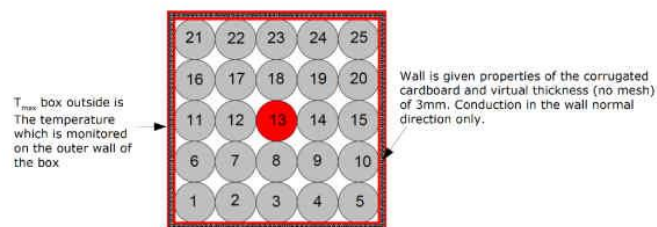


Figure 39: Schematic to go along simulations g06m01s02-s03

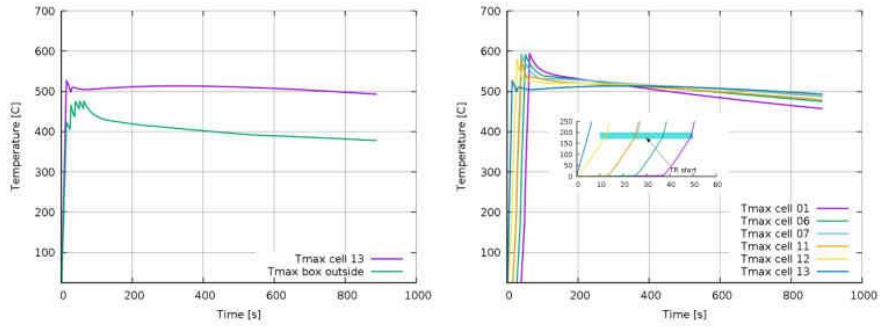


Figure 40: Time evolution of maximum temperature (g06m01s02)

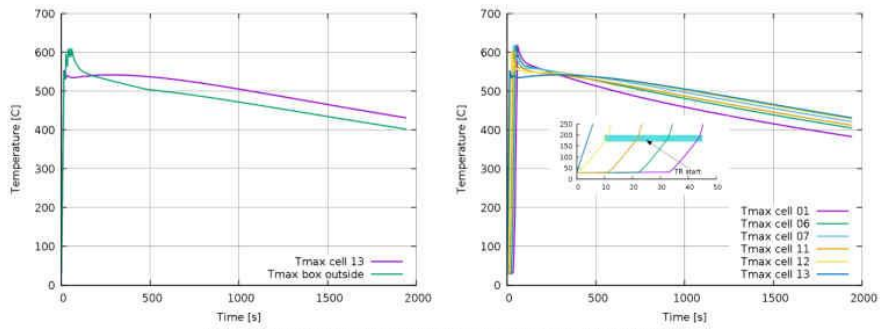


Figure 41: Time evolution of maximum temperature (g06m01s03)

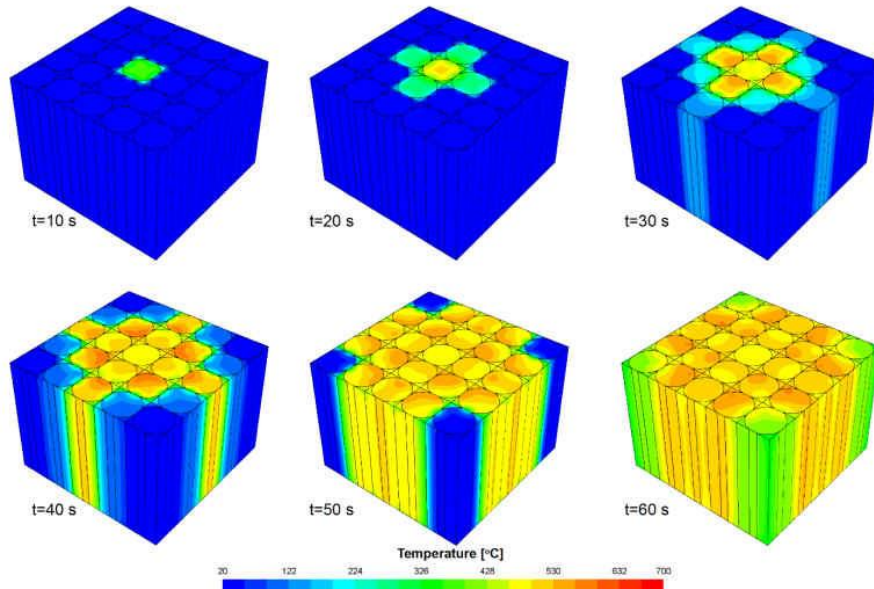


Figure 42: Temperature on the inner wall surface of the box (g06m01s02)

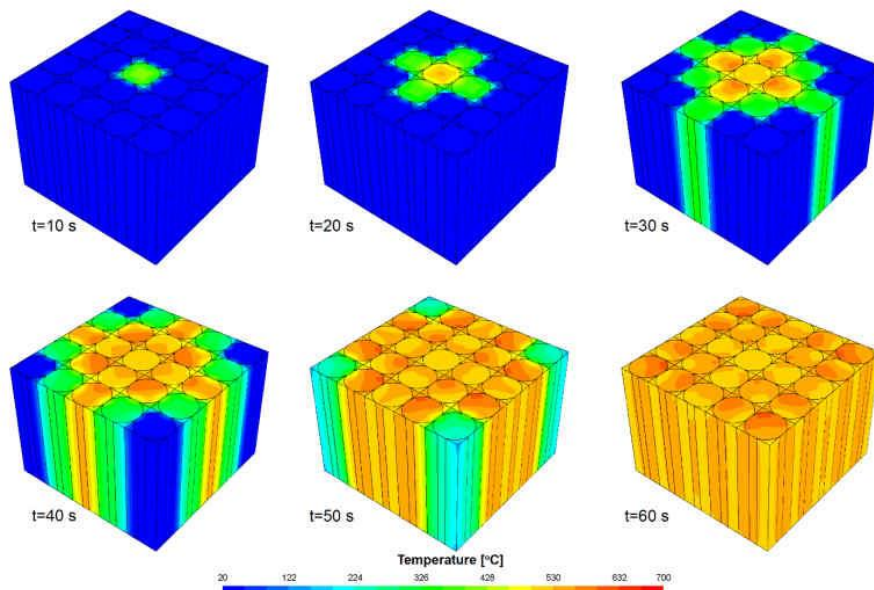


Figure 43: Temperature on the inner wall surface of the box (g06m01s03)

6 Heat propagation modelling in a pouch type cell and pouch cell array

The aim is to model heat distribution across the pouch cell. The heat source is a small heater represented as a boundary face attached to the front side of the cell. Simulations are performed for two values of temperature gradient, 15 and 5 °C/min, and these are prescribed as a boundary condition on the heater face. We are looking at temperature distribution across the cell in case the heat conduction coefficient k [W/mK] is not homogeneous but is orthotropic (directionally dependent with respect to XYZ as shown on the Figure 44). In this model cell tabs are not included. Their influence on heat redistribution will be investigated later on. Thermodynamic properties of the cell material are also given on Figure 44. In the numerical model, the cell is assumed to be fixed in a calm room temperature environment which suggests that it can give away heat to the environment by two mechanisms: convection and radiation. Therefore, mixed boundary condition is imposed everywhere on the cell boundary faces: convective heat transfer coefficient $h = 1$ W/m²K, free stream temperature $T_{\infty} = 25$ °C, external emissivity $\epsilon = 0.9$, external radiation temperature $T_r = 25$ °C.

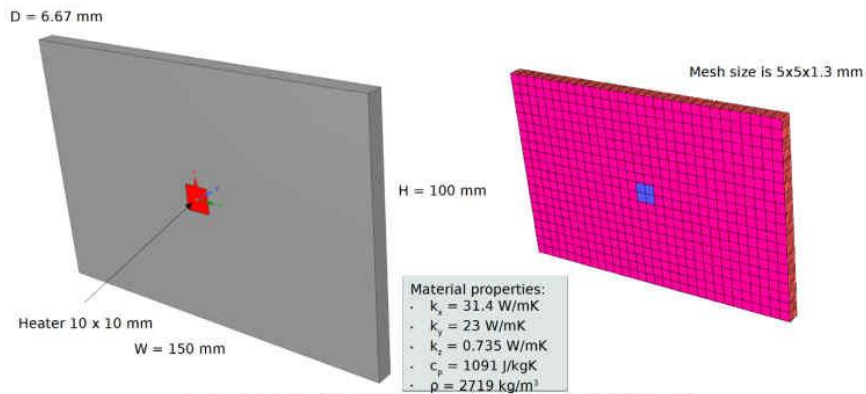


Figure 44: Geometrical model of the pouch cell and computational grid

Since the simulation computes temperature distribution due to heat conduction only, the transient energy equation is solved within cell domain. Simulation was running for 1000 timesteps with the timestep size of 5 s. Temperature is monitored at couple of points: top (bottom is the same) side, lateral side, and back of the cell just across from the heater. Contours of temperature distribution are shown on Figure 45.

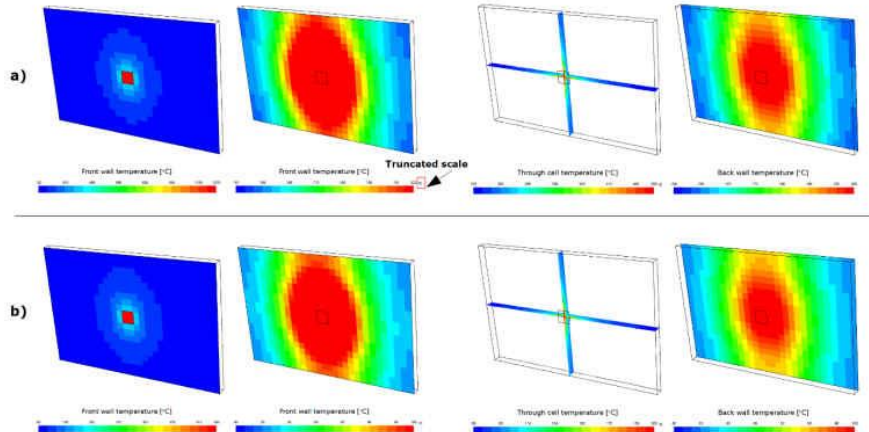


Figure 45: Contours of temperature on the cell walls: a) for the heater temperature ramp-up gradient of 15°C/min, b) 5°C/min (g08m01s01 and s02)

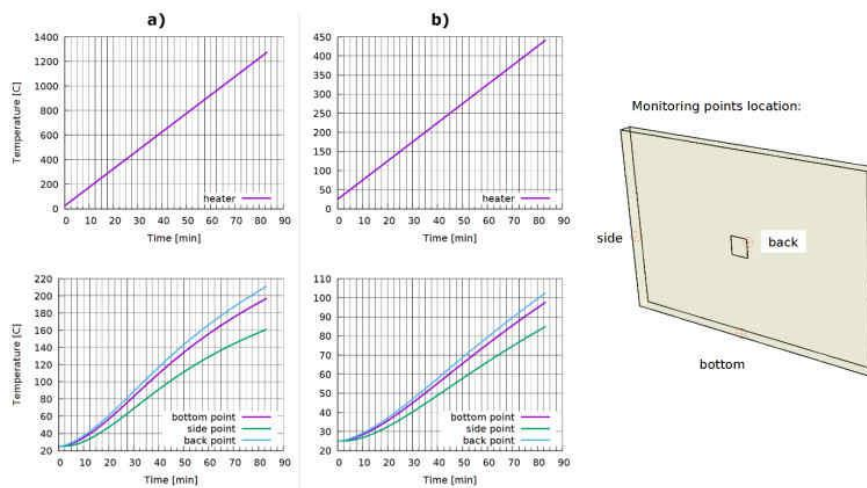


Figure 46: Temperature recordings at monitoring points (g08m0s01 and s02)

6.1 Heat distribution modelling in a pouch cell with tabs and pouch cell array with tabs

The first step is to model heat propagation in a single pouch cell with tabs (one made of copper and the other is aluminum) and to look at whether the tabs' influence is significant. They are essentially heat sinks. Apart from adding the tabs, boundary and initial conditions are the same as in the model g08m01s01. Temperature contours on the cell boundary are shown on Figure 47 and temperature time evolution at the back of the cell on Figure 48.

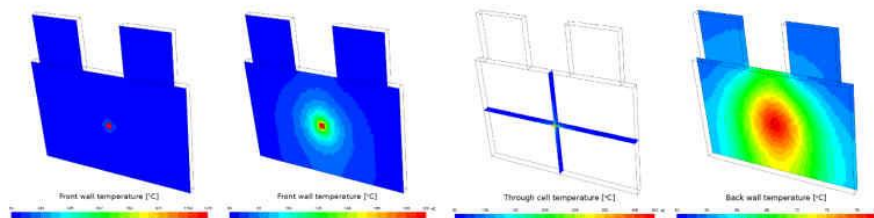


Figure 47: Temperature contours on the cell walls and through the cell (g09m01s01)

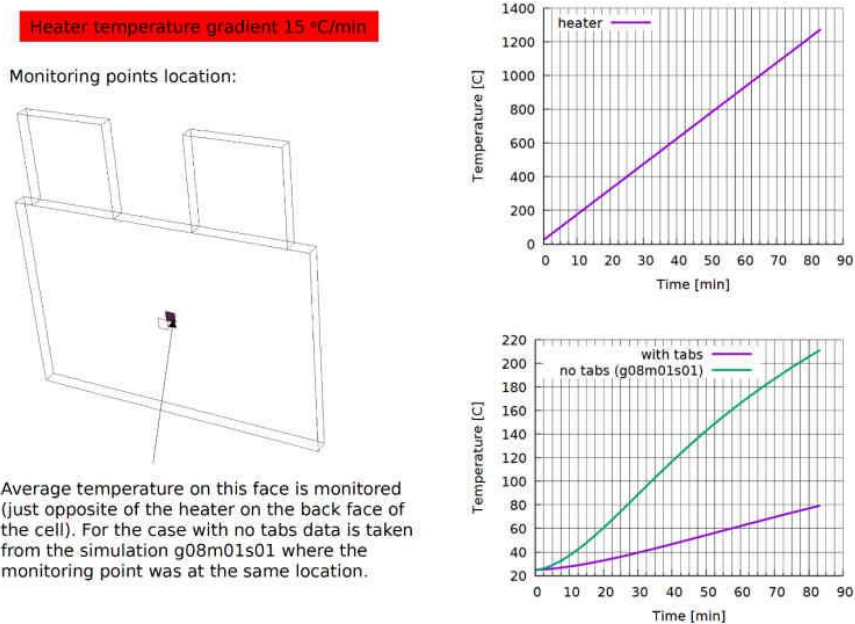


Figure 48: Comparison of the temperature logs (g08m01s01 (no tabs) and g09m01s01 (with tabs)) recorded at the back face of the cell opposite from the heater location

Model g09m01s01 represents a pack of five cells stacked next to each other and being separated by a thin solid cardboard divider. All the cells are wrapped up in a corrugated cardboard box. On the outer side of the box a convective boundary conditions is applied to allow for some energy dissipation to the environment. The heater which is attached to the front face of the cell 01 is not covered with a cardboard. The heater provides steady ramp-up temperature rise of 15 °C/min. Schematic of the model is shown on Figure 49. On Figure 50 temperature values on the inner side of the cardboard wall are shown as well as the temperature distribution through the pack after 90 minutes of being exposed to the steady temperature increase on the heater. Figure 51 shows temperature recordings in time from the monitoring points located at the back face of each cell in between the cells and cardboard divider.

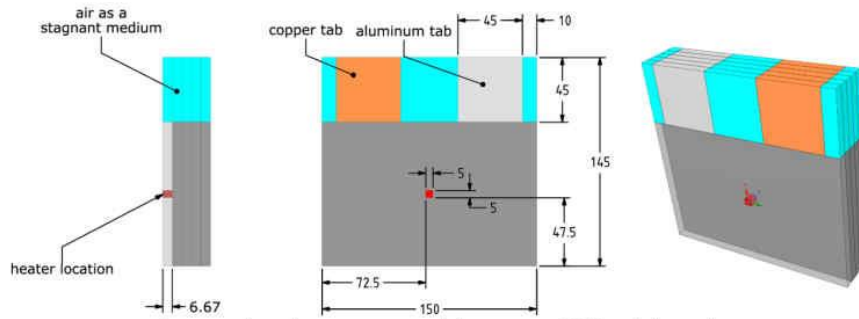


Figure 49: Schematic to accompany model g09m01s02 with five cells in a pack

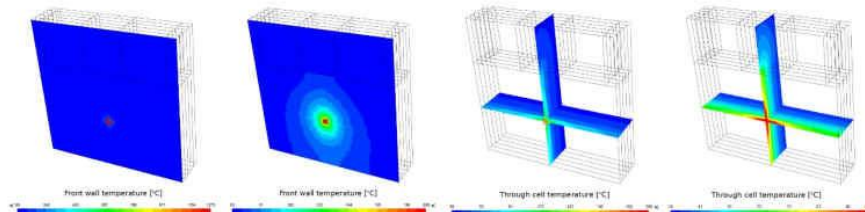


Figure 50: Temperature on the front face of cell 01 (inner wall of the cardboard box) and through the pack after 90 minutes (g09m01s02)

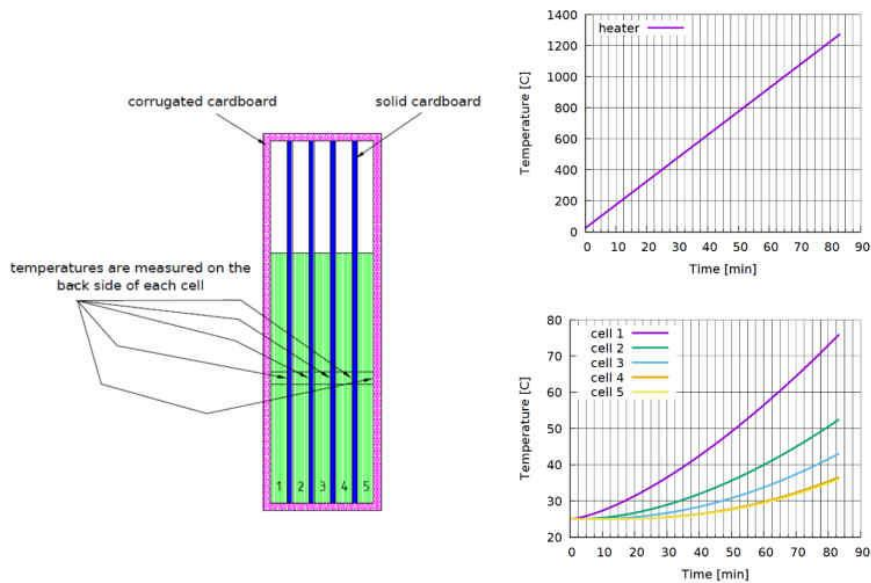


Figure 51: Temperature evolution in time recorded at the back face of each cell (virtual thermocouple is in between the back face of the cell and the solid cardboard divider)

7 Heat propagation modelling in cylindrical cell packs

The numerical model setup described in section 4 is applied to study the temperature propagation and distribution. The results are to be compared with the experiments of group of cells heated by a heater located on one cell. Once validated with sufficient match, the numerical simulations can be utilized to guide the experiments and set standards for heating of cells.

As per the current recommendations in the standards, a cell is heated on one side in such a way that the temperature at the opposite end of the cell rises at a rate of 5-20°C per minute until it reaches 200°C and maintained at that temperature for one hour.

In the simulations, 5x5 package with cylindrical cells described in the previous sections is heated with a heater of dimension 5mm x 5mm located at the center of cell number 3 as shown in figure 52. The heater temperature is increased from room temperature at a gradient of 120°C per minute in such a way that cell 3 temperature at the opposite end of the heater is increasing at a rate lies between 5-20°C per minute. The battery properties input for this simulation are as follows: $C_p = 830 \text{ [J/KgK]}$, $\rho = 2580 \text{ [Kg/m}^3\text{]}$, $K_x=K_y = 0.2 \text{ [W/mK]}$, $K_z = 30 \text{ [W/mK]}$. The boundary condition at corrugated cardboard is set as exposed to convection with $h=5 \text{ [W/m}^2\text{K]}$ and $T=20^\circ\text{C}$.

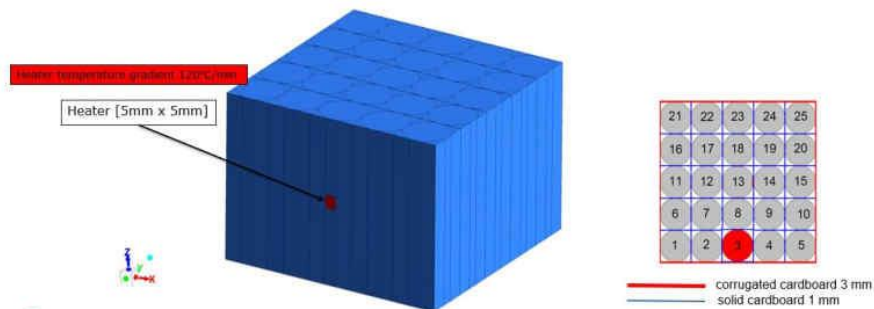


Figure 52: Heater located on cell 3 of the 5x5 cell package

In this simulation, thermal runaway is turned off as the main focus of interest is heat propagation and temperature distribution. The temperature evolution can be seen in figure 53. The temperature points monitored are at the heater, opposite point of the heater and side point of the heated cell. As can be seen in the figure, the temperature of the heater has to be much higher ($\sim 3500^\circ\text{C}$) for the opposite point to reach 200°C for heater temperature increase gradient of 120°C. Another point to notice is the temperature difference between the opposite point and the side point of the cell.

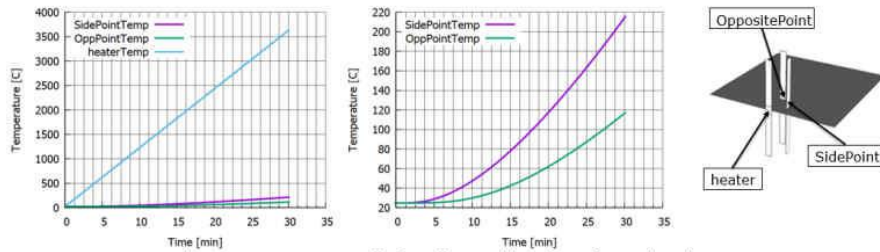


Figure 53: Temperature evolution at heater, side point and opposite point

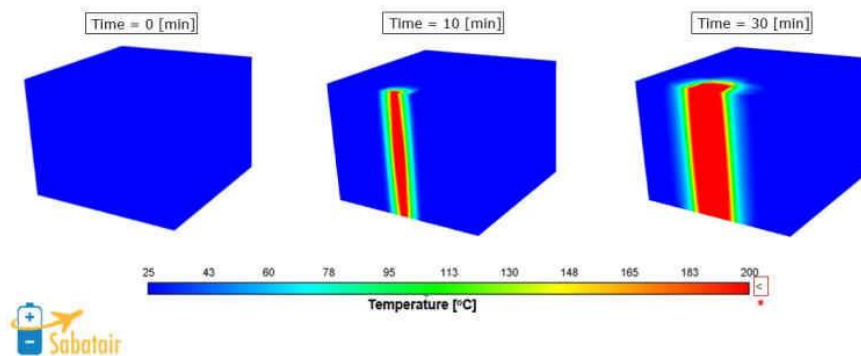


Figure 54: Temperature evolution contours at different time frame

The temperature distribution and heat propagation within the cell can be seen in Figure 54. As can be seen in the figure, the heat propagates according to the directional thermal conductivities. The heat propagates in the Z direction first and then propagates across the cell from the heater side to the opposite point side. The temperature contours are clipped to maximum temperature of 200°C for visualization. Similar analysis was done for a case without internal cardboard dividers between the cells. It portrayed similar temperature propagation except for the minor differences in the temperature contours due to the absence of internal cardboards.

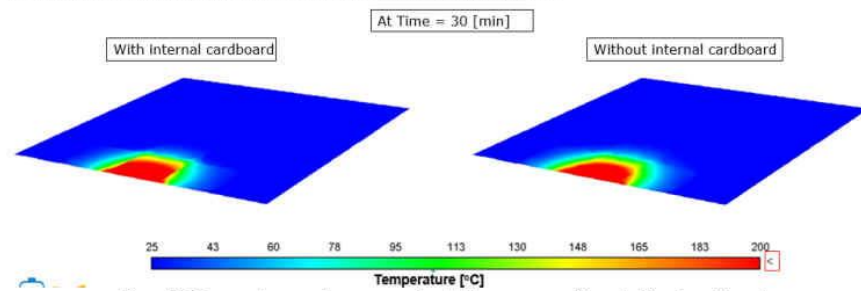


Figure 55: Temperature contours comparison between cases with and without cardboard

For another simulation case, the heater temperature profile was different from the previous case. The temperature increase was from 125°C + 30°C per minute instead of 25°C + 120°C per minute. Both the profiles yield similar rise of the temperature at cell opposite point. However, the temperature of the heater is much lower than the previous case as the temperature gradient of the heater is lower. Similar was the observation for the case with and without internal cardboards as for the previous heater gradient case.

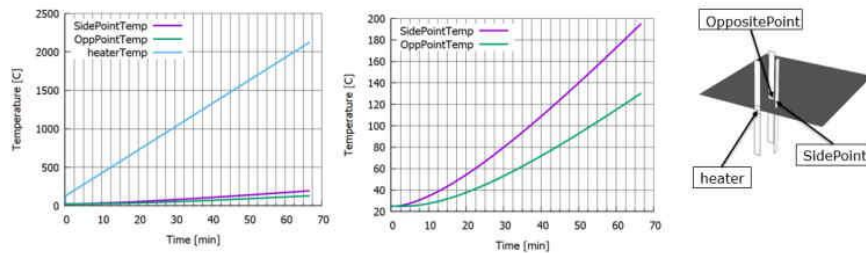


Figure 56: Temperature evolution at heater, side point and opposite point for heater gradient of 30°C pm

Overall, the learnings for the heat propagation study in cylindrical cells are as follows:

- For temperature at opposite cell point to reach 200°C at 5-20°C rise per minute without Thermal Runaway initiation, the heater temperature has to have very high temperature value
- Higher the heater temperature increase rate, higher is the temperature difference between the heater and point opposite the cell
- Even with a small heating region, the heat propagation still spreads across the cell according to directional thermal conductivities

8 Validation of thermal model

For the application of the thermal model in mitigation strategies for thermal runaway propagation prevention, it is important that the model is validated with experimental results. In this section, the validation of the model is performed with experimental data obtained from Sabatair partners. This is done using two kinds of experimental setup – first with 1 cell heated with a point heater source and insulated on all sides – second with measurements done on a group of cells placed together heated with a point source. The subsections 8.1 and 8.2 describe the experimental setup, computational setup and boundary conditions, and results for each of the cases respectively. In the subsection 8.3 implication of the results and conclusions are presented.

8.1 Comparison with temperature measurements for single cell case

In this section, the results from thermal model are compared with experiments conducted by Sabatair partner ALGOLION. For all experiments, 18650 LGMJ1 cell heated with a point source are presented. The thermal model results are compared with 2 experimental cases:

- a. case A with 30% SOC
- b. case B with 100% SOC

8.1.1 Experimental Setup

Understanding of the experimental setup is very important for validation of the thermal model. The experimental setup for the measurements of temperature can be seen in the following figure.



Figure 57: Experimental Setup at ALGOLiON for 1 cell heating temperature measurements

The cell and heater are placed in an explosion proof chamber to initiate thermal runaway with point heater. Thermocouples are attached to the cell in such a way that they do not come off when the cell goes into self-heating. The cell and the heater are clamped for keeping steady. The cell is insulated such that there is minimal heat loss from the cell to the surrounding. The thermocouple measurement points and insulation can be seen in the following figure. The temperatures at the respective points T1, T2, T3 and T4 are used for comparison with the results from the numerical model.



Figure 58: Thermocouple measurement points & setup insulation

8.1.2 Computational Setup & Boundary Conditions

To validate the model, the computation setup and boundary conditions were setup in a way to replicate the reality in the experiments as close as possible. The thermal properties of the cell are input from values used in a previous H2020 project with LGMJ1 18650 cells. The thermal properties used are as follows: $C_p = 918.8 \text{ [J/KgK]}$, $Rho = 2761.7 \text{ [Kg/m}^3\text{]}$, $K_x = K_y = 2.3 \text{ [W/mK]}$, $K_z = 24.3 \text{ [W/mK]}$. The heating was simulated using variable temperature boundary profile of the heater temperature (T1) imposed on the heater patch on the cell in computational domain. For the two cases A & B, apart from the

difference of SOC, there was also difference of insulation in the experiment. Experiment for Case A was poorly insulated while Case B was well-insulated. In the numerical simulation, boundary conditions were incorporated appropriately. In case A, convection boundary condition was imposed with an environmental temperature of 15°C and convective heat transfer coefficient of 15 W/m²K. Since Case B was well-insulated, it was imposed with a zero heat flux boundary condition. The computational mesh used for both simulation along with the heater zone highlighted can be seen in the following figure:

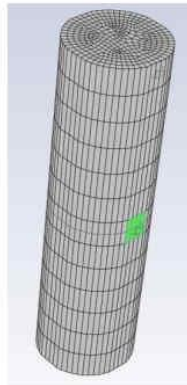
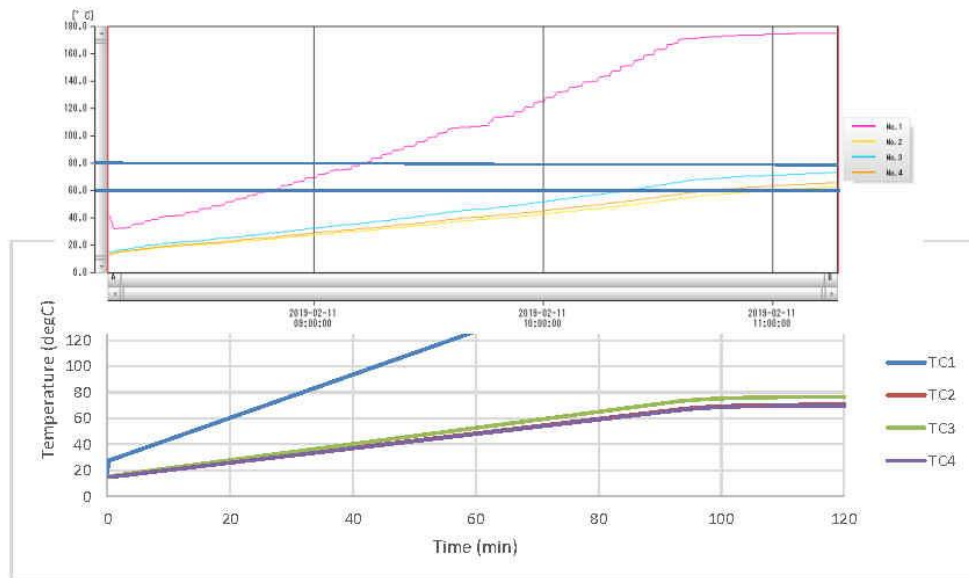


Figure 59: Computational mesh with heater zone highlighted

8.1.3 Results

The results for Case A and Case B can be seen in Figure 60 and 61 respectively.



08/05/2020

38/58

Figure 60: Case A - Experimental Data (Top) , Numerical results (Bottom) temperatures

As can be seen from Figure 60 for case A, there is a good match between the numerical results with experimental data. In the experiments the temperature of the heater was increased slowly in steps to a temperature close to 180 °C while in the numerical model the temperature was linearly increased to exactly 180 °C. Thus, the temperatures of points 1,2,3,4 from the numerical model are slightly higher than the experimental results. The temperature difference between temperature value at point 3 (higher point at cell on the same side of the heater) and temperature value at point 2 (point at the opposite side of heater) seem to be having similar values in the numerical results as in the experimental results. It has to be noted that from the experimental results it can be seen that there is no thermal runaway occurrence for cell with 30% SOC when heater temperature is maintained at close to 180 °C.

Similarly, the results are compared for Case B as seen in Figure 61.

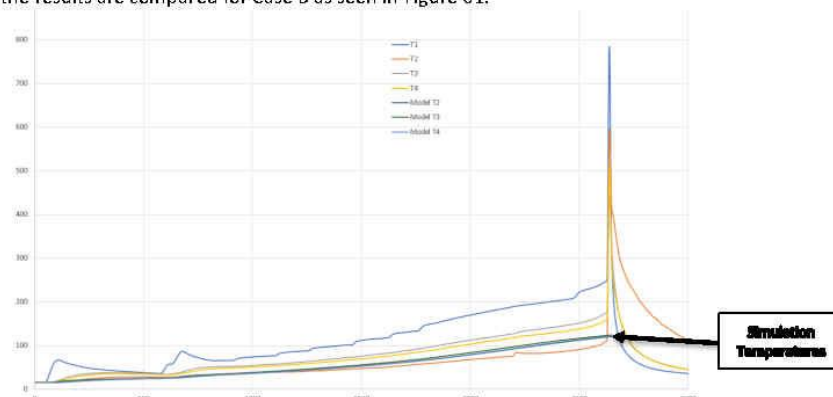


Figure 61: Case B – Experimental data and numerical data for measuring point temperatures

In the numerical model, thermal runaway was turned off. This was mainly because the temperature measurements T1 to T4 after the thermal runaway do not show temperature on the cell-remains but rather the temperature of the nearby air as they get detached from the cell-remains after the thermal runaway. The maximum temperature of the cell, however, was considered for the UDF input values for the TR model used later for TR propagation studies. In this section, therefore, the main focus has been on simulation before the thermal runaway.

In this case B, the temperature profile of the heater was exactly imposed as the temperature measurement profile of T1. The objective being comparison of the temperatures T2-T4 in the experiment and from the thermal model. As can be seen from Figure 61, there is an overall good match in the temperature-time trend. However, the temperature values from the numerical model do not provide temperature difference between T3 and T2 as it is there in the experiments. Moreover, the temperature T4 is quite higher in the experiments compared to the experiment value of T2. This result is not replicated exactly in the numerical simulations. One of the reasons is that, in the numerical simulations, boundary condition of total insulation, that is zero heat flux is applied on all boundary faces except for the heater. Numerically this implies less temperature gradient in itself within the boundary temperature points. In the experiment, it is difficult to obtain total insulation and there would be some minor heat flux losses leading to temperature gradients. Moreover, in the experiments there are other additions in the domain like thermocouple tape holders, cell holders etc. which influence heat transfer. These are not modelled in the computational domain of the numerical experiments which lead to differences in the temperature profile. Overall, however, the temperature

points of the cell are within the range from the experiments and provide sufficient accuracy to lead the development of mitigation strategies for thermal runaway propagation.

8.2 Comparison with temperature measurements for a group of cells

In this section, the results from thermal model are compared with experiments conducted by Sabatair partner Impact Solutions (IS). As in the experiments described above, the type of cells used are Li-ion 18650 LGMJ1 cells heated with a point source. In these experiments, the heating initiation cell is surrounded by other live cells and dummy cells. For computational domain representing the experimental setup, the thermal model results are generated and compared with several experiments with different degrees of experimental certainty. All the tests are numerically simulated with focus being on the last experiment being most controlled. This is the test comparison provided in this report. The experimental and numerical setups along with the results are presented as follows:

8.2.1 Experimental Setup

In these experiments, 1 cell is heated with a small heater of contact area of roughly 64mm^2 (8mm x 8mm). The heater cartridge is placed in an insulation of superwool as seen in the following figure and temperature measurements are done at several location points - 7 points on the initiation cell and 1 point at peripheral cell.

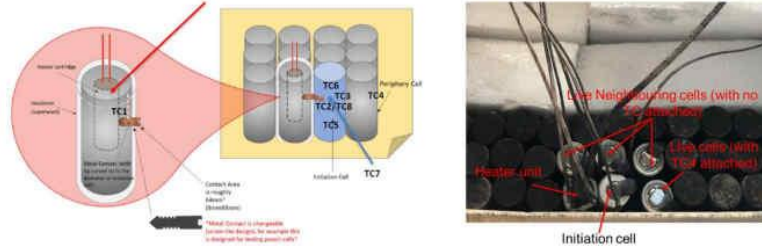


Figure 62: Heater and measurement setup depiction (Left) and an actual experimental setup (right)

In the experiment used for comparison of the temperature results from simulations, the initiation cell is surrounded by 4 live neighboring cells. The rest of the cells are dummy cells surrounding the live cells as seen in the figure 62. The heater temperature TC1 is slowly increased until the cell temperatures reach values around 200°C and the cell goes into thermal runaway. This setup is replicated in numerical simulations with computational setup represented in the following subsection.

8.2.2 Computational Setup & Boundary Conditions

The computational domain used for simulation of the experimental setup described above was similar to the computational domain used in section 5.6 and section 7. Instead of simulating more number of cells, a 25-cell domain mesh was used with the initiation cell at position 3 as shown in Figure 63.

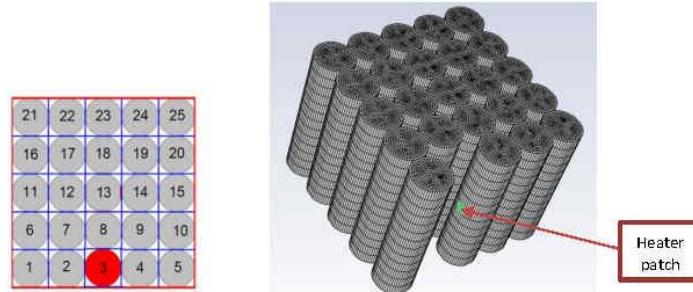


Figure 63: Computational domain for simulating IS experiments

Since the heater is at location 2 and it has insulation separation with the rest of the cells, the domain of the position 2 was removed from computations. However, to model its presence, zero heat flux boundary condition was applied at faces representing superwool insulation and small heater location was appropriately marked with an area of roughly 64mm². All the cells are given thermal properties of live cells with the thermal properties as follows: $C_p = 918.8$ [J/KgK], $Rho = 2761.7$ [Kg/m³], $K_x=K_y = 2.3$ [W/mK], $K_z = 24.3$ [W/mK]. The heating is simulated by imposing heater temperature profile T1 exactly as in the experiment. The outer cell faces are imposed with insulation boundary condition. The simulations are conducted just up to the point of time before thermal runaway occurs in experiments. The temperature results for this setup are compared for all the points T2-T2 and are provided in the following sub-section.

8.2.3 Results

The temperature points for comparison can be better seen in the following figure:

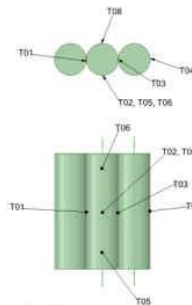


Figure 64: Measurement points for temperature comparison with IS experiments

At these points the temperature comparison is made between the numerical simulation results and the experimental results. The comparison of temperature plots can be seen in the following figure:

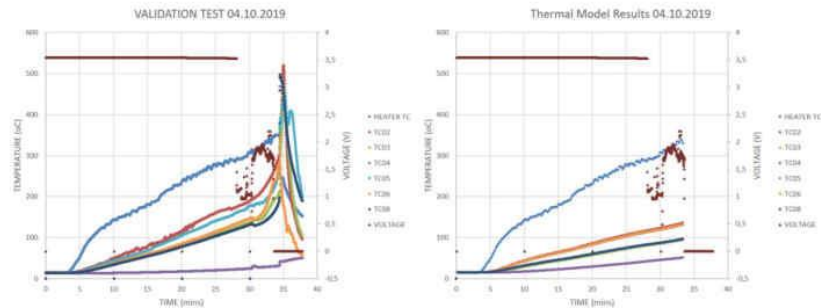


Figure 65: Temperature evolution in experiment (left) and in numerical results until TR (right)

As can be seen from figure 65, the temperature evolution modelled until thermal runaway point follows similar trend as in the experiments. The temperature distribution inside the initiation cell seems to be under-predicted while the temperature of the neighboring cell (TC08) seems to be well-predicted. This is useful for further application where the application of the thermal model is focused on the propagation of heat and thermal runaway. Moreover, the experiment measurements techniques influence the arrangement of the cell as well as temperature measured. With better replicability of the experimental setup, the numerical model results will be accurately closer to the experimental results.

8.3 Conclusions

In the limitations of experimental data and numerical results, the thermal model can be considered as validated and provides sufficient accuracy to approach mitigation strategies for prevention of thermal runaway. The thermal model can be therefore used to guide selection of appropriate mitigation strategies using qualitative assessment. For quantitative assessments, further experiments will need to be conducted and/or factor-of-safety will need to be used for translation of results from the numerical simulations into real life scenarios.

9 Thermal model application for mitigation strategies

Since conducting many experiments for studying thermal runaway propagation prevention is expensive, time-consuming and dangerous; use of numerical thermal model becomes a convenient way to find strategies for prevention of thermal runaway propagation. In this section, the numerical model validated in the previous section is applied to develop mitigation strategies for transport of a box with 25 cells of type LGMJ1 18650 in a 5x5 arrangement. Simulations are first performed for a base case similar to the one described in section 5.6. Furthermore, different cases are proposed as improvements for the base case and to observe the effect on prevention of thermal runaway propagation.

9.1 Base Case – Case 1

In this section, the base case for the study of mitigation strategies is described. All further cases for mitigation strategies are improvements made in reference to this case. Thus, the boundary conditions and properties described in this section are primarily used for all the cases. The details of the base case are as follows:

Description

The base case chosen for this study is one in which 25 cells are transported in a corrugated cardboard of 5mm thickness in a 5 x 5 cell configuration as shown in figure 66. All the cells used are Li-ion 18650 LGMJ1 type with the same thermal properties in the previous sections used for validation of the model. All cells are separated from one another by 2mm thick solid cardboard. The outer box is fully closed making the box with cells air-packed. The initial temperature of all cells are 20°C and the box is placed in an environment at 20°C with heat transfer coefficient of 5 W/m²K. The computational mesh and thermal properties for cardboard used are same as in section 5.6.

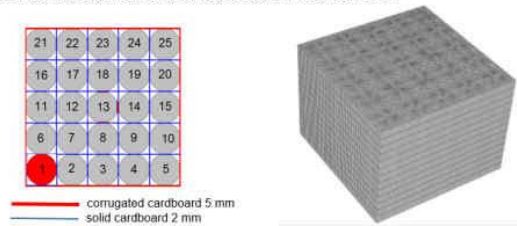


Figure 66: Base case for study of TR propagation mitigation strategies with computational mesh (right)

The location where Thermal Runaway first takes place is at the position 1. This position is chosen as from literature it is found that this has the most risk for initiation and wider propagation. The initiation in the numerical simulation can be considered similar to thermal transience effects from nail-penetration where 1 cell's temperature suddenly increases. In this study, the temperature of the initiation cell suddenly increases, starting from 180°C and follows heat generation profile as in section 5.6 to reach a temperature of around 600°C in about 14 seconds. This heat is propagated to the neighboring cells and the focus is to study how far and fast is thermal runaway propagated to the neighboring cells. The thermal runaway properties of neighboring cells are as in section 8.1 with onset temperature for heat generation pre-thermal runaway is 118°C and onset temperature for thermal runaway is 176°C. This corresponds to Li-ion 18650 LGMJ1 cell at 100% SOC as observed from the experiments. In the numerical model the heat generation is initiated as in section 5 when any computational control volume within the cell reaches these onset temperature. The results for this base case are as follows:

Results

The temporal evolution of maximum temperature in each of the cells can be seen in the following figure. In this base case, all 25 cells go into thermal runaway before 45 minutes from the start of initiation of the first cell thermal runaway.

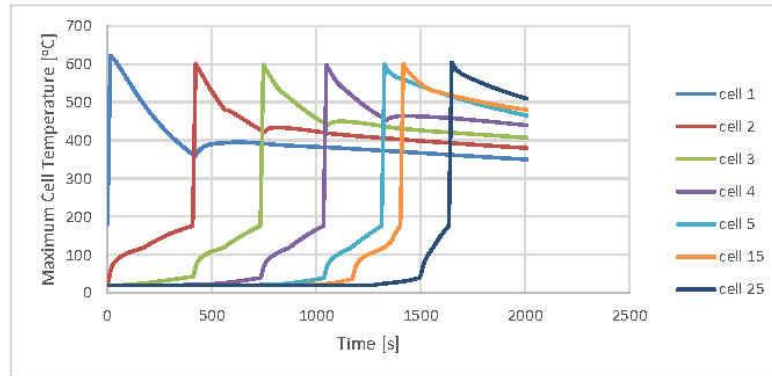


Figure 67: Base case cells maximum temperature temporal evolution

The heat is propagated from the initiation cell at position 1 to its adjacent cells first, i.e. cells 2 & 6 in figure 66. Once they reach their onset temperatures they have heat generation and reach TR temperature. The temperature contour at mid-height of the cells can be seen in Figure 68.

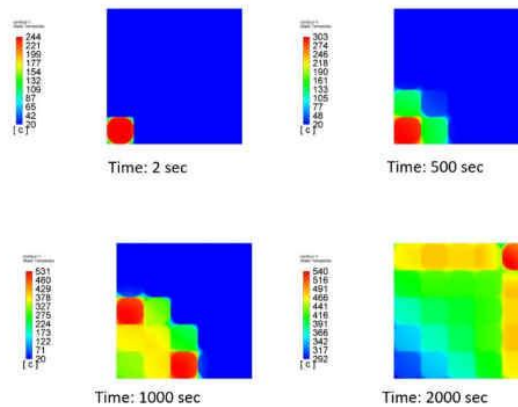


Figure 68: Temperature contour at mid-height level plane for base case at different times

From this base case, it can be understood that the current settings of separators do not suffice to prevent propagation of thermal runaway. Another important observation from this is that once the adjacent cells to the initiation cells go into complete thermal runaway, it is highly likely that all the cells would go into thermal runaway. This is because the environment for each subsequent cell gets hotter and it increases the chances of thermal runaway for the neighboring cells. Thus, in the further cases cells adjacent to initiation cell are focused to check thermal runaway.

From the current setting of cell properties, environmental conditions and initial conditions, different mitigation strategies are proposed in subsequent section to prevent thermal runaway propagation.

9.2 Mitigation Cases

In the base case in previous section, it is seen that thin solid cardboard separators of 2mm thickness do not prevent propagation of thermal runaway for the above case conditions. Thus, it was of interest to find different methods for prevention of thermal runaway propagation for this case of box-cell configuration and initial conditions. In this section several cases are examined to study the heat transfer propagation with different measures. In each case, everything is same as base case except for the parameter change of interest described for each case. The simulation temperature results are analyzed with special focus on temperature of TR initiation cell and 2 cells adjacent to the TR initiation cell. The cases' description and results are provided as follows:

Case 0

This case is a step back from the base case. In this case, there are no dividers separating the cells in the box. This simulation is performed to observe the effect of presence of solid cardboard separators of 2mm thickness. Thus, cells are placed in direct contact with one another while rest all of the conditions are exactly same as the base case. The temperature contour at mid-height of the cells for this case 0 can be seen in Figure 69.

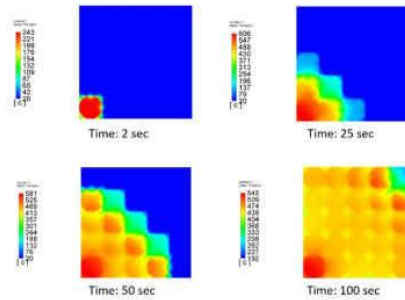


Figure 69: Temperature contour at mid-height level plane for case 0 at different times

As can be seen from figure 69, TR propagates through whole box for case 0 just as for the base case – case 1. However for the case 0 i.e. without any separators, the propagation is much faster. All cells in the box undergo thermal runaway by around 100 seconds. This is 20 times faster than the base case which has thin cardboard dividers. Thus, it can be said that having thin dividers help reduce the rate at which TR propagation takes place. The temperature evolution profile for initiation cell and its adjacent cells TC2 and TC6 can be seen in the following figure:

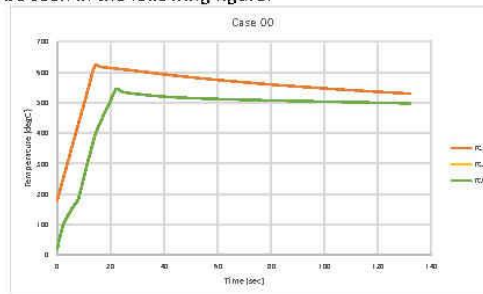


Figure 70: Temperature evolution for initiation cell and adjacent cells for Case 0

Once the initiation cell and adjacent cells undergo thermal runaway, the rest of the cells experience a hotter surrounding and undergo thermal runaway as well. As a next step to propose mitigation measures, thickness of cardboard separators are increased and simulations are performed as case 2.

Case 2

In this case the thickness of the separators is increased from 2mm to 4mm. The thermal properties of the cardboard are same as in base case and as in section 5.6. All other conditions are also kept exactly same as in the base case. The temperature contour at mid-height of the cells for this case 0 can be seen in Figure 71.

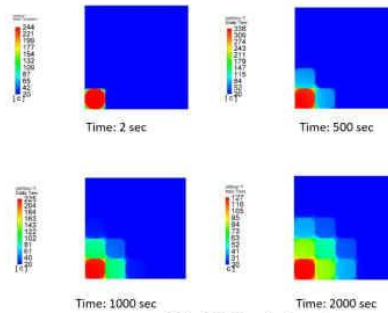


Figure 71: Temperature contour at mid-height level plane for case 2 at different times

As can be seen from the temperature contours of case 2 simulation, cells adjacent to the initiation cell do not undergo thermal runaway. Thus, the rest of the cells also do not undergo thermal runaway. This is with the increase in the thickness of separators which increases the effective thermal resistance between two adjacent cells. Also, the presence of thicker cell separators adds more thermal mass to the system which reduces the rate of heat transfer from one cell to another. Thus, cell separators with 4mm thickness can prevent TR propagation while cell separators with 2mm thickness fail to do so.

The temperature evolution profile for initiation cell and its adjacent cells for the base case (case 1) and case 2 can be compared as follows:

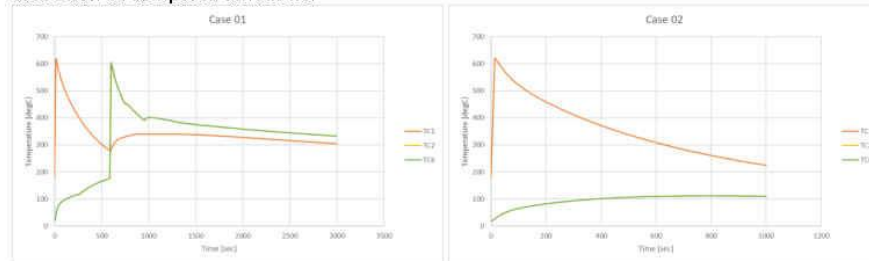


Figure 72: Temperature evolution for initiation cell and adjacent cells for Base Case- Case 1 (left) and Case 2 (right)

As can be seen in the figure 72, temperature of cells at position 2 and 6 never reach onset temperature and do not undergo thermal runaway. Thus, none of the other cells go into thermal runaway as the temperature of the initiation cell slowly reduces with time and heat dissipation. With this understanding, other possible measures for prevention of TR propagation can be seen in the subsequent cases.

Case 3

This case is same as the base case with the difference of external conditions outside of the cardboard box. For this case the effect of larger heat transfer coefficient and a colder environment is investigated. The heat transfer coefficient is increased from $5 \text{ W/m}^2\text{K}$ in base case to $50 \text{ W/m}^2\text{K}$ in this case 3. Along with this the outer environment temperature is reduced from 20°C to 0°C . The temperature evolution profile for initiation cell and its adjacent cells can be seen in the following figure:

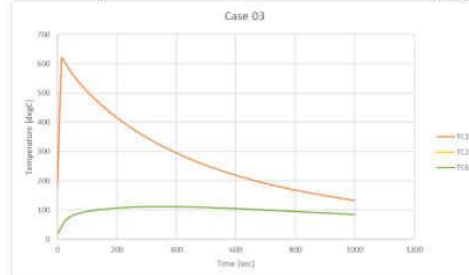


Figure 73: Temperature evolution for initiation cell and adjacent cells for Case 3

As can be seen from figure 73, the temperature of the initiation cell reduces much faster due to larger heat dissipation rate to the environment. This is due to lower external temperature and larger heat transfer. Larger heat transfer is achieved for example by having forced convection by a fan blower. The temperature of the adjacent cells do not reach onset temperature values so they do not undergo thermal runaway, nor do the rest of the cells. Thus, having mechanisms to cool down the box transporting cells can be one of the mitigation measures to prevent TR propagation.

Case 4 & Case 5

In Case 4 and Case 5, the effect of presence of fiberboard instead of thin cardboard separators is investigated. In both these cases, the base case is modified from having 2mm thick cardboard separators to 2mm thick fiberboard separators. The thermal properties of fiberboard input in the simulations are as follows: $C_p = 1700 \text{ [J/KgK]}$, $Rho = 750 \text{ [Kg/m}^3\text{]}$, $K = 0.3 \text{ [W/mK]}$. The rest of the properties and conditions for case 4 are same as in base case. For case 5, effect of presence of vermiculite instead of air in case 4 is investigated. The thermal properties of vermiculite input are as follows: $C_p = 920 \text{ [J/KgK]}$, $Rho = 100 \text{ [Kg/m}^3\text{]}$, $K = 0.06 \text{ [W/mK]}$.

The temperature evolution profile for initiation cell and its adjacent cells for case 4 and case 5 can be compared as follows:

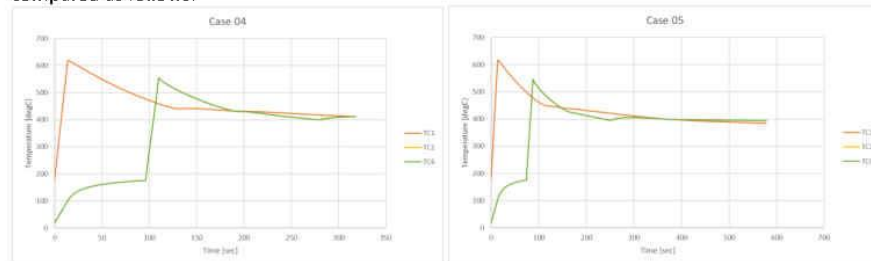


Figure 74: Temperature evolution for initiation cell and adjacent cells for Case 4 (left) and Case 5 (right)

For both the cases, case 4 and case 5 adjacent cells and further all the remaining cells undergo thermal runaway. Thus, having fiberboard of only 2mm thick is insufficient to prevent TR propagation in this case. The difference between presence of air and vermiculite is minimal for heat propagation. However

it should be kept in mind that this is only in terms of heat conduction and propagation and the model does not capture the benefits which vermiculite has in terms of absorption of electrolyte and gases.

Case 6

In this case, the study of presence of fiberboard is extended from the previous cases. In this case, 4mm thick fiberboard separators are used instead of 2mm thick. Rest all the inputs are exactly the same as Case 4. Since moving from case 1 (2mm) to case 2 (4mm) worked with solid cardboard separators to prevent TR propagation, it was of interest to see if it also works with fiberboard separators.

The temperature evolution profile for initiation cell and its adjacent cells can be seen in the following figure:

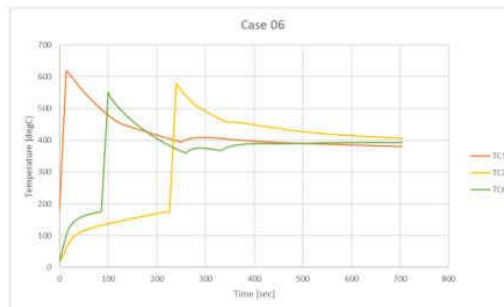


Figure 75: Temperature evolution for initiation cell and adjacent cells for Case 6

It can be seen from figure 75 that for the case of using thicker fiberboard with the input thermal properties does not prevent propagation of thermal runaway. Both the adjacent cells went into thermal runaway and subsequently all the cells went into thermal runaway. Moreover, it was strange that in this case compared to previous cases the temperature profiles TC6 and TC2 were not identical indicating heat propagation to be asymmetric. This is not to be expected, thus, in case fiberboard with the input thermal properties are planned to be used for mitigation measures then further investigation would be necessary.

Case 7

In this case the effect of presence of vermiculite in combination of thick solid cardboard separators is investigated. Thus, case 7 is exactly same as case 2 - in which no TR propagation occurred, except of addition of vermiculite instead of air. Results are plotted as for the other cases and it is seen that solid cardboard separators of 4mm thickness along with vermiculite can prevent TR propagation.

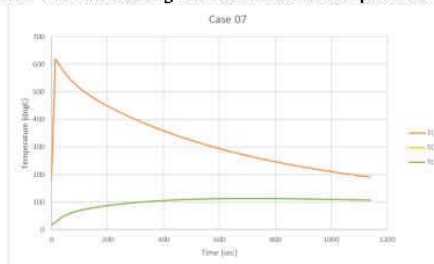


Figure 76: Temperature evolution for initiation cell and adjacent cells for Case 7

Case 8

This case is different from the previous cases as there are no cardboard solid separators. Instead the whole box is filled with sand between the cells to prevent thermal runaway propagation. The gap between the two cells is kept as 2mm and is considered to be filled with sand. Rest of the properties, initial conditions and boundary conditions are same as in the base case. The temperature evolution profile for initiation cell and its adjacent cells can be seen in the following figure:

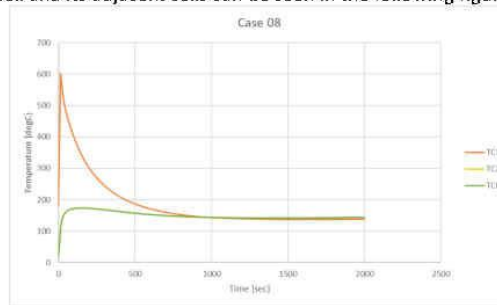


Figure 77: Temperature evolution for initiation cell and adjacent cells for Case 8

As can be seen from figure 77, the adjacent cells do not undergo thermal runaway and so is the case for the rest of the cells in the box. This is because the configuration of the case and sand thermal properties lead to sufficient heat insulation for neighboring cells initially and then dissipation of heat such that onset temperatures are not reached for the adjacent cells. However, it should be noted that the cells do reach onset temperature of pre-thermal runaway self-heating. Thus, for translating the results into real scenario it does not offer sufficient factor-of-safety to be sure of thermal runaway propagation prevention. A possible means of improvement can be to increase the gap between the adjacent from 2mm to 4mm or higher to ensure that there is no thermal runaway propagation.

Case 9 & Case 10

All the cases thus far mainly rely on the fact that the adjacent cells are sufficiently insulated from the initiation cell and the heat release out of the box is sufficient that the remaining cells do not undergo thermal runaway. While for case 9 and case 10, the main mitigation strategy is to have material with high thermal conductivity between the cells such that the heat is dissipated away from the initiation cell much faster and the adjacent cells do not reach onset temperatures. For these cases special boxes with materials covering the whole box and inter-cell region are used. Thus, they act as heat sinks when one cell goes into thermal runaway. The material used in case 9 is alumina (Al_2O_3) with following properties: $C_p = 3970$ [J/KgK], $Rho = 765$ [Kg/m³], $K = 36$ [W/mK]. For case 10 graphite is used instead of alumina with the properties as follows: $C_p = 850$ [J/KgK], $Rho = 1600$ [Kg/m³], $K = 160$ [W/mK]. It can be observed that the thermal conductivity for these materials is more than 100 times higher than for the previous cases. The gap between the adjacent cells is fixed to be having 4mm made of the respective dissipative material while the outer box is made with same material having 5mm thickness. From the temperature evolution profile for initiation cell and its adjacent cells for case 9 and case 10, it can be seen that the temperature of the initiation cell is reduced very fast and within 100 seconds the risk of TR propagation is eliminated. The temperature evolution for the 2 cases vary due to differences in thermal properties but both act as good heat sinks and provide extremely efficient measure for preventing risks of thermal runaway propagation.

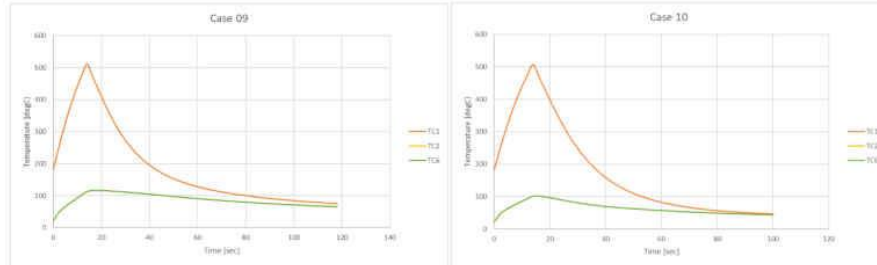


Figure 78: Temperature evolution for initiation cell and adjacent cells for Case 9 (left) and Case 10 (right)

9.3 Results Summary

The thermal numerical model provides good understanding of heat propagation from an TR initiation cell to remaining cells in a box. It is also used to study the effect of different mitigation strategies for prevention of thermal runaway propagation.

The summary of results of all cases presented in section 9 is provided as follows:

Case Name	Mitigation Strategy	Description	Result
Case 00	None	No separators	TR for all cells
Case 01	Thin cardboard separators	BASE CASE	TR for all cells
Case 02	Thicker cardboard separators	Base Case with 4mm separator thickness	no TR propagation
Case 03	Colder environment with higher h	Base Case with more convection heat transfer: h=50, T=0	no TR propagation
Case 04	Thin fiberboard separators	Base Case with 2mm fiberboard separators	TR for all cells
Case 05	Thin fiberboard + vermiculite	Base Case with 2mm fiberboard separators & vermiculite	TR for all cells
Case 06	Thicker fiberboard	Base Case with 2mm fiberboard separators	TR for all cells
Case 07	Thicker cardboard + vermiculite	Base Case with 4mm separator thickness & vermiculite	no TR propagation
Case 08	Sand filled cardboard box	Base Case sand filled with cells at 2mm separation	adjacent cells vented but no TR propagation
Case 09	Alumina full container	Base Case layout in Alumina container with 4mm cell separation	no TR propagation
Case 10	Graphite full container	Base Case layout in Graphite container with 4mm cell separation	no TR propagation

From different cases analysed, the following results can be summarised:

1. Thicker cardboard separators are required to prevent TR propagation.
2. Box placed in an colder environment with high heat transfer coefficient can prevent TR propagation.
3. Conductive fiberboard needs more thickness for TR prevention in comparison to less conductive cardboard.
4. Presence of vermiculite instead of air is a good option when used with cardboard separators.
5. Container filled with sand can prevent TR propagation when the cells are kept with sufficient separation distance between them.
6. Thermally conductive holder boxes made from graphite or alumina helps in thermal dissipation and prevents TR propagation.

Thus, from these possibilities in the above cases, appropriate thickness of separators, material for filling and holding of the cells can be selected. Furthermore, it should be noted that the success or failure from the above simulation cases is for one type of thermal runaway i.e. one cell suddenly goes into TR while the other cells are at room temperature. This can be considered similar to the case of a sudden nail penetration for the corner cell. If the initial condition and initiation conditions are changed then some measures can become more effective or less effective depending on the case at hand.

While the model provides good basis for qualitative assessments, it should be noted that the thermal model has several limitations. The simulations can be used to predict well the heat propagation by conduction and radiation. However in a thermal runaway, there are other complex physics such as gas release, flames etc which are not modelled in the current model. The model currently utilizes only thermal properties of the materials to predict heat propagation. Thus, the benefit of vermiculite, for example, compared to just air is not visible through this model. Another consideration which is important is that for separators and boxes made from cardboard it would be better to have flame-resistant coating as the temperatures reach up to 600°C while flame point of most carboards is around 450°C. While the temperature reaching 600°C is modelled the effect of presence of flames is cannot be modelled in the current model.

For exact quantitative measures for prevention of TR propagation, it would be preferred that the model is supported with more experimental data. The results from the model can be used to guide forming appropriate experiments to develop mitigation strategies for prevention of thermal runaway propagation.

10 Study for cell internal temperature distribution

It is of interest to study how the internal cell temperature distribution is and heat propagates within a cell first along with studying how cell propagates from one cell to another. In this section, the focus is to investigate the internal cell temperature distribution.

10.1 Single Cell Simulations

In this sub-section, simulations using the numerical model for heating of a single cell are presented. The computational setup is similar to the one in section 8.1, however, with more focus on the internal temperature distribution and rate of temperature rise. As in the section 8.1, the thermal properties of the cell input in the model are as follows: $C_p = 918.8$ [J/KgK], $Rho = 2761.7$ [Kg/m³], $K_x=K_y = 2.3$ [W/mK], $K_z = 24.3$ [W/mK]. Since the effect of explicit modelling of can properties is of focus in this section, the can properties are input in addition to the overall cell properties. A can of 0.2mm thickness and with thermal properties as follows is modelled: $C_p = 460$ [J/KgK], $Rho = 7917$ [Kg/m³], $K = 14$ [W/mK] [from Ref. T. D. Hatchard, D. D. MacNeil, A. Basu, and J. R. Dahn, *J. Electrochem. Soc.*, **148**, A755 (2001)]. The simulations are performed with convection boundary condition imposed having an environmental temperature of 15°C and convective heat transfer coefficient of 15 [W/m²K]. The cell is heated from one side with a small heater as in section 8.1 with a heater heating rate of 15°C+20°C per minute and simulations are stopped when the temperature at the opposite point of the cell reaches 200°C. The internal cell temperature distribution contour at the mid-height plane of the cell is observed. Along with this the temperature increase rates at the surface and interior of the cell are noted. This base case is referred to case 1 in the subsequent parts of this section 8.1. The results obtained for base case are as follows:

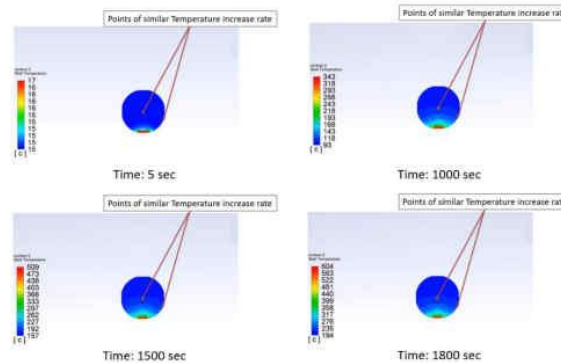


Figure 79: Internal temperature contour at mid-height plane for Case-1 simulation

As can be seen from the temperature contours, the maximum cell temperature inside the cell reaches to values greater than 400°C. The opposite point temperature takes about 1800 seconds to reach around 200°C with a rate of about 6°C increase per minute. The temperature at the interior of the cell, near the center around 9mm from the heating point increases at a rate similar to a side point the cell.

Case 2

In case 1 presented above, the single cell is imposed with a convection boundary condition. However, when placed inside a package the surrounding will be more insulating than the free convection boundary condition applied in case 1. As a follow-up to case 1, case 2 is simulated with an extreme

case boundary condition of adiabatic or zero-flux boundary condition. The results obtained for case 2 are as follows:

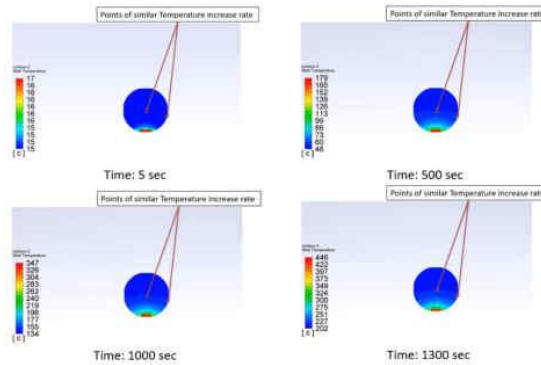


Figure 80: Internal temperature contour at mid-height plane for Case-2 simulation

As can be seen from the temperature contours, the maximum cell temperature inside the cell reaches to values greater than 300°C. The opposite point temperature takes about 1300 seconds to reach around 200°C with a rate of about 8.5°C increase per minute. Since the case is of adiabatic, there is no heat loss from the cell to the surrounding. Thus, all of the input heat is leads to temperature increase of the cell. So the time taken for the opposite point to reach 200°C is less than case 1. Moreover, temperature gradient within the cell is also lower compared to case 1. Similar to case 1, the temperature at the interior of the cell, near the center around 9mm from the heating point increases at a rate similar to a side point the cell.

Case 3

In this case a hypothetical scenario is simulated where the computational setup is exactly same as in case 1 except the can thickness is modelled to be 1mm thick. This hypothetical case is to see the effect of rate of temperature increase at a point on the surface compared to interior temperatures. The results obtained for case 3 are as follows:

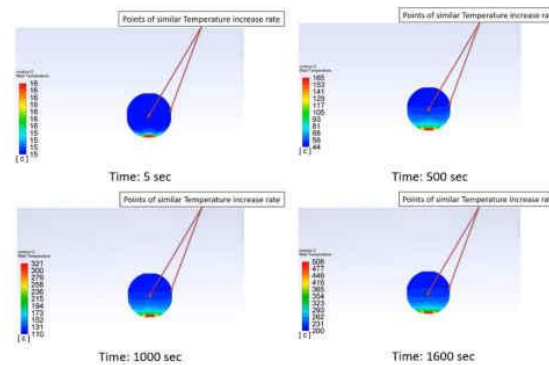


Figure 81: Internal temperature contour at mid-height plane for Case-3 simulation

As can be seen from the temperature contours, the maximum cell temperature inside the cell reaches to values greater than 350°C. The opposite point temperature takes about 1600 seconds to reach around 200°C with a rate of about 6.8°C increase per minute. Compared to case with can thickness of 0.2mm the point on the surface, which has similar temperature increase rate as that of the interior center of the cell, is shifted further away from heating side.

Case 4

This case is to observe the effect of higher heating rate compared to case one. In case 1, the heating rate of the heater is 15°C+20°C per minute. While in this case the heater heating rate is 15°C+40°C per minute. Keeping all the parameters same, the effect of higher heating rate is observed. The results obtained for case 4 are as follows:

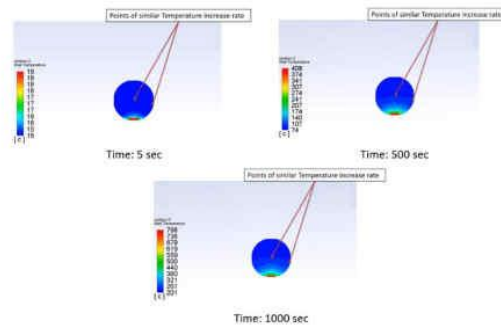


Figure 82: Internal temperature contour at mid-height plane for Case-4 simulation

As can be seen from the temperature contours, the maximum cell temperature inside the cell reaches to values greater than 500°C. The opposite point temperature takes about 1000 seconds to reach around 200°C with a rate of about 11°C increase per minute. Thus, with a higher heating rate there is a higher gradient within the cell and the rate of temperature increase at the back point is also higher.

To summarize the results from single cell simulation:

- The cell internal temperature center heat increase rate is similar to the temperature increase rate of cell side point at same height level as of the heater
- Internal cell maximum temperature depends on external environment of a cell and the heating rate

Case	Opposite Point Temperature increase rate to 200°C	Internal Max Temp
Base Case + convection environment (20°C/min heating rate)	~6°C per minute	>400°C
Base case + Adiabatic environment (20°C/min heating rate)	~8.5°C per minute	>300°C
Thicker Can (1mm) convection environment (20°C/min heating rate)	~6.8°C per minute	>350°C
Higher Heating Rate + convection environment (40°C/min heating rate)	~11°C per minute	>500°C

10.2 Simulations of multiple cells in a pack

In this sub-section, cells in a pack are simulated with a computation setup that can help with the SAE G27 guidelines. Thus, the location of the initiated cell is at location 3 in the following figure 83. The cell at this location is heated with a heater at location 2 which is insulated on all sides except one small region, only to heat the cell at location 3 with a small heating area. Thus, this setup is similar to the setups performed by Sabatair partner Impact Solutions, similar to the experiment described in section 8.2.

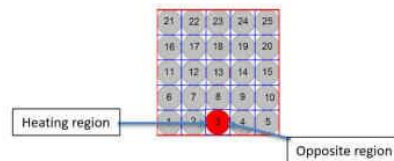


Figure 83: Initiation heating cell at location 3, heater from the side of location 2 cell

In this study, following effects are studied:

- Internal temperature contours at different height levels
- Effect of heater size
- Effect of heater heating rate

These effects are studied by starting from one reference case and adding the other effects in numerical model for the next 2 cases. The simulations are performed for same thermal properties and boundary conditions as in section 9 with a few changes. For the simulations in this section, the computational domain does not contain mesh control volumes of cells at location 2. This is because the heater is located at location 2 and is insulated from the rest of the box. This effect can be simulated numerically by imposing a zero-flux boundary condition and heater patch of regulated temperature increase. The computational domain with heater patch can be seen in the following figure:

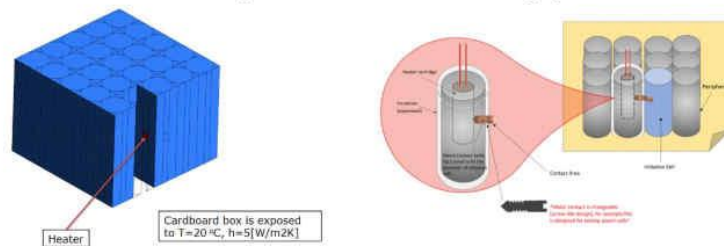


Figure 84: Computational domain for heating guidelines study (left); representing an equivalent experimental setup (right)

The reference case for this study is with computation setup having a small heater patch of about 20mm^2 similar to size of heater in section 8.1. The heater patch is imposed a temperature increase rate profile of $25^\circ\text{C}+24^\circ\text{C}$ per minute. The material properties and boundary conditions for the simulations are as in the reference case in section 9 where cells are packed air-tight in a cardboard package. The heater location is at mid-height of the cell and the temperatures contours are observed at mid-height horizontal plane, horizontal plane at 75% of the height and vertical plane at the location of the heater. The simulations are run with thermal runaway turned off in the model. The simulations are stopped when the temperature at the opposite side of the cell reaches 200°C . The results obtained of temperature contours for this reference case 1 are as follows in figure 85:

As can be seen from the figure 85, the temperature progressively increases with time as the heater temperature increases. The temperature distribution within the heated cell at one point of time follows a gradient as per the thermal conductivity of the cell. For visualization, maximum temperature in display is clipped to 450°C. This temperature of 450°C also corresponds close to the ignition temperature of standard corrugated cardboard. Likewise, the temperature contour at vertical plane at heater location is presented in figure 86. From the figures 85 and 86, the overall temperature distribution around the heater for case 1 can be studied.

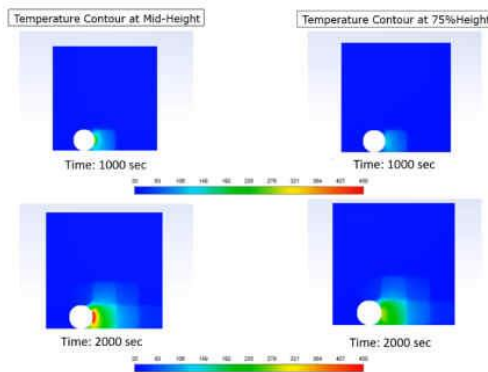


Figure 85: Temperature contour for horizontal planes at mid-height (left); at 75% of the height (right)

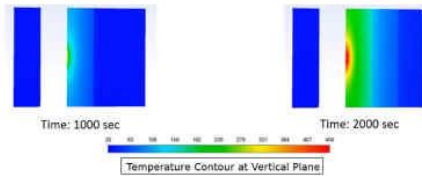


Figure 86: Temperature contour for vertical plane at heater location for case 1

Overall, the opposite point temperature takes about 2190 seconds to reach around 200°C with a rate of about 4.9°C increase per minute. The maximum cell temperature inside the cell reaches to values greater than 500°C. The temperatures at heater height level are higher than at heights above or below the heater level.

Case 2

The computational setup for case 2 is exactly the same as case 1 except for the change in parameter of heater area size. The heater size for this case is 64mm² similar to the experimental setup heater in section 8.2. The temperature contours for this case are obtained similar to the reference case 1.

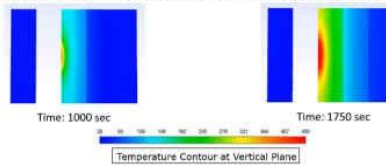


Figure 87: Temperature contour for vertical plane at heater location for case 2

The opposite point temperature takes about 1750 seconds to reach around 200°C with a rate of about 6.3°C increase per minute. The maximum cell temperature inside the cell reaches to values greater than 550°C. Overall, since the heater area is larger for the same heating rate as in case 1, larger internal volume has temperatures higher than 450°C as seen in the figure 87. The time required for the opposite point temperature to reach 200°C is less than in case 1.

Case 3

In the case, the effect of heating rate is studied. Thus, compared to the reference case 1, this case 3 has only the difference of higher heating rate. The heater patch of around 20mm² is imposed a boundary condition temperature increase rate profile of 25°C+48°C per minute.

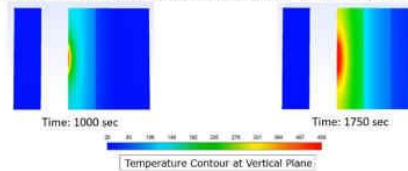


Figure 88: Temperature contour for vertical plane at heater location for case 3

The opposite point temperature takes less than 1750 seconds to reach around 200°C with a rate of about 8°C increases per minute. The maximum cell temperature inside the cell reaches to values greater than 600°C. Overall, since the heater temperature increase rate is higher than in case 1, larger internal volume has temperatures higher than 450°C as seen in the figure 88. The time required for the opposite point temperature to reach 200°C is less than in case 1. Moreover, the temperature gradient within the cell at different locations is higher at same point of time.

Overall, from this study in section 10.2 following results can be summarized:

- Temperatures at same height as of heater are higher than temperatures at heights higher and lower than heater location height.
- Bigger surface area of the heater leads to faster heating and higher average internal temperature.
- Higher heating rate of the heater leads to more faster heating and higher maximum internal temperature.

10.3 Extension of study to pouch cells

The numerical model is mainly used as a tool to study the temperature distribution and propagation for cylindrical cells. However, similar studies can be extended for pouch cells by appropriate computational domain modelling, thermal properties and boundary condition input as demonstrated in section 6. The effect of heater heating rate, heater size and heater location on cell surface temperatures and internal temperatures can be studied accordingly.

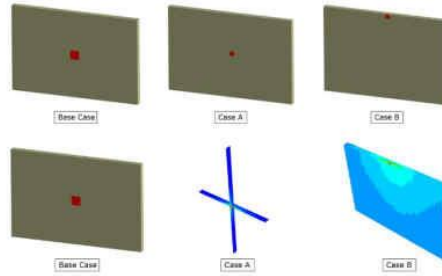


Figure 88: Extension of the model to pouch cells

As observed from sample cases, the temperature distribution is influenced by effective thermal conductivities, heating rates, heater areas and boundary conditions; similar to cases with cylindrical cells.



Sabatair_Heat
transfer modeling o